
**UNIVERSITÀ DEGLI STUDI DI MILANO**

PhD Course in Molecular and Cellular Biology

**XXXV Cycle**

# A novel Rit2-LRRK2 axis modulates lysosome function: Insight for Parkinson's disease pathophysiology

**Sara Pizzi**

PhD Thesis

**Scientific Supervisor: Prof. Graziella Cappelletti**

**Co-Tutor: Dr. Mattia Volta**

Academic Year: 2021-2022

# Table of Contents

# Abbreviations

**ALP** autophagy-lysosomal pathway

**AMPK** adenosine monophosphate-activated protein kinase

**Atg** autophagy-related gene

**BCA** bicinchoninic acid

**BSA** bovine serum albumin

**CaMKK-β** calcium-dependent protein kinase kinase-β

**CMA** chaperone-mediated autophagy

**COR** C-terminal of Roc

**CQ** chloroquine

**DA** dopamine

**DAT** dopamine transporter

**ESCRT** endosomal sorting complex required for transport

**GAP** GTPase activating protein

**GBA** Glucocerebrosidase

**GDI** GDP dissociation inhibitors

**GEF** guanine nucleotide exchanging factor

**GWAS** genome-wide association study

**HSC70** heat shock cognate 70

**KI** knock-in

**KO** knock-out

**LAMP2A** lysosome-associated membrane protein 2A

**LC3** microtubule-associated protein 1A/1B-light chain 3

**LRRK2** Leucine-rich repeat kinase 2

**MAO-B** monoamine oxidase-B

**MAPK** mitogen-activated protein kinase

**MPTP** 1-methyl-4-phenyl-1,2,3,6-tetrahydropyridine

**mTORC1** mammalian target of rapamycin complex 1

**NAADP** nicotinic acid adenine dinucleotide phosphate

**PD** Parkinson's disease

**PI3K** phosphatidylinositol 3-kinase

**PVDF** polyvinylidene difluoride

**RBD** rapid eye movement behavior disorder

**RIT2** Ras-like without CAAX 2

**ROC** Ras of complex

**SNpc** *Substantia Nigra pars compacta*

**TBS** Tris-buffered saline

**TBS-T** Tris-buffered saline-Tween 20

**TFEB** transcription factor EB

**TH** tyrosine hydroxylase

**TPC2** two-pore channel 2

**TRPML1** transient receptor potential mucolipin 1

**ULK** Unc-51-like kinase

**UPS** ubiquitin-proteasome system

**VPS35** vacuolar protein sorting 35

**WIPI** WD-repeat protein interacting with phosphoinositide

**WT** wild-type

**αSyn** α-Synuclein

**PBS** phosphate buffered saline

**PLA** proximity ligation assay

# Riassunto

La disfunzione lisosomiale è un fattore determinante nella patogenesi della malattia di Parkinson (PD). L'attività chinasica di Leucine-rich repeat kinase 2 (LRRK2) modula autofagia e funzionalità lisosomiale, e la sua inibizione farmacologica è protettiva per neurodegenerazione e patologia di α-sinucleina (αSyn). Tuttavia, rimane da chiarire la via di segnalazione che coinvolge LRRK2, ed il ruolo patogenico delle relative alterazioni.

In questo lavoro, abbiamo rivelato una nuova interazione funzionale tra LRRK2 e la piccola GTPasi Rit2. Quest'ultima è coinvolta nella via di segnalazione regolata da MAPK, nell'accrescimento dei neuriti e nel traffico del trasportatore della dopamina. Polimorfismi nel locus genico contenente *RIT2* sono stati associati ad un incrementato rischio di sviluppare PD, che si presuppone collegato ad alterata espressione genica di *RIT2*. Abbiamo osservato che i livelli di mRNA di *RIT2* sono ridotti nei neuroni dopaminergici della *substantia nigra pars compacta* (SNpc) e in modelli *in vitro* che *in vivo* di PD. L'overespressione di Rit2 in cellule di neuroblastoma esprimenti G2019S LRRK2 ha revertito difetti lisosomiali e diminuito l'accumulo di αSyn, mostrando un effetto simile a quello dell'inibizione chinasica di LRRK2. Inoltre, l'overespressione selettiva di Rit2 selettivamente nei neuroni dopaminergici della SNpc in topi iniettati con virus contenente A53T αSyn ha mostrato effetti neuroprotettivi. A livello molecolare, abbiamo identificato un'interazione tra Rit2 e LRRK2, e un'inibizione dell'attività chinasica di LRRK2 da parte di Rit2. Per di più, abbiamo osservato che l'ablazione dell'espressione di Rit2 comporta difetti lisosomiali sia in cellule che in neuroni dopaminergici, indicando che Rit2 è indispensabile per una corretta funzione lisosomiale. Abbiamo inoltre mostrato il coinvolgimento di Rit2 nel rilascio di calcio dai lisosomi, che rappresenta un punto di convergenza nella modulazione dell'autofagia dipendente da LRRK2. Concludendo, proponiamo Rit2 e la sua interazione con LRRK2 come possibili nuovi target per lo sviluppo di approcci terapeutici per PD.

# Abstract

Lysosome dysfunction is recognized as a critical factor in Parkinson's disease (PD) pathogenesis. Leucine-rich repeat kinase 2 (LRRK2) has a kinase-dependent role in autophagy and lysosomal function, and its pharmacological inhibition is protective against neurodegeneration and α-synuclein (αSyn) pathology. However, the precise signaling pathways involving LRRK2 and how alterations lead to pathology have not been clarified yet. In this work, we unravel a novel functional interaction between LRRK2 and the small GTPase Rit2, previously reported to participate in MAPK-signaling, neurite outgrowth and dopamine transporter trafficking. Polymorphisms in the *RIT2* locus are associated to increased risk of PD and are predicted to alter gene expression. We found that *RIT2* mRNA levels are reduced in *substantia nigra pars compacta* (SNpc) dopaminergic neurons of idiopathic PD patients and in different *in vitro* and *in vivo* PD models. Rit2 overexpression in G2019S-LRRK2 neuroblastoma cells restores lysosomal defects and diminishes αSyn accumulation, phenocopying pharmacological LRRK2 kinase inhibition. Moreover, Rit2 selective overexpression in SNpc dopaminergic neurons in A53T-αSyn virally injected mice reduces neurodegeneration and αSyn pathology. Notably, we uncovered that Rit2 interacts with LRRK2, and its overexpression inhibits LRRK2 kinase activity both *in vitro* and *in vivo*. In addition, Rit2 is required for lysosomal function, since its gene silencing in cell lines and DA neurons leads to lysosomal defects. We showed promising preliminary data indicating that the mechanism of Rit2 action in autophagy might involve lysosomal calcium release, that represents a convergent point in LRRK2-mediated regulation of autophagy. We propose Rit2 and its interplay with LRRK2 as novel targets for future, disease-modifying therapeutic approaches in PD.

# Aim of the project

Degeneration of nigral dopaminergic neurons and αSyn pathology are the pathological hallmarks of PD. Alterations in the autophagy-lysosome pathway (ALP) have been found in PD brains and experimental models, and different lines of research suggest that these alterations may underlie disease pathogenesis. LRRK2 is a large multidomain protein involved in different signaling cascades and it plays a role in autophagy. Nevertheless, the precise mechanism underlying LRRK2-mediated regulation of autophagy are still unclear, as contradictory reports exists with regard to the direction of such modulation. LRRK2 mutations, such as the G2019S, are the most common genetic cause of PD and produce hyperactivation of its kinase function. Of note, pharmacological LRRK2 kinase inhibition has been proven effective against experimentally induced αSyn pathology and neurodegeneration. Recently, GWAS studies associated variations in the locus containing the *RIT2* gene with an increased risk of PD. Moreover, Rit2 expression is downregulated in nigral dopaminergic neurons from PD patients. The *RIT2* gene encodes a small GTPase belonging to the Ras superfamily that also includes Rab proteins, which are validated LRRK2 substrates and interactors. Rit2 is involved in MAPK/ERK signaling, a cascade in which LRRK2 is also implicated, neurite outgrowth and differentiation, calcium signaling, and dopamine transporter trafficking.

On this basis, we aim to investigate whether LRRK2 and Rit2 functionally interact in a disease-relevant molecular mechanism. First of all, we sought to investigate whether Rit2 downregulation could be recapitulated in our G2019S LRRK2 SH-SY5Y cell model, that displays αSyn accumulation and lysosomal defects. Secondly, we explored whether the restoration of Rit2 expression would be beneficial in this cell model of PD, in terms of reduction of pathologic αSyn burden and amelioration of lysosomal function, thus linking Rit2 and LRRK2 functions. In this regard, we sought to investigate whether Rit2 interacts with LRRK2, by utilizing proximity ligation assay and co-immunoprecipitation, and whether Rit2 might modulate LRRK2 kinase activity. Besides, since very little is known about Rit2 physiological function, we aimed at elucidating its possible participation in the regulation of the ALP, dissecting different steps of this pathway in a Rit2-KO cell line. In this view, we further examined the molecular mechanism through which Rit2 could modulate autophagy. In

particular, we explored the hypothesis that Rit2 could regulate lysosomal calcium release from TPC2 channels, which was reported to regulate autophagy and be modulated by LRRK2 itself. To this purpose we used two different approaches to measure calcium transients: a more general Fura-2-based calcium imaging method and more specific calcium imaging using a novel genetically encoded calcium indicator fused to the lysosomal calcium channel TPC2. The results obtained from this study will contribute shading a light on pathophysiological mechanisms underlying PD, with the ultimate aim to find a disease-modifying therapeutic approach, that is urgently needed for PD.

# 1. Introduction

## 1.1 Parkinson's disease: clinical manifestations and therapy

PD is the second most common neurodegenerative disorder affecting more than 6 million people worldwide, a number that is expected to double by 2050 [1]. The prevalence of PD in the global population is estimated to be 0,3%, but it increases up to 3-4% in people over the age of 80 [2], making age the major risk factor for developing PD. However, it is worth mentioning that there are cases manifesting the disease before the age of 40. They enter the category of early-onset PD, among which young-onset PD (onset between age 21 and 40) and juvenile parkinsonism (onset before the age of 21) can be distinguished [3]. This age-related disorder is generally characterized by a slow progression (disease duration can span decades) and affected individuals accumulate disability over time. This results in a great impact on caregivers, health systems, and patients themselves, therefore, PD represents a surging socioeconomic burden from the perspective of aging-population [4].

Two centuries have passed since James Parkinson's first description of the malady in "An essay on the Shaking Palsy" [5]. He identified the cardinal motor symptoms of the disease, then grouped under the acronym TRAP: Tremor at rest, muscular Rigidity, Akinesia (namely bradykinesia), and Postural instability [6]. Following the UK Parkinson's disease Society Brain Bank clinical diagnostic criteria, bradykinesia plus rigidity and/or resting tremor are necessary for clinical diagnosis of PD, in the absence of an alternative cause of parkinsonism [7]. But due to the heterogenicity of clinical manifestations, and similarity to other neurodegenerative diseases or secondary parkinsonism, diagnosis is not always a straightforward process. Indeed, only 75%-95% of cases have a definitive diagnosis of PD after *post-mortem* examination, when histopathology assesses the loss of pigmented neurons in the SNpc and the presence of Lewy bodies in the surviving neurons [8]. Nevertheless, if motor symptoms characterize the clinical and late stage of the disease, there is growing evidence that non-motor symptoms are a major component of the early prodromal phase of PD (**Fig.1.1**), namely the window of time in which signs of disease progression become evident but they are not sufficient to drive a diagnosis. Non-motor symptoms that have a significant value in predicting PD diagnosis consist of rapid eye movement sleep behavior

disorder (RBD), loss of olfaction, cognitive and behavioral disturbances (e.g., attention and memory deficits, depression/anxiety), constipation, somnolence, orthostatic hypotension [9].

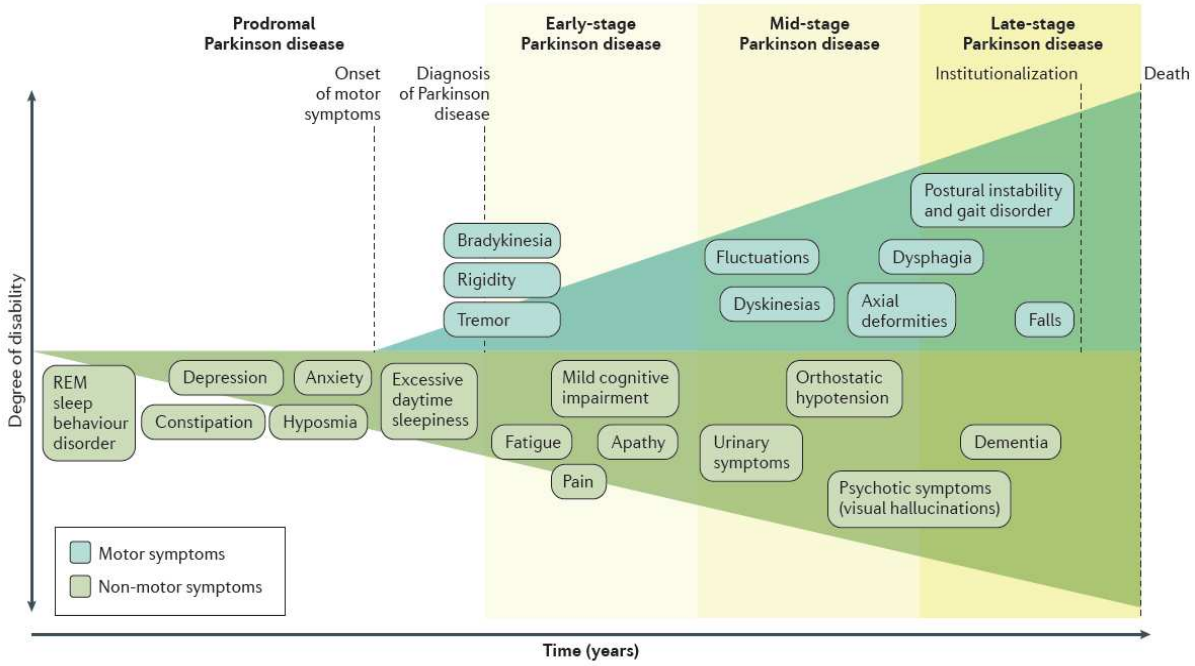


***Fig.1.1:*** **Symptomatology during the progression of Parkinson's disease.** Schematic representation of symptomatology progression during different stages of PD. The prodromal phase is characterized by specific non-motor symptoms, that can anticipate of decades the onset of the cardinal motor symptoms that lead to a diagnosis. Progressive disability is given by increasing severity of both motor and non-motor symptoms (from Poewe *et al.*, 2017 [2]).

The premotor phase can precede the onset of the cardinal motor symptoms by decades. It is becoming evident that, during this phase, pathogenic processes that cause PD have already begun. According to the Braak staging model, pathology might initiate in the enteric nervous system, or the olfactory bulb, affect the autonomic nervous system, and then spread throughout the brain, contributing to the view that PD is rather a multisystemic disorder [10]. Moreover, it is estimated that 40%-60% of dopaminergic neurons are lost and synaptic function is reduced by up to 80% at the moment of diagnosis, indicating that at this stage pathology is already quite advanced [11]. Therefore, an effort has been made in the last years to develop criteria to help standardize the diagnosis of PD during the prodromal phase, both for research and clinical purposes [12, 13]. Indeed, the prodromal period offers the possibility to study the early stages of the disease, for a better understanding of the pathology progression, and provides a potential temporal window during which disease-modifying therapies, once they will become available, might be administered to prevent, or delay the

development and progression of the disease. In this view, the need for specific and sensitive biomarkers that can keep track of disease progression is urgent. Neuroimaging markers have been proven helpful in predicting PD. These markers include abnormal tracer uptake of the presynaptic dopaminergic system with PET/SPECT (e.g., DaTSCAN), SNpc hyperechogenicity, and absence of the "swallow-tail sign" (due to the loss of nigrosome 1 in SNpc) at MRI. Additionally, in early PD patients, αSyn deposition has been found peripherally in the enteric nervous system, autonomic nerve fibers, submandibular gland, and skin biopsies. On the other hand, markers in biofluid (e.g., cerebrospinal fluid, blood) still require a standardization of methodologies and validation in large cohort studies, but they represent a promising alternative [9, 14, 15].

Unfortunately, a therapy capable of preventing or just slowing down the progression of PD is currently unavailable. Patients receive symptomatic treatments, aimed to alleviate motor and non-motor symptoms. The cardinal motor symptoms are due to the degeneration of dopaminergic neurons of SNpc that project to the striatum, which is mainly populated by medium spiny neurons, a major synaptic target of SNpc neurons. In physiological conditions, dopamine (DA) release in the striatum produces activation of the direct pathway and inhibition of the indirect pathway of the basal ganglia-thalamocortical motor circuit, with a net effect of facilitation of movement. Consequently, in PD conditions, the loss of DA unbalances the motor circuit, with a downstream inhibitory effect on the cerebral cortex, and therefore inhibition of movement that is manifested as akinesia/bradykinesia [16]. For this reason, the treatments are meant to restore DA tone in the brain. Preparations of levodopa, the DA precursor, are the main medication used soon after diagnosis and can be administered in combination with DA agonists and/or monoamine oxidase-B (MAO-B) inhibitors. Concurrently, nonpharmacological approaches, such as an appropriate exercise regimen and rehabilitative therapies (i.e., physical, occupational, and speech therapies), are highly recommended. However, long-term treatment with levodopa is associated with motor fluctuations, characterized by both off periods (due to medication wearing off) and dyskinesia. For some selected patients, deep brain stimulation of the subthalamic nucleus or globus pallidus internus may be advisable to improve motor symptoms [17]. At the moment, several therapeutic approaches aiming at disease modification are under evaluation. New therapeutic strategies range from pharmacological therapy, immunotherapy, gene therapy to

cell therapy and transplantation, and the targets under consideration are equally diversified: αSyn, LRRK2, β-glucocerebrosidase (GBA), neuroinflammation, lysosomal calcium, mitochondrial function, calcium homeostasis, insulin resistance, iron content [18].

## 1.2 Pathology and etiopathogenesis of Parkinson's disease

The histopathological hallmark of the disease is the presence of proteinaceous intraneuronal inclusions found *post-mortem* in patients' brains. These inclusions are called Lewy bodies and Lewy neurites, based on their localization in the cell body or neurites of neurons, respectively. Misfolded and aggregated αSyn is the main protein component of these inclusions and this has led to the classification of PD as a proteinopathy, specifically a synucleinopathy [19].

αSyn is a small (140 amino acids), intrinsically disordered protein, enriched in the brain, and predominantly localized at nerve terminals in association with synaptic vesicles. In physiological conditions, it is mainly monomeric and soluble, but pathological conditions trigger conformational changes that make αSyn prone to aggregate, first in small oligomers, then in fibrils with a β-sheet rich secondary structure, which are eventually incorporated in highly ordered structures such as Lewy bodies [20]. Besides, there is evidence that αSyn pathology can be transmitted cell-to-cell in a prion-like modality. Braak and colleagues developed a spatiotemporal staging of the pathology, based on autoptic observations in diseased brains. From these observations, the researchers concluded that the disease propagates in a time-dependent ascending manner between synaptically connected areas that exhibit a selective vulnerability toward the pathology. According to this staging, neuropathological lesions first appear in the olfactory bulb and/or in the dorsal motor nucleus of the vagus nerve, spreading through the lower brain stem and midbrain, and eventually reaching the neocortex [21]. In support of the intercellular transmission hypothesis, αSyn aggregates were found in grafted neurons in the brains of patients who received transplantation of human fetal-brain-derived cells as a therapy for PD, indicating a host-to-graft transmission [22, 23]. Additionally, the treatment with pathological seeds (synthetic preformed fibrils or pathological αSyn isolated from transgenic mice or human brain) in neuronal cultures and their stereotactic injection in several animal models has been found to induce αSyn pathology and neurodegeneration, sometimes far from the injection site

(reviewed in [24-26]). Nevertheless, the precise mechanism and conditions that trigger αSyn misfolding and seed aggregation are not clear. Uncertainty exists also on the mechanism/s of αSyn-induced neurotoxicity and, in this regard, small oligomers are believed to bear toxic properties, rather than large aggregates, that have been suggested to be benign or even protective.

However, the central role of αSyn in PD pathogenesis has been corroborated by the finding in families with PD of missense mutations and copy number variations (i.e., duplication and triplication) in its encoding gene *SNCA*, and genomic variants in the *SNCA* locus are considered a risk factor for idiopathic PD [27]. Before 1997, when the first mutation in *SNCA* has been discovered [28], PD was supposed to be exclusively the result of exposure to environmental factors, such as viruses (e.g. influenza) and neurotoxins (i.e. paraquat, rotenone, 1-methyl-4-phenyl-1,2,3,6-tetrahydropyridine (MPTP)). Since then, enormous progress has been achieved in uncovering genetic and genomic factors linked to the development of PD. Familial PD, once being even disbelieved, is now known to account for 10-15% of total cases and is due to rare monogenic mutations that display Mendelian inheritance. The genes, mutations of which are pathogenic for PD are listed in **Table 1.1**, together with gene functions and the associated clinical phenotype observed in patients [29].

| | **Gene (HGNC[1] Approved Name)** | **Alternative Gene Names** | **Inheritance** | **Pathogenicity** | **PD Phenotype** | **Function** |
|---|---|---|---|---|---|---|
| High penetrance | *SNCA* | *PARK1, PARK4, NCAP* | AD[2] | Pathogenic | Early-onset | Uncertain (encodes α-synuclein) |
| | *VPS35* | *PARK17, MEM3* | AD | Pathogenic | Typical | Retromer and endosomal trafficking |
| | *PINK1* | *PARK 6* | AR[3] | Pathogenic | Early-onset | Mitochondrial |
| | *PARK7* | *DJ-1* | AR | Pathogenic | Early-onset | |
| | *PRKN* | *PARK2, PARKIN* | AR | Pathogenic | Early-onset | |
| | *PLA2G6* | *PARK 14, IPLA2* | AR | Pathogenic | Early-onset, atypical parkinsonism; neuroaxonal dystrophy; neuro-degeneration associated with brain iron accumulation; Karak syndrome | Cell membrane |

| | | | | | | |
|---|---|---|---|---|---|---|
| | *ATP13A2* | *PARK9* | AR | Pathogenic | Early-onset, atypical parkinsonism; Kufor-Rakeb syndrome | Lysosomal |
| | *FBXO7* | *PARK15, FBX7* | AR | Pathogenic | Early-onset, atypical parkinsonism-pyramidal syndrome | Mitochondrial |
| | *POLG* | *POLG1, POLGA* | AD | Pathogenic | Variable phenotypic presentation. Early-onset, atypical parkinsonism, ataxia | Mitochondrial DNA maintenance |
| | *DNAJC6* | *PARK19, DJC6* | AR | Likely pathogenic | Early-onset, atypical parkinsonism; variable neurological defects | Synaptic vesicle formation and trafficking |
| | *DNAJC13* | *PARK21, RME8* | AD | Conflicting reports | Typical | |
| | *TMEM230* | *C20ORF30* | AD | Conflicting reports | Typical | |
| | *SYNJ1* | *PARK20* | AR | Pathogenic | Early-onset, atypical parkinsonism; variable neurological defects | |
| | *VPS13C* | *PARK23* | AR | Pathogenic | Early-onset | Mitochondrial |
| | *CHCHD2* | - | AD | Pathogenic | Typical | Uncertain |
| | *DCTN1* | - | AD | Pathogenic | Atypical parkinsonism, Perry syndrome | Microtubule |
| Variable penetrance | *LRRK2* | *PARK8, DARDARIN* | AD | Pathogenic | Typical | Lysosomal, mitochondrial, microtubule |
| | *GBA* | *GBA1* | AD | Pathogenic | Typical | Lysosomal |
| Associated with PD but unlikely to be pathogenic | *HTRA2* | - | AD | Uncertain/ likely benign | - | Mitochondrial |
| | *UCHL1* | *PARK5* | AD | Uncertain/ likely benign | - | Ubiquitin-proteasome |
| | *GIGYF2* | *PARK11* | AD | Uncertain/ likely benign | - | Uncertain |
| | *EIF4G1* | - | AD | Benign | - | mRNA translation |
| | *LRP10* | *LRP9* | AD | Uncertain | - | Uncertain |

[1]HGNC = HUGO Gene Nomenclature Committee; [2]AD = Autosomal Dominant; [3]AR = Autosomal Recessive

**Table 1.1: Summary of pathogenic genes associated with Parkinson's disease** (Modified from Day and Mullin, 2021 [29]).

Most of the cases enter the category of sporadic PD, for which the causes are unknown (for this reason it is defined as idiopathic). The idea that PD is a multifactorial disorder is now commonly accepted. Lifestyle, environmental factors and genetic background, together play a key role in the determination of the risk of developing the disease. An extensive review of lifestyle habits and environmental factors that act as risk modifiers for PD can be found in [30]. Moreover, a recent genome-wide association study (GWAS) revealed 90 common risk variants across 78 different genomic regions, 37 of which were novel loci [31]. This study helped to corroborate the view that genetic predisposition is a great component in determining the risk of developing PD, updating the contribution of common genetic variants up to 16-36% of the overall risk of developing PD.

Knowing the genetics underlying the disease represents a great opportunity to understand the pathogenic mechanisms that lead to the pathology. Indeed, the progress made in the fields of genetics and genomics of PD made possible the development of genetic disease models that boosted the understanding of the biological processes altered during pathogenesis. Moreover, several loci nominated by GWAS contain genes that are known to cause monogenic PD (such as *SNCA*, *LRRK2*, and *GBA1*), building a bridge between familial and sporadic disease. This is extremely important from the perspective of finding a unifying pathogenic mechanism that could be targeted by a universal therapeutic approach. On the other hand, it is getting clearer that PD is a highly heterogeneous disorder, that can be subdivided into different subtypes based on the clinical manifestation and neuropathology. The knowledge derived from the study of the genetic architecture of PD will help the stratification of patients, giving more power to future clinical trials and opening a window to precision medicine.

## 1.3 Molecular mechanisms deregulated in Parkinson's disease

The picture of PD etiopathogenesis is extremely complex. According to the multiple-hit hypothesis, a combination of diverse factors (genetic, environmental, etc.) is necessary to trigger the pathogenesis. This has made the finding of a unifying mechanism owning causality nexus to pathology development and neurodegeneration challenging. Genetic and toxin models allowed the identification of different, but possibly converging, molecular and cellular

mechanisms that are implicated in the pathogenesis of PD. The main functions associated with pathogenic genes are schematically included in **Table 1.1**. Protein homeostasis (alias proteostasis, with particular attention to αSyn), autophagy-lysosomal pathway (ALP), the ubiquitin-proteasome system (UPS), vesicular and membrane trafficking, mitochondrial function and quality control, metabolic and oxidative stress, calcium homeostasis, synaptic activity, neuroinflammation, axonal transport, and microtubule function are the main cellular processes that have been found altered in PD [2, 32, 33]. For brevity and pertinence to my research activity, I will specifically focus on the involvement of the ALP in PD.

## 1.4 Autophagy

The two main catabolic processes that allow the maintenance of cell homeostasis are the UPS and the ALP. Autophagy, whose etymological meaning is "self-eating", is the evolutionarily conserved process that ensures the degradation and the recycling of cytoplasmic constituents, including proteins, lipids, and dysfunctional or superfluous organelles. Three different types of ALP can be distinguished based on the modality used to direct substrates to lysosomes for degradation: microautophagy, chaperone-mediated autophagy (CMA), and macroautophagy (**Fig.1.2**).

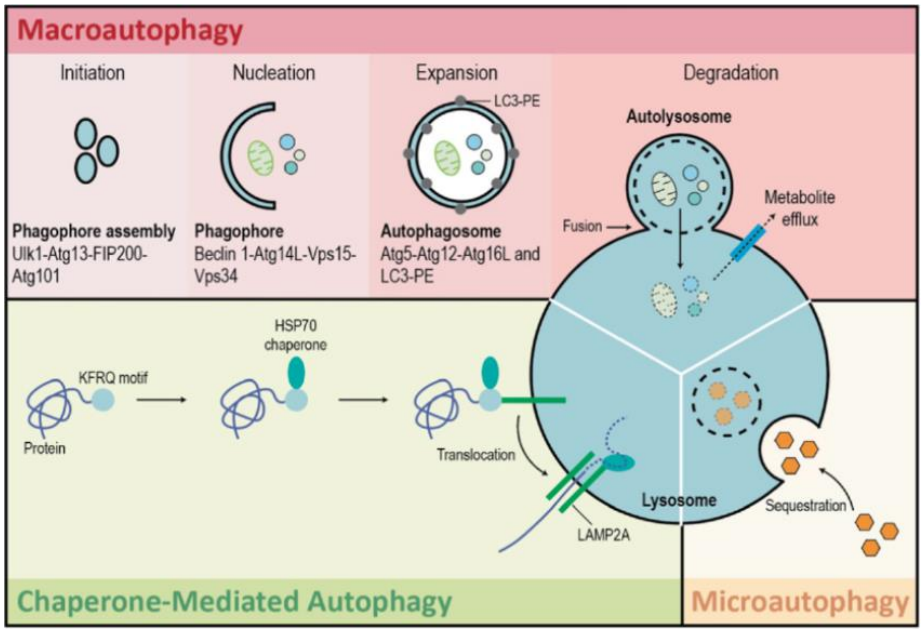

***Fig.1.2*: Schematic overview of different types of autophagy.** During macroautophagy , cellular component are engulfed in nascent autophagosome, which eventually fuses with lysosome, where degradation takes place. The formation of autophagosome can be subdivided in steps and it is regulated by the assembly of different molecular complexes. During chaperone-mediated autophagy, cytosolic proteins containing KFERQ-like motif are targeted to lysosomal degradation in chaperone mediated manner. During microautophagy, cellular components are directly uptaken inside the lysosome through an unknown mechanism (from Ho *et al.*, 2019 [34])

In microautophagy, the cytoplasmic components directly enter the lysosome or the late endosome through membrane invagination, but to date, the mechanism of this process is still poorly understood (reviewed in [35]).

CMA allows the selective degradation of proteins. The chaperone heat shock cognate 70 (HSC70) recognizes and binds a pentapeptide KFERQ-consensus motif on the cytosolic target protein (the CMA substrate) which is then unfolded and guided to the lysosomal membrane, where the chaperone-substrate complex binds the lysosome-associated membrane protein 2A (LAMP2A). This triggers its oligomerization, forming a channel that permits the translocation of the substrate inside the lysosome for degradation (reviewed in [36]).

Macroautophagy, the most studied and molecularly defined among the three autophagic processes, hereafter referred to as autophagy, involves the formation of the autophagosome, a double membrane vesicle that encloses cytosolic components, and its fusion with the lysosome where degradation takes place, after the merging with endocytic vesicles. Even though autophagy has been considered predominantly a bulk degradation process, a certain degree of selectivity is now emerging. Specific cargo recognition is mediated by selective autophagy receptors (e.g., p62/SQSTM1) that target the ubiquitinated substrate to the forming autophagosome by interacting with LC3 (microtubule-associated protein 1A/1B-light chain 3). Different types of selective autophagy can be distinguished based on the substrate that has to be degraded: aggrephagy, referring to protein aggregates; mitophagy, referring to mitochondria; lysophagy, referring to lysosomes; lipophagy, referring to lipid droplets; nucleophagy, referring to parts of the nucleus; xenophagy; referring to intracellular pathogens; etc. (reviewed in [37]).

Autophagy is a complex, multistep and extremely fine regulated process. A more detailed molecular understanding of the process was obtained with the discovery of the autophagy-related proteins (Atg). A subset of these proteins takes part in the autophagy "core" molecular machinery that coordinates autophagosome biogenesis. Atg proteins interact

to form different complexes that regulate the various steps of this process. The Atg1/Unc-51-like kinase (ULK) complex and the class IIII phosphatidylinositol 3-kinase (PI3K) complex are recruited to the phagophore assembly site and are indispensable for autophagy induction. Conversely, the two ubiquitin-like conjugation systems Atg12 and Atg8/LC3/GABARAP are required during elongation of the phagophore membrane, and a key step is the conjugation of the latter to phosphatidylethanolamine in the elongating membranes. Other proteins involved in the autophagosome formation are Atg2, Atg9, vacuole membrane protein 1, WD-repeat protein interacting with phosphoinositide (WIPI) and Double-FYVE-containing protein 1 (extensively reviewed in [38-40]). The phagophore membrane is then closed by the endosomal sorting complex required for transport (ESCRT) [41], and eventually, mature autophagosomes (which result from fusion with endocytic vesicles) fuses with the lysosome with the coordination of SNARE proteins (such as syntaxin 17 and SNAP29), small GTPases (such as Rab proteins), and other tethering proteins. The subcellular localization of both autophagosome and lysosome is critical for the fusion step, and it is determined by transport along microtubules [42, 43].

Constitutive levels of autophagy are necessary to maintain cell homeostasis, especially in post-mitotic and long-lived cells like neurons, where the constant quality control of cellular elements is necessary for neuron functionality and survival. On the other hand, autophagy can be induced by diverse stress stimuli and several signaling pathways participate in its regulation. Nutrient deprivation stimulates autophagy through the negative regulation of two signaling pathways, the mammalian target of rapamycin (mTOR) and Ras/cAMP-dependent-PKA pathways. Growth factors deprivation and decreased ATP/AMP ratio also induce autophagy through the inactivation of mTOR, although exploiting a different signaling cascades. Besides, growth factors and amino acids can regulate autophagy through the Ras-MAPK (mitogen activated protein kinase) pathway. A plethora of extra- and intracellular stresses are able to induce autophagy, from endoplasmic reticulum stress to accumulation of misfolded proteins, oxidative stress, and pathogen infection (reviewed in [44]). Calcium is a universal second messenger and specifically calcium released from the lysosomes is emerging as a key player in the regulation of ALP at different levels [45]. Interestingly, while mTOR-mediated phosphorylation of transcription factor EB (TFEB, a master transcriptional regulator of genes involved in autophagy and lysosomal biogenesis) prevents its nuclear translocation,

thus inhibiting autophagy [46], lysosomal calcium release from the channel TRPML1 (transient receptor potential mucolipin 1) induces TFEB dephosphorylation and consequent nuclear translocation, through the activation of calmodulin and the phosphatase calcineurin [47].

### *1.4.1 Autophagy in Parkinson's disease*

Given the physiological relevance of autophagy in sustaining cell survival, cell growth, differentiation and development, and its involvement in immunity [48], deregulation of the autophagic machinery is thought to underly many human diseases, such as, cancer, infectious and autoimmune diseases, diabetes and obesity, lysosomal storage disorders and neurodegeneration, and even the physiological process of aging [49]. The importance of autophagy for the nervous system has been pointed out with the generation of mice lacking Atg7, an E1-like enzyme indispensable for the conjugation systems, specifically in the nerve tissue. These mice exhibited motor disorders, neuronal loss, and premature death. Defective autophagy, but not UPS, led to the formation of ubiquitin-containing inclusion bodies in the neurons, pointing out the impairment of autophagy as a hot topic in the pathogenesis of neurodegenerative disorders [50]. In another seminal work, mice lacking Atg7 in dopaminergic neurons recapitulate some aspects of PD pathology including loss of dopaminergic neurons, motor dysfunctions, and Lewy body-like inclusions associated with aging, making a direct link between protein-quality control failure and PD pathogenesis. In particular, the authors observed that this conditional Atg7 knockout (KO) mice displayed age-related formation of p62 aggregates, containing mitochondria, in peripheral axons and dendrites, and that these aggregates were also positive for αSyn [51]. Besides, an increased number of autophagosomes [52] and reduced levels of lysosomal markers [53, 54] have been found in post-mortem PD brains. Moreover, a role in the ALP has been revealed for several e PD-associated proteins, such as LRRK2, αSyn, GBA, VPS35 (vacuolar protein sorting 35), ATP13A2, Parkin/PINK1/DJ-1 [55, 56]. Altogether, these observations suggest a causative role for autophagy dysfunctions at least in a proportion of PD cases.

As already mentioned, αSyn proteostasis is a key factor in PD pathogenesis. In normal conditions, αSyn is thought to be degraded mainly by CMA, with a minor contribution of macroautophagy. Indeed, αSyn contains the pentapeptide sequence $_{95}$VKKDQ$_{99}$ (variation of

the KFERQ motif) that targets αSyn to lysosomal degradation via CMA. Besides, αSyn mutants (A30P and A53T) have higher affinity for LAMP2A, but cannot be translocated inside lysosomes, competing with other CMA substrates and thus clogging CMA. In this situation compensatory activation of macroautophagy would take over the degradation of mutated and aggregated αSyn [57]. If on the one hand activation of macroautophagy has proven effective in enhancing the clearance of different forms of αSyn, on the other side αSyn itself can impair macroautophagy [58], thus creating a vicious cycle that leads to the disruption of proteostasis. Additionally, several studies demonstrated that autophagy impairment would result in increased secretion of αSyn via exosomes, amplifying cell-to-cell transmission and thus contributing to the spread of the pathology [59].

A proof of the involvement of lysosomal impairment in PD pathogenesis come from the finding of mutations in *GBA1* gene in PD patients [60]. Deficiency of GBA is the cause of Gaucher's disorder, a lysosomal storage disorder that can manifest with neurological symptoms. *GBA1* encodes for the β-glucocerebrosidase lysosomal enzyme that digests glycolipids within the lysosomal membrane. Several evidence links GBA deficiency/loss-of-function with promotion of αSyn accumulation. Conversely, αSyn might interfere with GBA trafficking associated to its decreased lysosomal activity. Moreover, the accumulation of the GBA substrate glucosylceramide, caused by GBA dysfunction, has been shown to stabilize αSyn oligomers [56, 61, 62].

VPS35 is part of the endosomal retromer complex which recycles the receptors that mediate the sorting of hydrolases to lysosome. Indeed, VPS35 deficiency and its PD-linked D620N mutation are associated to lysosomal and autophagy defects. LAMP2A reduction and αSyn accumulation were found in D620N-VPS35 mice. Moreover, VPS35 knockdown perturbed the maturation of cathepsin D with concomitant accumulation of αSyn in the lysosomes. VPS35 has been found to interact with parkin and with LRRK2-Rab29 pathway [63], suggesting a larger molecular picture of molecular interactions involving different PD-linked genes, sharing an effect on intracellular vesicle and organelle trafficking.

ATP13A2 encodes a lysosomal P-type ATPase involved in the selective transport of cations through the lysosomal membrane. Mutations in ATP13A2 have been found to increase lysosomal pH, increase lysosomal permeability, and impair maturation of cathepsins, eventually leading to autophagy defects and αSyn accumulation [64].

Upon damage and/or depolarization, mitochondria are directed to degradation via mitophagy. The PINK1/Parkin axis operates in the mitochondrial quality control, and PINK1-Parkin deficiency or loss-of-function lead to mitochondrial dysfunction. PINK1 is a ubiquitin kinase that accumulates on the outer membrane of mitochondria when they are depolarized. Then, PINK1 autophosphorylation recruits the E3-ubiquitin ligase Parkin, which is phosphorylated and activated by PINK1. Activated Parkin catalyzes ubiquitin transfer to mitochondrial proteins and recruit the UPS and autophagy machineries (mediated by the adaptor protein Optineurin) for mitochondrial clearance. Furthermore, DJ-1, a protein mainly involved in protection against oxidative stress, has been proposed to participate in mitochondrial quality control acting in a pathway parallel to PINK1/Parkin [65, 66].

LRRK2 is a large multi-domain protein involved in a wide range of cellular pathways, and a great consensus exist on its participation in ALP. I will discuss the role of this PD-related protein in ALP in larger detail the next section.

### *1.4.2 LRRK2 and autophagy*

Among PD genes, LRRK2 mutations represent the most frequent cause of familial PD and major risk factors for sporadic PD. The G2019S missense mutation is the most common one with a frequency that can reach 42% of familial cases in some ethnic groups [67]. Moreover, the majority of LRRK2 PD patients develop late-onset PD, clinically and neuropathologically identical to idiopathic PD. But it is worth to mention that LRRK2-PD is associated to incomplete penetrance Lewy pathology is limited to ~50% of manifesting carriers [68].

LRRK2 is a large (~280 kDa) multidomain protein containing a GTPase-kinase catalytic core surrounded by protein-protein interaction domains. From the N-terminal to the C-terminal, LRRK2 comprises the following domains: an armadillo, an ankyrin, a leucine-rich repeat, a tandem Ras of complex (ROC, with GTPase activity) and C-terminal of Roc (COR), a serine/threonine kinase, and a WD40. All PD pathogenic mutations reside in the catalytic core: N1437H, R1441C/G/H, R1628P, and Y1669C in the ROC-COR domain; I2012T, G2019S, and I2020T in the kinase domain [69]. An increased LRRK2 kinase activity has been reported for pathogenic mutations, resulting in enhanced LRRK2 autophosphorylation at Ser1292 and enhanced phosphorylation of validated LRRK2

substrates (mainly Rab GTPases) [70-72]. Mutations in the kinase domain have a direct effect on the kinase activity, while mutations in the ROC-COR domain are thought to act by altering the capacity of binding and hydrolysis of GTP, which has been shown determinant in modulating the activity of the kinase domain [73, 74]. Importantly, enhanced LRRK2 kinase activity has been found also in idiopathic PD, in the absence of mutations [75]. Besides, some studies have proven the protective effect of LRRK2 kinase inhibition in cell and animal models [76-79], making LRRK2 pharmacological inhibition a promising and highly pursued therapeutic strategy for both familial and sporadic PD. Indeed, Denali Therapeutics has developed two compounds that are undergoing clinical trials (DNL201 [80] and DNL151-BIIB122 [ClinicalTrials.gov]). However, some concerns arose regarding the strategy of inhibiting LRRK2. LRRK2 expression is reported in the kidneys, lungs, and cells of the immune system. Critically, peripheral expression levels are significantly higher than in the brain. Pharmacologically, the systemic administration of LRRK2 inhibitors in primates led to a vacuolated phenotype in lung cells (type-II pneumocytes). The same phenotype has been reported also in LRRK2 KO mice and rats, which also display kidney and liver pathology. Besides, in cell assays pharmacological LRRK2 kinase inhibition of the wild-type (WT) protein has been found to show effects similar to pathogenic mutants [81, 82]. This is thought to be due to a mechanism that leads to LRRK2 protein instability. Phosphorylation at different residues (Ser910, Ser935, Ser937, and Ser955) is essential for the binding to 14-3-3 proteins, which in turns controls LRRK2 protein stability and localization [83, 84]. LRRK2 inhibitors, as well as LRRK2 mutants, cause dephosphorylation at Ser910/Ser935, and this is associated to LRRK2 re-localization and reduction of protein levels [85]. These data suggest that LRRK2 function is important in cellular homeostasis and cannot be abolished completely, which is consistent with its multi domain, and thus multifunctional, biochemical nature.

The high complexity of LRRK2 protein structure, of its enzymatic function regulation, and of the molecular network in which it is implicated have made it hard to dissect both physiological and pathological roles of LRRK2, and a lot of controversies and missing gaps exist. Despite this, research efforts have highlighted the involvement of LRRK2 in a plethora of cellular processes including synaptic transmission, vesicle trafficking, mitochondrial function, immune response, and cytoskeletal dynamics. Moreover, given the central role that the ALP plays in PD pathogenesis (as discussed in the previous section), there is a great

interest in the involvement of LRRK2 in this process, and accumulating evidence strengthen its role in ALP [86-88]. Different experimental settings have been used to study LRRK2 function: from cellular and animal models generated through overexpression of both WT and mutant LRRK2, knock-down/KO, and kinase inhibition (either pharmacological or genetic, with the introduction of kinase-dead variants), to patient-derived cell cultures. Unfortunately, the use of different model systems in addition to different ways to induce/inhibit autophagy and the modality of autophagic flux investigation have led to discordant reports. Thus, even though the involvement of LRRK2 in autophagy is indisputable, a clear view on the mechanism/s operated by LRRK2 in the regulation of this process and the net direction of such regulation is still lacking [86, 88].

LRRK2 KO mice provided a strong link between LRRK2 and its physiological function in regulating ALP. Accumulation of autophagic markers (LC3II and p62), and lysosomal abnormalities have been found in the kidneys of these animals in an age-dependent manner [89-91]. However, there were no evidence of ALP alterations in the brain. The generation of double LRRK2-LRRK1 KO mice revealed a possible compensatory effect driven by LRRK1 (i.e., functional homolog of LRRK2) given that these mice display age-dependent increased levels of p62, LC3II and accumulation of autophagic vesicles in the brain [92]. Data from LRRK2 KO primary cultures show increased autophagic flux [93-95]. On the other side, the same effect on autophagic flux has been observed in other studies when LRRK2 is overexpressed [96, 97], significantly muddying the waters.

Pharmacological LRRK2 kinase inhibition also produced contradictory results, with some studies reporting an enhancement [94, 98] while others showing an inhibitory effect [99, 100] on the autophagic flux, but altogether demonstrating the role of kinase activity in the regulation of ALP.

Concerning LRRK2 mutations, animal models bearing G2019S or R1441C/G mutations display signs of reduced autophagic flux [95, 101-104]. Besides, an age-dependent impairment of CMA has been observed in R1441G knock-in (KI) animals, associated to lysosomal impairment and reduced clearance of αSyn. CMA was previously found to be inhibited also in the context of G2019S LRRK2 overexpression, and macroautophagy was found to be increased as a putative compensatory mechanism [97]. Some evidence highlights that G2019S LRRK2 produces a toxic enhancement of autophagy induction, elicited by

activation of MAPK/ERK pathway [105, 106]. Besides, LRRK2 overexpression has been shown to induce autophagosome formation via the activation of calcium-dependent protein kinase kinase-β (CaMKK-β)/adenosine monophosphate-activated protein kinase (AMPK) pathway, involving activation of nicotinic acid adenine dinucleotide phosphate (NAADP)-sensitive two-pore channel 2 (TPC2) located on the membrane of the lysosomes. A specific antagonist of NAADP, Ned-19, was able to revert the increase in autophagosome number and lysosomal alkalinization elicited by LRRK2 overexpression [96]. In line with this work, G2019S LRRK2 patient-derived fibroblasts displayed lysosomal morphological defects and alkalinization, that were restored by TPC2 inhibition [107]. Lysosomal alkalinization and dysfunction has also been found in association with R1441C LRRK2, caused by the disruption of the interaction with the V-type $H^+$ ATPase proton pump and its consequent downregulation and mislocalization [95]. A schematic overview of molecular pathways through which LRRK2 has been proposed to modulate autophagy is represented in **Fig.1.3**.

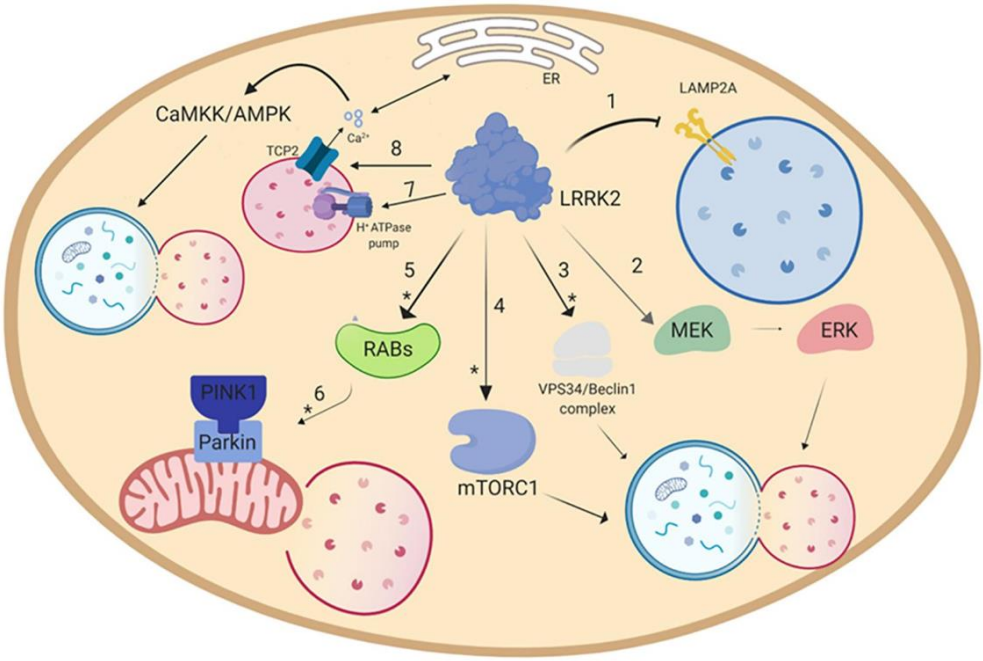


**Fig.1.3*:* Proposed molecular pathways through which LRRK2 modulates autophagy.** CMA is blocked by overexpressed/mutant LRRK2 (1). LRRK2-mediated autophagy modulation can be achieved via MEK/ERK pathway (2), activation of VPS34/Beclin-1 complex (3), mTOR pathway (4), calcium-sensitive CaMKK/AMPK pathway (8). LRRK2 modulates lysosomal pH via $H^+$-ATPase pump (7) and calcium efflux (8). LRRK2/RABs axis can modulate autophagy at diverse levels (5) and even PINK1/Parkin-mediated mitophagy (6). Asterisks (*) indicate pathways modulated by pharmacological LRRK2 kinase inhibition (From Albanese *et al.*, 2019 [88]).

Some members of the Rab family of GTPases are well validated LRRK2 substrates, and they are involved in vesicle trafficking and regulation of ALP. It has been shown that LRRK2 can be recruited to membranes and activated through the interaction with RAB7L1 (or RAB29, a PD-associated risk factor) [108-111]. Interestingly, Eguchi and coworkers found that LRRK2 is recruited by RAB29 to the membrane of stressed lysosomes, leading to recruitment and phosphorylation of RAB10 and RAB8 with consequent regulation of lysosomal homeostasis [112]. LRRK2 recruitment and phosphorylation of RAB8A on damaged/dysfunctional lysosomes mediated lysosomal membrane repair [113]. Besides, presence of active LRRK2 on lysosomal membrane upon lysosomal damage recruits and phosphorylates RAB10 and RAB35. This is necessary for recruitment of the motor adaptor protein JIP4, that contributes to the formation of a lysosomal tubule which is then sorted into vesicles (a process the authors termed LYTL, LYsosomal Tubulation/sorting driven by LRRK2) [69, 114]. These data suggest that LRRK2, in concert with its downstream target RABs, might operate in maintaining lysosomal homeostasis. On the other hand, pathological conditions (e.g. variations in *LRRK2* and/or *RAB7L1* genes, membrane damage or other stress stimuli) might perturb this function, leading to lysosomal defects and underlying PD-pathogenesis. However, precise molecular mechanisms that link LRRK2 to ALP defects in PD remain largely obscure, as well as the relevance of the above-mentioned pathways in PD pathogenesis.

## 1.5 Rit2 in Parkinson's disease

*RIT2* (Ras-like without CAAX 2) encodes the small (~25kDa) GTPase Rit2 (a.k.a. Rin, i.e., Ras-like expressed in neurons) and together with its close homolog *RIT1* (encoding Rit1, a.k.a. Rit, i.e. Ras-like expressed in many tissue) belongs to a subfamily of Ras-related proteins. Rit1 is expressed ubiquitously, while Rit2 expression is restricted to the brain with specific expression pattern within certain subsets of neurons. These GTPases have been shown to be associated to the plasma membrane, despite the lack of the C-terminal sequence target of isoprenylation [115], a modification generally required for membrane binding of Ras proteins. Similarly to all Ras-like proteins, Rit2 and Rit1 are able to bind and hydrolyze GTP, suggesting that they can act as molecular switches. Indeed, Ras-related GTPases can cycle between active GTP-bound and inactive GDP-bound structural state, depending on their

intrinsic rate of GTP hydrolysis and on the regulation operated by GTPase activating proteins (GAPs) guanine nucleotide exchanging factors (GEFs) and GDP dissociation inhibitors (GDIs). As a consequence of this property, Ras-like proteins are involved in signal transduction inside a variety of cellular processes. Intriguingly, Rit2 and Rit1 possess a different G2 effector protein binding domain (one of the five G domain that are generally highly conserved among Ras-related proteins) and a high intrinsic rate of GTP hydrolysis. Moreover, they have a different pattern of interaction with Ras effectors, indicating their differential involvement in signaling pathways and cellular processes [116]. It has been observed that Rit2 interacts with calmodulin in a calcium-dependent manner, suggesting its involvement in calcium signaling pathways, which are essential in the regulation of neuronal processes [115].

Both Rit2 and Rit1 have been found to be key players in NGF-dependent neuritogenesis and the signaling cascades in which they participate require activation of ERK- and p38-MAPK. Moreover, Rit2 and Rit1 are involved in PACAP38-stimulated neurite outgrowth, but with two different signaling cascades. Rit2 can also induce neurite outgrowth in calmodulin- or Rac/Cdc42-dependent signaling pathway. However, these evidence were obtained in different cell lines with little neuronal identity, and a strong indication on the neuronal relevance of Rit2 involvement in these signaling cascades is still lacking. On the other hand, Rit1 activation has been associated to proliferative pathways, promotion of cell survival, and transformation (reviewed in [117]). In a drug screening, *RIT2* KO SH-SY5Y cells display ERK hyperphosphorylation, that can be counteracted by dabrafenib, a B-Raf inhibitor approved for melanoma treatment, eliciting cell survival. The authors proposed dabrafenib as a drug for PD treatment, also given its neuroprotective effect in MPTP treated mice [118]. The generation of Rit1 KO and transgenic mice helped increase our knowledge on its physiological role in the promotion of cell survival and resistance to oxidative stress, through activation of p38-Akt cascade [119-121].

Variations in *RIT2* gene have been associated to different neurological disorders, such as schizophrenia (gene deletions [122], 5 instead of 11 GA short tandem repeat in the promoter associated to reduced gene expression [123], rs16976358 polymorphism [124]), autism spectrum disorder (rs16976358 polymorphism [124-126]) and PD. One polymorphism, namely rs12456492G/A, in the *RIT2* gene locus has been associated to increased PD

susceptibility in different GWAS [31, 127-134], with one study reporting an increased but not significant association between this variant and PD in a Taiwanese population [135] and successively belied [136]. This polymorphism reside in an intronic region, upstream of the promoter, and it has been proposed that it might influence gene expression either by affecting splicing or by creating a CpG site that, if hypo-methylated, would reduce gene expression [134]. Accordingly, two studies reported reduced *RIT2* expression in PD conditions. In the rat brain *RIT2* was found to be enriched in dopaminergic neurons of SNpc and ventral tegmental area. Treating rats with 6-hydroxydopamine, used to model the nigral degeneration occurring in PD, Zhou and colleagues found downregulation of *RIT2* with respect to non-treated rats [137]. Additionally, in post-mortem human brain, 36% reduction in *RIT2* expression was found in SNpc of PD patients with respect to neurologically healthy controls [138]. Altogether, these data suggest a role for *RIT2* in determining susceptibility towards DA-related neurological disorders. Reinforcing the significant role of *RIT2* in the regulation of the dopaminergic system, an interaction at the level of the plasma membrane between Rit2 and the DA transporter (DAT) has been reported. DAT is responsible for the reuptake of DA in the synaptic space, thus controlling DA signaling termination. Importantly, *RIT2* silencing attenuates PKC-mediated DAT internalization both in cell line [139] and *in vivo* (specifically in dopaminergic terminals of ventral striatum) [140]. The authors proposed that DAT is stabilized at cell membrane by a PKC-sensitive endocytic brake. This brake requires Rit2 to be released upon PKC-activation, and then, Rit2 dissociates from the internalizing DAT [140]. The same group also revealed a sex-specific role of Rit2 in response to cocaine. Conditional, inducible *RIT2* knockdown in dopaminergic neurons produced an anxiolytic effect in both male and female mice. Conversely, *RIT2* silencing in males increased cocaine-induced locomotor activity, whereas in females this response was reduced. This might be a consequence of differential stimulation on the two types of striatal medium spiny neurons. They also measured increased DA uptake upon *RIT2* knockdown, consistent with DAT internalization inhibition [141]. These results were recapitulated also in *Drosophila melanogaster*. The ortholog of Rit2, Ric, interacts with dDAT and constitutively active Ric stabilizes dDAT at the membrane and stimulates its function. Moreover, active Ric leads to reduced sleep consolidation and increased amphetamine sensitivity in a DAT-dependent manner [142]. Further corroborating the specific function of Rit2 in dopaminergic neurons,

very recently, the group of Zhenyu Yue, with a single-cell transcriptomic approach, has reported the finding of molecularly distinct subtypes of dopaminergic neurons in the SNpc of aged human brain, all of them degenerating in PD. They discovered one neuronal subtype, positive for neuromelanin (i.e., a pigment that is formed when free cytosolic DA oxidizes and polymerizes), that is highly enriched in *RIT2* expression. Intriguingly, this subtype, differently from the others, does not express/have reduced expression of tyrosine hydroxylase (TH, i.e., the enzyme necessary for the synthesis of levodopa) and other DA markers in healthy aged brains. Moreover, *RIT2* is downregulated in this neuronal subtype in PD patients' brains. Even though the physiological role of Rit2-enriched dopaminergic neurons is still to be determined, overall, the evidence reported here support a role for Rit2 in regulating dopaminergic neuron physiology, and alterations of its expression or activity may underlie susceptibility towards pathological alterations [143].

# 2. Results and Discussion

## 2.1 G2019S LRRK2 promotes formation of αSyn inclusions inhibiting autolysosome formation and function in a kinase-dependent manner

In 2020 we published the results obtained on SH-SY5Y neuroblastoma cells stably overexpressing G2019S LRRK2. I will give an overview of the study, to which I contributed, that will serve as an introduction to the main work I carried out during my doctoral studies. The integral previous work can be found at https://doi.org/10.1038/s41420-020-0279-y [144].

G2019S LRRK2 expressing cells, with respect to naïve SH-SY5Y and WT LRRK2 cells, displayed overactive LRRK2 kinase activity and intracellular inclusions, positive for pSer129-αSyn, the pathological form present in PD patients' brain. Moreover, by immunofluorescence, we found accumulation of puncta positive for LC3, used to stain autophagosomes. Since elevation in autophagosome number could be due to either upstream enhanced autophagy activation or downstream defects in lysosomal degradation (or even a combination), we assessed the autophagic flux to understand which step could be affected. First, by Western blotting we measured conversion of LC3-I to LC3-II upon chloroquine (CQ) treatment, which inhibits autophagosome-lysosome fusion [145]. We also used the GFP-LC3-mCherry tandem reporter [146] (where GFP fluorescence is quenched in the acidic pH of lysosomes) to measure the relative abundance of autophagosome and autolysosomes, thus following autophagosome maturation. With both approaches we did not observe any changes between cell lines, indicating that expression of WT or G2019S LRRK2 does not affect autophagy initiation nor the overall autophagic flux. Accumulation of $LC3^{+}$-autophagosomes without an increase in their production suggested defects in lysosome functions. Therefore, we stained lysosomes with Lysotracker Deep Red, a lysosomotropic dye, to evaluate lysosomal morphology. Both WT and G2019S LRRK2 overexpressing cells displayed fewer but larger lysosomes, an indication of clustered (and likely malfunctional) lysosomes. Consequently, we used the DQ-Red-BSA assay to investigate lysosomal proteolytic activity. DQ-Red-BSA is endocytosed and trafficked to lysosomes where it is degraded by proteases with consequent release of fluorescence[147]. Surprisingly, WT LRRK2 cells showed increased number of DQ-Red-BSA puncta with respect to naïve SH-SY5Y cells, but such enhancement was absent in G2019S LRRK2 expressing cells. This suggested that the

mutation may hamper lysosomal activity. We then asked whether the phenotypes we observed in G2019S LRRK2 cells depended on LRRK2 kinase activity, since this mutation strongly overactivates LRRK2 *in vitro* and *in vivo* [76, 148]. We verified that the treatment with the LRRK2 kinase inhibitor PF-06447475 (PF-475) was effective in reducing LRRK2 autophosphorylation at Ser1292. Importantly, we found that pharmacological LRRK2 kinase inhibition reduced accumulation of pS129- αSyn, diminished $LC3^{+}$-autophagosome number without an effect on autophagy initiation, promoted autophagosome-lysosome fusion, rescued lysosome morphology and proteolytic activity. Moreover, blocking autophagosome-lysosome fusion with CQ before the treatment with PF-475 abolished the LRRK2 kinase inhibition protective effect against accumulation of pS129-αSyn. Concluding, these results further corroborated that: 1) PF-475 exerted its protective effect promoting the step of autophagosome-lysosome fusion and 2) LRRK2-mediated defects in this step were directly correlated to pS129-αSyn accumulation.

## 2.2 *RIT2* expression is downregulated in recombinant LRRK2 cells

Genomic variations in *RIT2* have been associated to increased risk of developing PD [31]. The PD-related polymorphism is located in an intronic region, upstream of the promoter, and it has been proposed to alter gene expression [134]. Besides, *RIT2* expression was downregulated in one animal model of PD [137] and in SNpc of idiopathic PD patients [138, 143]. Given our interest in discovering a functional link between LRRK2 and other PD-linked genes, with the ultimate aim of reconstructing molecular pathways of pathogenic relevance, we investigated *RIT2* expression in our SH-SY5Y cell lines stably overexpressing WT and G2019S LRRK2. To this purpose, we used droplet digital PCR (ddPCR) that allows absolute quantification of mRNA and enables detection of extremely low abundance targets, which is the case for *RIT2* in SH-SY5Y cells [140]. According to the reports of *RIT2* downregulation in PD models, we found reduced levels of *RIT2* mRNA in both WT and G2019S LRRK2 overexpressing cells (**Fig.2.1**).

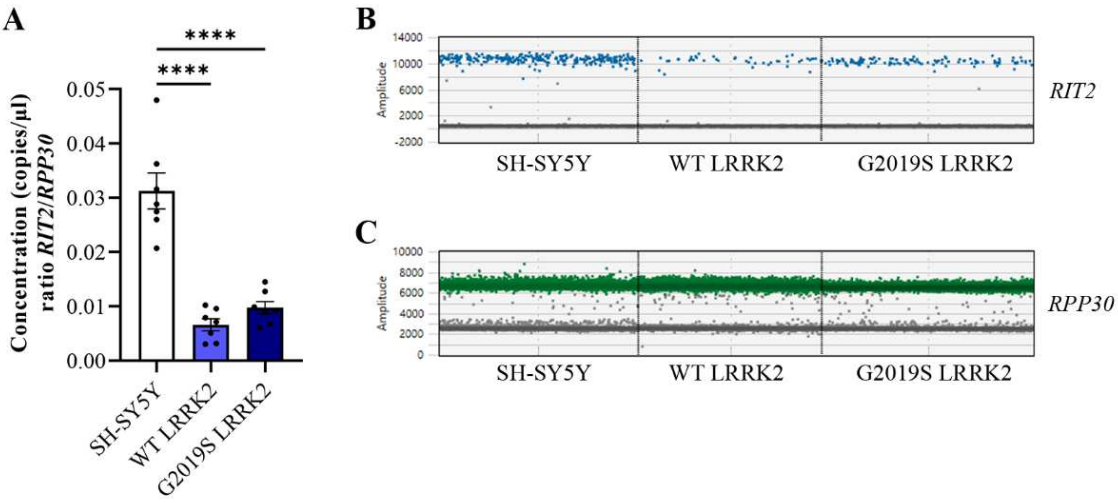


**Fig.2.1**: ***RIT2* mRNA expression is reduced in WT and G2019S LRRK2 cells**. **A**. Graphical representation of the ratio between *RIT2* and *RPP30* mRNA concentrations. Data are shown as mean ± SEM (n=7); ****p<0.0001 one-way ANOVA followed by Bonferroni's post-hoc test. **B**, **C** Example of 1D amplitude view of ddPCR reaction for *RIT2* and *RPP30*.

In a manuscript that our group has recently submitted to revision, we also show that *RIT2* expression is reduced in laser-capture microdissected nigral dopaminergic neurons of PD patients, in dopaminergic neurons of mice treated with viral-induced A53T αSyn overexpression, in iPSC-derived dopaminergic neurons obtained from a carrier of the A53T αSyn mutation, and in our SK-N-SH neuroblastoma cell line overexpressing A53T αSyn (***Appendix I***). We speculated that LRRK2 hyperactivation, found also in idiopathic PD patients [75], could affect *RIT2* expression. Therefore, we treated G2019S LRRK2 cell with PF-475, but we did not detect any changes. This implicates that LRRK2 kinase activity does not impact directly on *RIT2* expression, or alternatively the treatment time was not long enough to induce changes in gene transcription (***Appendix I***). Although the mechanism/s leading to *RIT2* downregulation are still unknown, reduced levels of *RIT2* expression in PD appears consistent across cellular and animal models, and patient-derived tissue samples.

## 2.3 Rit2 overexpression in G2019S LRRK2 cells rescues lysosomal defects

ALP alterations are an underlying theme in PD and are thought to lead to altered αSyn proteostasis [149]. Besides, in G2019S LRRK2 cells we detected ALP defects and accumulation of pSer129-αSyn, which were modulated by LRRK2 kinase activity [144]. *RIT2* downregulation in PD models constitutes the rationale to explore the effects of restoring its

expression. Therefore, we transiently overexpressed Rit2 in G2019S LRRK2 cells (**Fig.2.2**) and we investigated different steps of ALP.

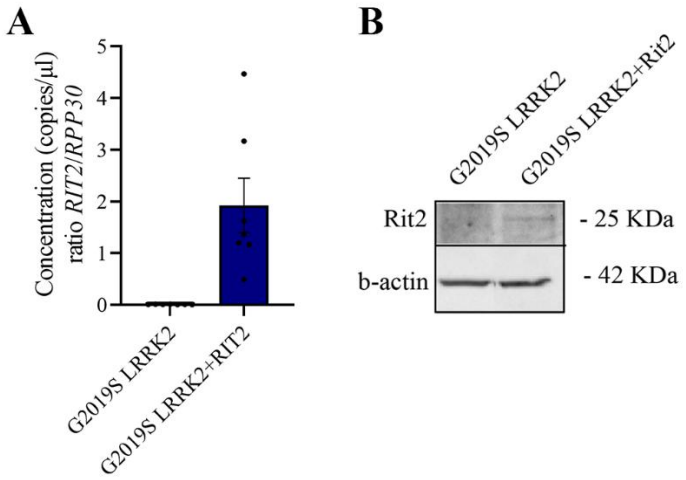


**Fig.2.2**: **Rit2 overexpression in G2019S LRRK2 cells. A** Graphical representation of the ratio between *RIT2* and *RPP30* mRNA concentrations. Data are shown as mean ± SEM (n=7). **B** Representative Western blot image of Rit2 in G2019S LRRK2 and G2019S LRRK2+Rit2 cells.

First of all, we assessed the autophagic flux, measuring the turnover of autophagosomes upon CQ treatment. We had previously reported that G2019S LRRK2 cells did not display alterations in the autophagic flux with respect to naïve cells [144]. Here, we used a complementary approach, i.e. the Cyto-ID assay, that is designed to specifically accumulate inside autophagosomes and autolysosomes, allowing fluorescent labelling of these autophagic vesicles (**Fig.2.3A**). With this approach, we were able to observe an increase in the number of autophagic vesicles upon CQ treatment, as expected (**Fig.2.3B-C**). Intriguingly, we detected significantly less Cyto-ID-positive vesicles in G2019S LRRK2 cells with respect to naïve SH-SY5Y cells upon CQ treatment (**Fig.2.3B**). This result would suggest an impairment of autophagic flux, possibly a delayed autophagy initiation, in G2019S LRRK2 cells. This result differs from what we observed in the previous work, possibly due to increased sensitivity of Cyto-ID assay with respect to quantification of LC3B protein levels by Western blotting and overexpression of the (exogenous) GFP-LC3-mCherry tandem reporter. Moreover, we examined the amount of autophagosomes upon Rit2 overexpression in G2019S LRRK2 cells, and we did not observe any change (**Fig.2.3C**), suggesting that Rit2 does not influence autophagy initiation in this cell model. We also performed Western blotting for LC3B (**Fig.2.3D)** and we found that Rit2 overexpression in G2019S LRRK2 cells

did not affect either the LC3B-II/LC3B-I ratio nor the levels of LC3B-II, indicating no alterations in the autophagosome turnover (**Fig.2.3E-F**). Moreover, Rit2 overexpression did not produce differences in LC3B in G2019S LRRK2 cells upon CQ treatment either (**Fig.2.3E-F**), further corroborating that Rit2 might not have a specific role in autophagy initiation.

**Fig.2.3: Rit2 overexpression does not impact on the autophagic flux. A** Representative images of Cyto-ID staining for autophagic vesicles in SH-SY5Y, G2019S LRRK2 and G2019S LRRK2+Rit2 cells upon CQ treatment (100 μM for 3h). **B-C** Quantification of Cyto-ID positive puncta per cell. Data are shown as mean ± SEM (n=4). ****p<0.0001 non-parametric two-way ANOVA followed by Bonferroni's post-hoc test. **D** Representative Western blot of LC3B in G2019S LRRK2 and G2019S LRRK2+Rit2 cells upon CQ treatment (100 μM for 3h). **E-F** Graphical representation of LC3B-II/LC3B-I ratio and LC3II normalized on b-actin. Data are shown as mean ± SEM (n=3). No differences were detected by two-way ANOVA followed by Bonferroni's post-hoc test.

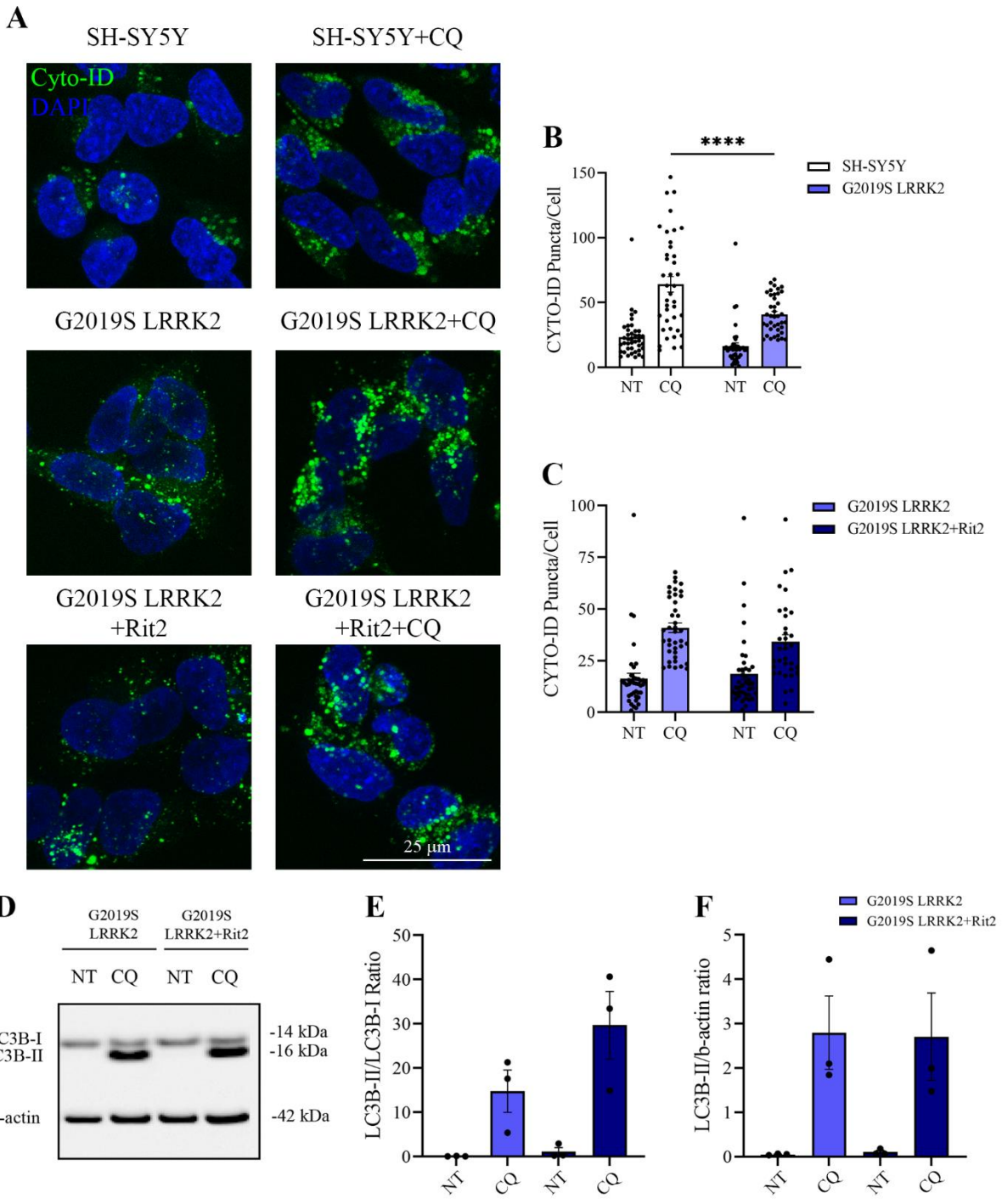
A
SH-SY5Y
SH-SY5Y+CQ
Cyto-ID
DAPI
G2019S LRRK2
G2019S LRRK2+CQ
G2019S LRRK2
+Rit2
G2019S LRRK2
+Rit2+CQ
25 µm
B
****
SH-SY5Y
G2019S LRRK2
CYTO-ID Puncta/Cell
150
100
50
0
NT
CQ
NT
CQ
C
G2019S LRRK2
G2019S LRRK2+Rit2
CYTO-ID Puncta/Cell
100
75
50
25
0
NT
CQ
NT
CQ
D
G2019S LRRK2
G2019S LRRK2+Rit2
NT
CQ
NT
CQ
LC3B-I
LC3B-II
b-actin
-14 kDa
-16 kDa
-42 kDa
E
LC3B-II/LC3B-I Ratio
50
40
30
20
10
0
NT
CQ
NT
CQ
F
G2019S LRRK2
G2019S LRRK2+Rit2
LC3B-II/b-actin ratio
5
4
3
2
1
0
NT
CQ
NT
CQ

We previously reported that G2019S LRRK2 impaired lysosomal functionality in a kinase dependent manner [144]. Thus, we investigated whether Rit2 overexpression could restore lysosomal defects in G2019S LRRK2 cells. Therefore, we first looked at lysosomal morphology using Lysotracker staining, a dye that specifically accumulates inside acidic organelles, such as the lysosomes (**Fig.2.4A**). Interestingly, we observed that Rit2 overexpression increased the number of lysosomes (**Fig.2.4B**) and decreased their diameter (**Fig.2.4C**), thus rescuing the morphological defects we observed in G2019S LRRK2 cells. Lysosomal morphological defects could be a sign of dysfunctional activity, and we have already observed proteolytic deficit in G2019S LRRK2 cells [144]. Hence, we assessed lysosomal proteolytic activity upon Rit2 overexpression using the DQ-Red-BSA assay (**Fig.2.4D**). We quantified the fluorescence signal produced by the proteolysis of DQ-Red-BSA molecules, and we found that Rit2 overexpression in G2019S LRRK2 increased the number of fluorescent spots, indicating enhancement of lysosomal proteolytic activity and/or increase in number of active lysosomes (**Fig.2.4E**).

We also tested whether Rit2 overexpression could have an effect on ALP in cell overexpressing WT LRRK2. As previously reported, these cells did not display alteration of the autophagic flux, albeit showing lysosomal morphological defects similar to G2019S LRRK2 cells. However, their lysosomal activity was significantly increased with respect to G2019 LRRK2 cells [144]. First of all, we ensured that Rit2 was successfully overexpressed in WT LRRK2 cells by ddPCR (**Fig2.5A**) and Western blotting (**Fig.2.5B**). Similar to what found in G2019S LRRK2 cells, Rit2 overexpression did not alter autophagosome turnover in WT LRRK2 cells, assessed by Cyto-ID staining (**Fig.2.5C-D**). Interestingly, assessing lysosomal morphology by Lysotracker staining revealed that Rit2 overexpression in WT LRRK2 cells reduced lysosomal diameter without significantly affecting lysosome number (**Fig.2.5E-G**). Besides, lysosomal proteolytic activity, assessed by DQ-Red-BSA assay, was not changed by Rit2 overexpression in WT LRRK2 cells (**Fig.2.5H-I**). We can speculate that the slight alterations in lysosomal morphology produced by overexpression of WT LRRK2 does not translate in alterations to lysosomal functionality, possibly through the activation of a hypothetical compensatory mechanism. Interestingly, restoration of Rit2 expression in both WT and G2019S LRRK2 cell lines rescued lysosome morphology, suggesting that Rit2 could have an overarching role in the regulation of lysosome biology. Importantly, Rit2 seems to

have a specific effect on G2019S LRRK2-mediated lysosomal activity defects, phenocopying pharmacological LRRK2 kinase inhibition [144], indicating that it may act in a disease-relevant pathway shared with LRRK2.

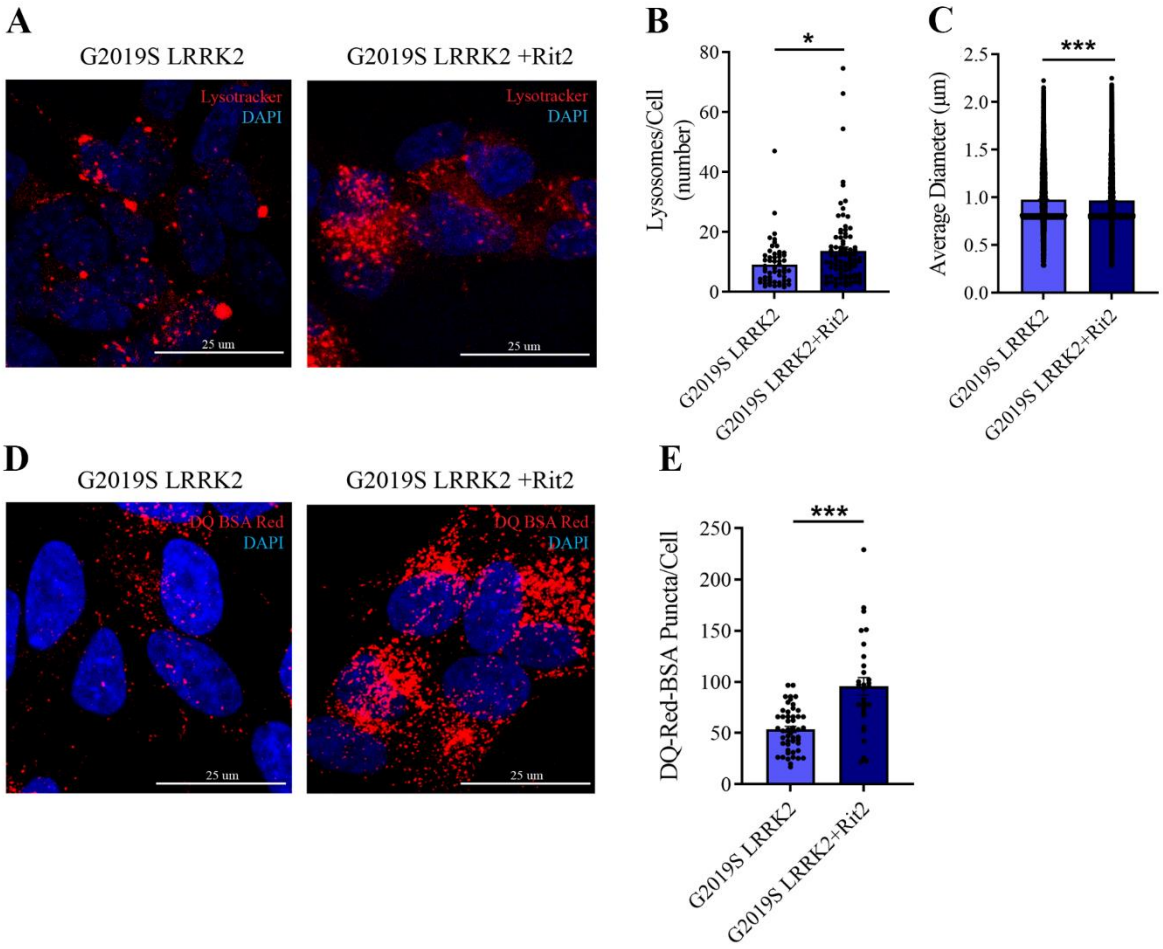


**Fig.2.4: Rit2 overexpression rescues lysosomal morphology and functionality in G2019S LRRK2 cells. A** Representative images of Lysotracker Deep Red staining in G2019S LRRK2 and G2019S LRRK2+Rit2 cells. **B** Quantification of lysosomes number per cell and **C** average lysosomal diameter. Data are shown as mean ± SEM (n=3). *p<0.05, ***p<0.001 Mann-Whitney test. **D** Representative images of DQ-Red-BSA assay in G2019S LRRK2 and G2019S LRRK2+Rit2 cells. **E** Quantification of DQ-Red-BSA puncta revealed significant increase in G2019S LRRK2+Rit2 cells. Data are shown as mean ± SEM (n=3). ***p<0.001 two-tailed Student's t-test.

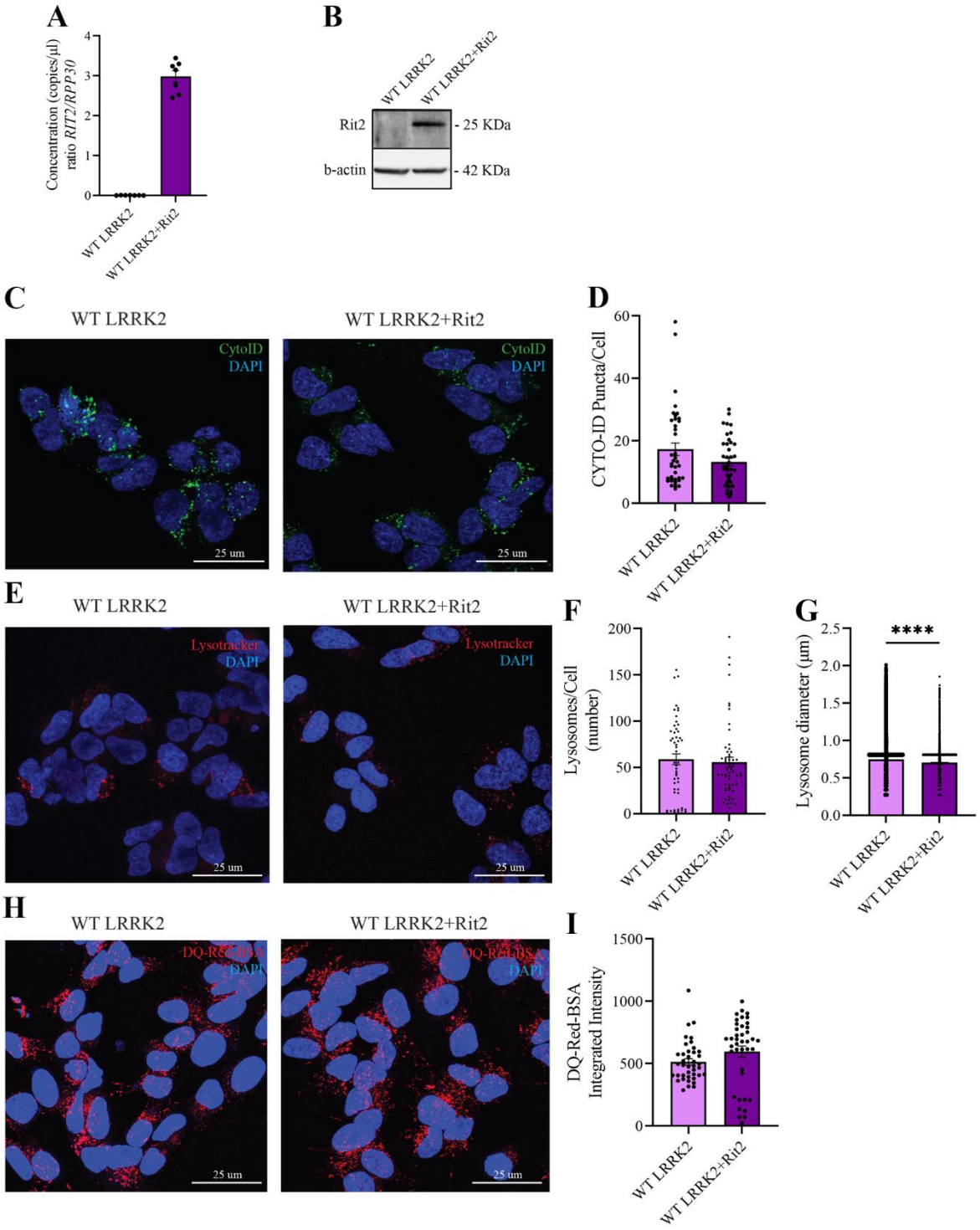
A
Concentration (copies/µl) ratio RIT2/RPP30
WT LRRK2
WT LRRK2+Rit2
B
WT LRRK2
WT LRRK2+Rit2
Rit2
- 25 KDa
b-actin
- 42 KDa
C
WT LRRK2
WT LRRK2+Rit2
CytoID
DAPI
25 um
D
CYTO-ID Puncta/Cell
E
Lysotracker
F
Lysosomes/Cell (number)
G
Lysosome diameter (µm)
****
H
DQ-Red-BSA
I
DQ-Red-BSA Integrated Intensity

**Fig.2.5: Rit2 overexpression rescues lysosomal morphology in WT LRRK2 cells. A** Graphical representation of the ratio between *RIT2* and *RPP30* mRNA concentrations. Data are shown as mean ± SEM (n=7). **B** Representative Western blot of Rit2 in WT LRRK2 and WT LRRK2+Rit2 cells. **C** Representative images of Cyto-ID staining for autophagic vesicles in WT LRRK2 and WT LRRK2+Rit2 cells. **D** Quantification of Cyto-ID positive puncta per cell. Data are shown as mean ± SEM (n=4). No differences were detected by Mann-Whitney test. **E** Representative images of Lysotracker Deep Red staining in WT LRRK2 and WT LRRK2+Rit2 cells. **F** Quantification of lysosomes number per cell and **G** average lysosomal diameter. Data are shown as mean ± SEM (n=3). ****p<0.0001 Mann-Whitney test. **H** Representative images of DQ-Red-BSA assay in G2019S LRRK2 and G2019S LRRK2+Rit2 cells. **I** Quantification of DQ-Red-BSA puncta revealed significant increase in G2019S LRRK2+Rit2 cells. Data are shown as mean ± SEM (n=3). ***p<0.001 two-tailed Student's t-test.

## 2.4 Rit2 overexpression reduces pSer129-αSyn inclusions in G2019S LRRK2 cells

αSyn pathology is the hallmark of PD, and enrichment of phosphorylation at Ser129 is found in pathological aggregates [150]. In transgenic animals G2019S LRRK2 was found to promote αSyn phosphorylation and aggregation in a kinase-dependent manner [151, 152]. Moreover, in our previous work, we demonstrated that the stimulation of autophagosome-lysosome fusion and lysosomal activity by LRRK2 kinase inhibition was linked to clearing of pSer129-αSyn inclusions from G2019S LRRK2 cells [144]. Since we found that Rit2 overexpression rescued lysosomal activity in G2019S LRRK2 cells phenocopying pharmacological LRRK2 kinase inhibition, we decided to explore whether it could also be able to reduce the burden of pSer129-αSyn in the same cell model. G2019S LRRK2 cells nucleofected to overexpress Rit2 were fixed and processed for pS129-αSyn immunofluorescence after 72h (**Fig.2.6A**). The analysis revealed diminished count of pSer129-αSyn positive objects upon Rit2 overexpression (**Fig.2.6B**). We also assessed the level of total αSyn protein by Western blotting (**Fig.2.6C**). We did not detect changes between non-transfected and Rit2 overexpressing G2019S LRRK2 cells (**Fig.2.6D**), indicating that the effect of Rit2 could be specific on the phosphorylated, pathological form, rather than a non-specific effect on protein levels. This result indicates that the restoration of Rit2 expression could be protective against αSyn pathology.

To further test this hypothesis our collaborators, the group of Prof. Martin Lévesque (CERVO Brain Research Centre, Université Laval, Quebec, Canada), used DAT-Ires-Cre mice injected in the midbrain with an A53T αSyn-carrying virus to induce neurodegeneration and αSyn neuropathology. Importantly, co-injection of an AAV containing a Flex-Rit2

construct, to drive overexpression of Rit2 selectively in dopaminergic neurons, was able to prevent accumulation of pSer129-αSyn in the midbrain and loss of dopaminergic neurons in the same area elicited by overexpression of mutated αSyn (***Appendix I***). This indicates that restoration of Rit2 expression provided neuroprotection *in vivo*, notably, in a non-LRRK2-based PD animal model, thus opening a window for exploration of the restoration of Rit2 levels as a general therapeutic approach in other PD models, possibly aiming at a therapeutic strategy applicable to both idiopathic and familial PD.

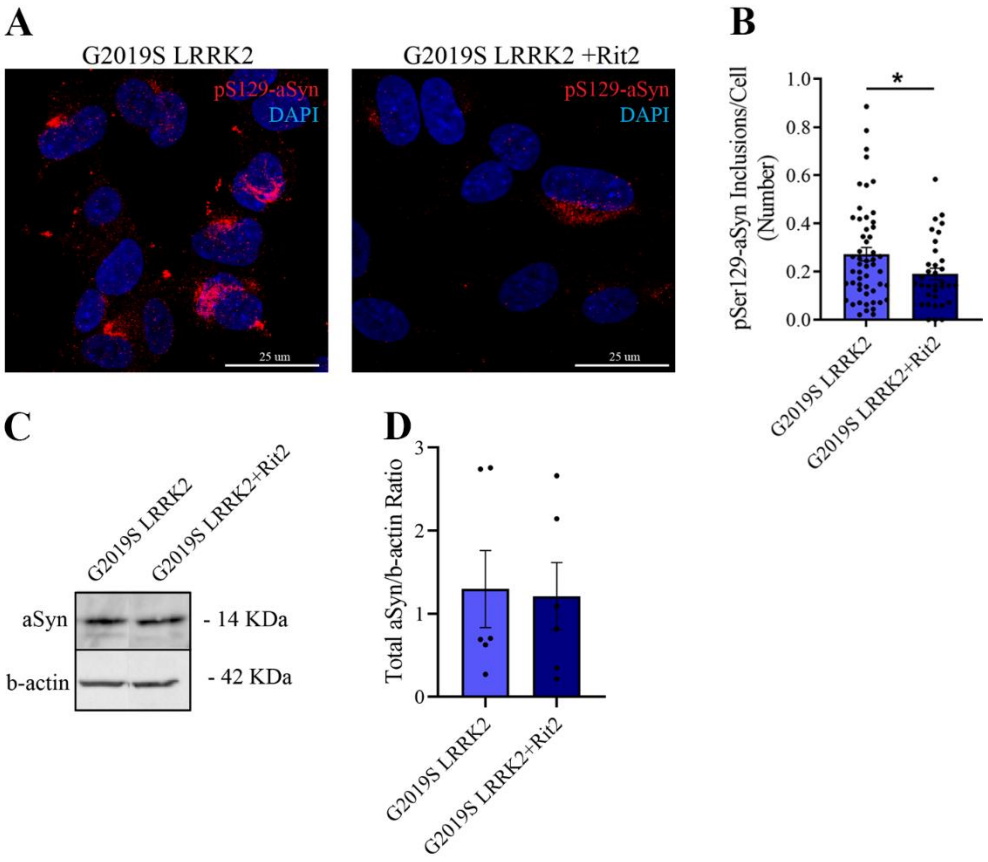


**Fig.2.6: Rit2 overexpression reduces inclusions of pSer129- αSyn in G2019S cells**. **A** Representative images of pSer129-αSyn immunostaining in G2019S LRRK2 and G2019S LRRK2+Rit2 cells. **B** Quantification of the number of pSer129-αSyn positive objects per cell. Data are shown as mean ± SEM (n=4). *p<0.05 two-tailed Student's t-test. **C** Representative Western blot for total αSyn in G2019S LRRK2 and G2019S LRRK2+Rit2 cells. **D** Quantification of total αSyn normalized to b-actin. Data are shown as mean ± SEM (n=6). No difference was revealed by two-tailed Student's t-test.

## 2.5 A close interplay between Rit2 and LRRK2 exists in the cell

The data presented so far suggest a functional interaction between Rit2 and LRRK2 in cell biology. LRRK2 is a large multidomain protein with several protein-protein interaction domains, and it has been suggested to act as a scaffold in protein complexes [153]. Moreover, small Ras-like GTPases are well established LRRK2 interactors and kinase substrates [71]. Therefore, we decided to explore whether an interaction between Rit2 and LRRK2 exists. We first used proximity ligation assay (PLA) for Rit2 and LRRK2. This technique allows *in situ* detection of protein-protein interactions and post-translational modifications using a pair of oligonucleotide-labeled secondary antibodies that binds to the primary antibodies raised against the target proteins. If the distance between the target proteins is shorter than 40 nm, ligation and amplification of the PLA probes take place, and the amplicon can be detected by hybridization of fluorescent oligo probes. Since Rit2 levels in SH-SY5Y cells (naïve, WT LRRK2, G2019S LRRK2) is extremely low, we decided to perform PLA experiments on cells nucleofected with Rit2 (**Fig.2.7A**). Analysis of PLA puncta revealed a low signal in SH-SY5Y cells, just above the sensitivity limit of the assay, probably due to low LRRK2 abundance as well. However, we detected a strong signal when both Rit2 and WT LRRK2 were overexpressed, indicating that the two proteins are very close in a cellular context. PLA signal was also readily detectable in G2019S LRRK2+Rit2 cells but in a significantly lower magnitude with respect to WT LRRK2+Rit2 cells (**Fig.2.7B**), suggesting that Rit2-LRRK2 interaction might be affected by the G2019S mutation. Nevertheless, we wanted to rule out a possible bias in this result due to different levels of LRRK2 overexpression in our stable overexpressing lines (WT and G2019S LRRK2, as reported in [144]). Therefore, we performed the same PLA experiment in HEK293T cells with transient, stoichiometrically comparable expression of LRRK2 (either WT or G2019S) together with Rit2-GFP (**Fig.2.7C**). Also in this experimental setting we were able to detect PLA signal, and WT LRRK2+Rit2 cells showed a greater number of PLA puncta with respect to G2019S LRRK2+Rit2 cells (**Fig.2.7D**), reinforcing the result of decreased interaction between the two proteins in the presence of the G2019S mutation.

Nevertheless, PLA informs on the spatial vicinity between two proteins inside the cell but it does not provide information on their actual physical interaction. To specifically address this aspect, we performed co-immunoprecipitation using HEK293T cells transfected with

either Rit2, LRRK2 (WT or G2019S) or both (**Fig.2.7E**). We were able to specifically precipitate LRRK2, as can be observed from the absence of LRRK2 immunoreactive bands when precipitation was carried out using control IgG (**Fig.2.7F**) and from the presence of a greater amount of LRRK2 immunoreactivity in supernatants (**Fig.2.7G**). Unfortunately, the immunoprecipitation was not very efficient, as a fair amount of LRRK2 protein still remained in the supernatants (**Fig.2.7G**). Importantly, we found that Rit2 was specifically co-immunoprecipitated with LRRK2, even in non-transfected cells (**Fig.2.7F**), indicating that the interaction between the two proteins occurs at the level of endogenous proteins. We also observed a slight increase in the intensity of Rit2 immunoreactive bands when both LRRK2 and Rit2 were overexpressed. However, we did not detect a clear quantitative difference between the intensity of Rit2 signal in the presence of WT or G2019S LRRK2. A better optimization of the conditions of immunoprecipitation is needed to quantify whether Rit2-LRRK2 physical interaction is quantitively affected by the G2019S mutation in LRRK2.

Altogether, these data indicate that Rit2 and LRRK2 share a common localization and, possibly, directly interact or at least are part of a common multiprotein complex. Regardless of the molecular details, these results support our view that the two proteins are deeply functional related. Our collaborators at the Université Laval observed the occurrence of an endogenous Rit2-LRRK2 interaction also in the mouse brain, highlighting its relevance *in vivo* in brain physiology (***Appendix I***). A better biochemical and molecular characterization at the protein level is needed to understand the fine dynamics of this interaction, whether it is regulated by Rit2 or LRRK2 enzymatic activity, which domains are involved in said interaction, whether this is direct or it occurs in a larger multiprotein complex (and in this case, which are the other components?), what upstream signals trigger the interaction and what downstream effectors are modulated.

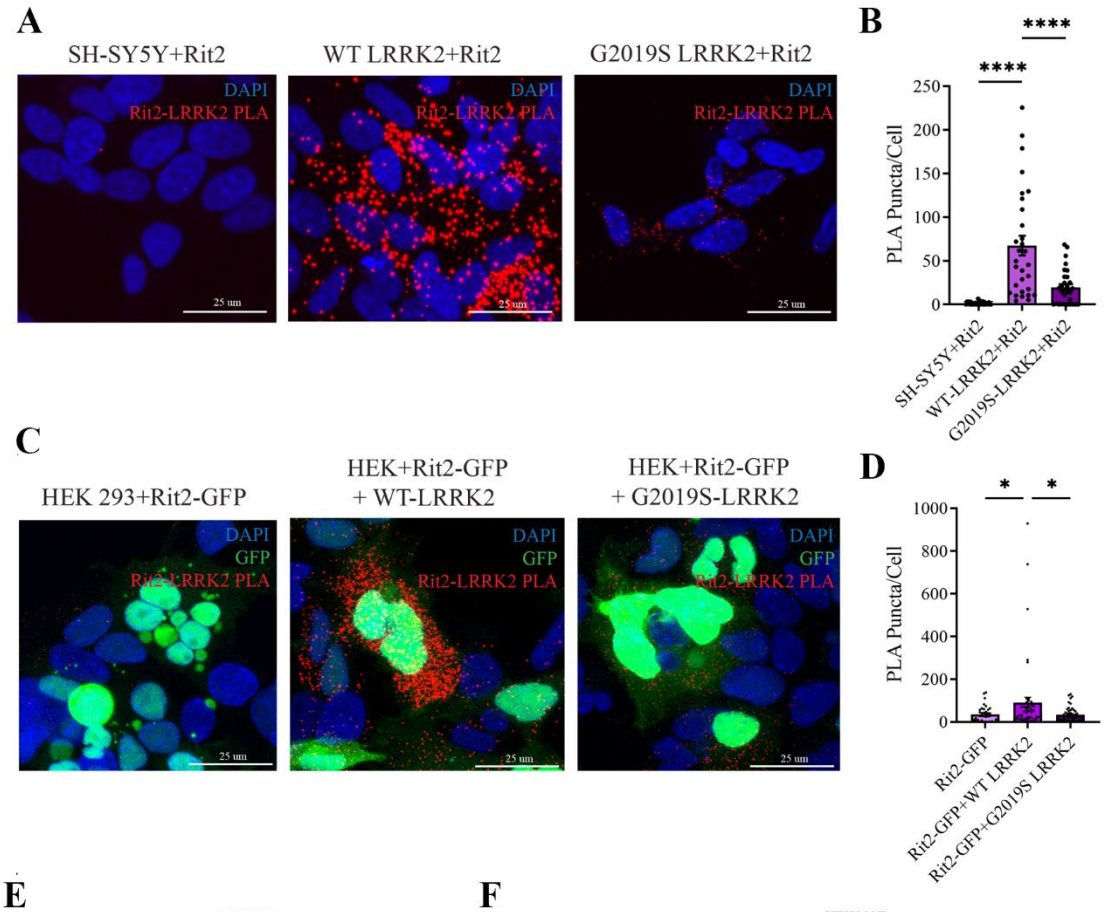
A
SH-SY5Y+Rit2
WT LRRK2+Rit2
G2019S LRRK2+Rit2
DAPI
Rit2-LRRK2 PLA
25 um
B
****
****
PLA Puncta/Cell
250
200
150
100
50
0
SH-SY5Y+Rit2
WT-LRRK2+Rit2
G2019S-LRRK2+Rit2
C
HEK 293+Rit2-GFP
HEK+Rit2-GFP
+ WT-LRRK2
HEK+Rit2-GFP
+ G2019S-LRRK2
DAPI
GFP
Rit2-LRRK2 PLA
25 um
D
*
*
PLA Puncta/Cell
1000
800
600
400
200
0
Rit2-GFP
Rit2-GFP+WT LRRK2
Rit2-GFP+G2019S LRRK2
E
HEK293T
RIT2
LRRK2 WT
LRRK2 G2019S
Input
LRRK2
280 kDa
b-actin
42 kDa
Rit2
25 kDa
F
HEK293T
RIT2
LRRK2 WT
LRRK2 G2019S
CO-IP
LRRK2
280 kDa
Rit2
25 kDa
LRRK2
IgG
G
HEK293T
RIT2
LRRK2 WT
LRRK2 G2019S
Supernatant
LRRK2
280 kDa
Rit2
25 kDa
LRRK2
IgG

**Fig.2.7: Rit2 and LRRK2 are in close proximity in the cell and co-immunoprecipitate. A** Representative images of Rit2-LRRK2 PLA in SH-SY5Y naïve, WT LRRK2, and G2019S LRRK2 cells overexpressing Rit2. **B** Quantification of PLA puncta per cells. Data are shown as mean ± SEM (n=3). ****p<0.0001 one-way ANOVA followed by Bonferroni's post-hoc test. **C** Representative images of Rit2-LRRK2 PLA in HEK293T overexpressing Rit2-GFP, WT LRRK2+Rit2-GFP, G2019S LRRK2+Rit2-GFP. **D** Quantification of PLA puncta per cells. Data are shown as mean ± SEM (n=5). *p<0.05 one-way ANOVA followed by Bonferroni's post-hoc test. **E-F** Representative Western blot images of Rit2 and LRRK2 in input samples, immunoprecipitation, and CO-IP supernatants.

## 2.6 Rit2 overexpression inhibits LRRK2 kinase activity

The finding of a Rit2-LRRK2 interaction combined with the observations that Rit2 overexpression phenocopies pharmacological LRRK2 kinase inhibition, rescuing lysosomal defects and reducing pS129-αSyn load in G2019S LRRK2 cells, led us to hypothesize that Rit2 might inhibit LRRK2 kinase activity. It is well established that the G2019S LRRK2 mutation increases LRRK2 kinase activity, and this gain-of-function is linked to pathogenicity [73, 76]. A commonly accepted read-out of LRRK2 kinase activity is its autophosphorylation at the Ser1292 residue [70, 148]. Recently, a PLA method has been validated to detect pSer1292 *in situ*. Only a small portion of endogenous LRRK2 is phosphorylated at Ser1292 at basal levels, hampering its detection by conventional immunofluorescence. PLA against pSer1292-LRRK2 and total LRRK2 allows a greater amplification of the signal and helps increasing its specificity [75]. We performed PLA for pSer1292-LRRK2 in our cell lines (**Fig.2.8A**). According to kinase hyperactivation caused by mutation in LRRK2, we detected a very large increase in PLA signal only in G2019S LRRK2 cells, while naïve SH-SY5Y and WT LRRK2 cells showed a negligible, almost undetectable signal level (**Fig.2.8B**). Importantly, when Rit2 is overexpressed in G2019S LRRK2 cells, the PLA signal is significantly decreased, indicating that high Rit2 levels limit the activation of the LRRK2 kinase (**Fig.2.8A-B**). As a positive control for this assay, we used pharmacological LRRK2 kinase inhibition (PF-475, 500 nM for 6h), which correctly completely abolished the pS1292 LRRK2 PLA signal (**Fig.2.8A-B**).

We confirmed these results measuring pSer1292 and pSer935 LRRK2 levels by Western blotting. We previously reported that pSer1292 LRRK2 was specifically increased by G2019S LRRK2 and that treatment with the LRRK2 kinase inhibitor PF-475 reduced LRRK2 phosphorylation at Ser1292 and Ser935 (which is not a autophosphorylation site, but is sensitive to pharmacological LRRK2 kinase inhibition [144, 154]). This approach

confirmed that the overexpression of Rit2 in G2019S LRRK2 cells diminished the pSer1292 LRRK2-total LRRK2 ratio (**Fig.2.8C-D**), indicating inhibition of LRRK2 kinase activity. Intriguingly, we found that phosphorylation at Ser935, as well as total levels of LRRK2, were increased when Rit2 was overexpressed in G2019S LRRK2 cells (**Fig.2.8E-G**). This effect is contrary to that produced by treatment with pharmacological kinase inhibitors, which is related to LRRK2 protein destabilization [85] and cellular abnormalities in the lung of animal models, similar to those found in LRRK2 KO animals [155]. The mechanism/s that lead to LRRK2 protein destabilization upon pharmacological kinase inhibition are not fully understood. It has been proposed that LRRK2 is stabilized by pS935-dependent binding to 14-3-3 proteins [83, 84] and that protein stability depends on its kinase activity [89]. But, if on one hand LRRK2 destabilization has been associated to a toxic effect, especially in the periphery, LRRK2 antisense oligonucleotides have been found to protect against αSyn pathology, therefore caution must be exercised in the view of therapeutic approaches.

Other crucial points in LRRK2 biology are how its kinase activity is regulated and what physiological roles it plays. Membrane-bound LRRK2 is thought to be kinase active [109]. Rab29 was found to recruit and activate LRRK2 to the trans Golgi network [110] and stressed lysosomes [112], where LRRK2 exerts its function phosphorylating a subset of Rab proteins. We reported that Rit2 interacts with LRRK2 and inhibits LRRK2 hyperactivation. To the best of our knowledge, this is the first report of a small GTPase capable of reducing LRRK2 kinase activity. This opens new possibilities to the investigation of how LRRK2 kinase activity is regulated in physiology and pathology. It would be interesting to explore the downstream effects of this interplay in future studies. Here we reported that Rit2 overexpression rescued LRRK2-dependent lysosomal defects, suggesting their interplay in a mechanism that aims at the maintenance of lysosomal homeostasis. Further studies are needed to address whether Rit2 and LRRK2 could be recruited at the lysosomal membrane (as suggested for LRRK2 and other Rabs) and how phosphorylation on different Rabs changes upon Rit2-mediated LRRK2 kinase inhibition.

The Rit2-mediated inhibition of LRRK2 kinase activity has an *in vivo* relevance. Indeed, our collaborators at Université Laval found that viral-mediated A53T αSyn overexpression elicited LRRK2 hyperactivation in nigral dopaminergic neurons, assessed by pSer1292 LRRK2 PLA (result in accordance with previous report [75]). Importantly, the co-

injection of a Rit2-carrying virus was able to prevent LRRK2 hyperactivation (***Appendix I***). This result coupled to Rit2-mediated protective effect against αSyn pathology and neurodegeneration, makes approaches aimed at restoring Rit2 expression valuable candidates for the development of disease-modifying treatments for PD. Additionally, both Rit2 downregulation and LRRK2 hyperactivation have been found in non-LRRK2-based models and idiopathic PD patients, opening to the possibility of a universal treatment for PD. From our experimental paradigm we can infer that restoration of Rit2 expression would be beneficial in early stages of the disease (since Rit2 overexpression was concomitant to pathogenic insult). It remains to be elucidated whether it would also be effective when applied to later stages of the disease, when the pathogenic and pathologic processes are well underway.

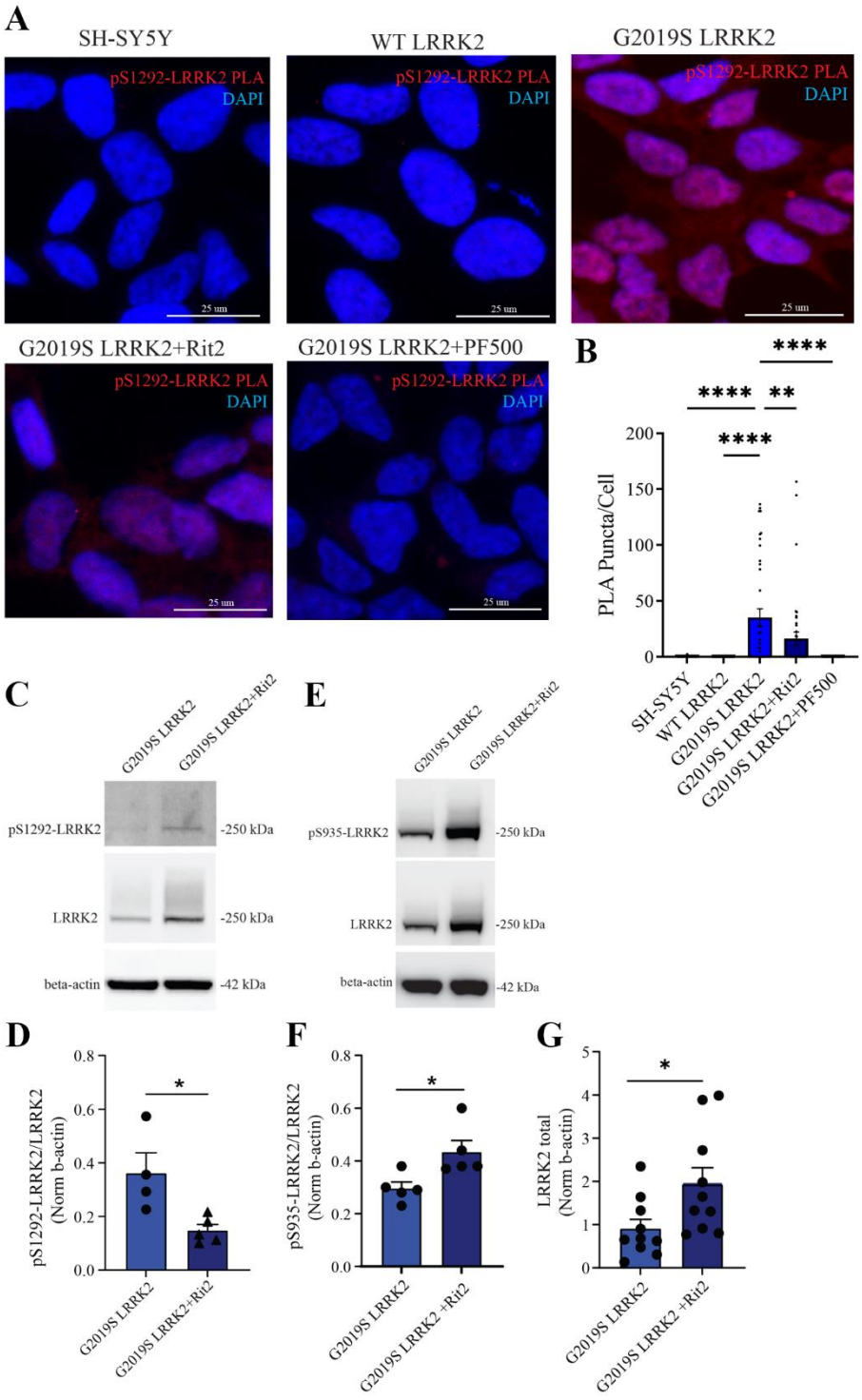
A
SH-SY5Y
WT LRRK2
G2019S LRRK2
pS1292-LRRK2 PLA
DAPI
25 um
G2019S LRRK2+Rit2
G2019S LRRK2+PF500
B
****
**
PLA Puncta/Cell
200
150
100
50
0
SH-SY5Y
WT LRRK2
G2019S LRRK2
G2019S LRRK2+Rit2
G2019S LRRK2+PF500
C
G2019S LRRK2
G2019S LRRK2+Rit2
pS1292-LRRK2
-250 kDa
LRRK2
beta-actin
-42 kDa
E
pS935-LRRK2
D
pS1292-LRRK2/LRRK2
(Norm b-actin)
0.8
0.6
0.4
0.2
0.0
*
F
pS935-LRRK2/LRRK2
(Norm b-actin)
G
LRRK2 total
(Norm b-actin)
5
4
3
2
1
0

**Fig.2.8: Rit2 overexpression reduces LRRK2 hyperactivation elicited by the G2019S mutation. A** Representative images of pSer1292 LRRK2 PLA in naïve SH-SY5Y, WT LRRK2, G2019S LRRK2, G2019S LRRK2+Rit2 and G2019S LRRK2+PF-475 cells (500 nM for 6h). **B** Quantification of PLA puncta per cell. Data are shown as mean ± SEM (n=5). **p<0.01, ****p<0.0001 one-way ANOVA followed by Bonferroni's post-hoc test. **C-E** Representative Western blotting of pSer1292 LRRK2, pSer935 LRRK2 and total LRRK2. **D-F-G** Quantification of the levels of pSer1292 LRRK2 (normalized on total LRRK2), pSer935 (normalized on total LRRK2), total LRRK2 (normalized on b-actin). Data are shown as mean ± SEM. *p<0.05 two tailed Student's t-test.

## 2.7 Effect of Rit2 overexpression in G2019S LRRK2 cells on ALP substrates

As mentioned above, we found that Rit2 overexpression rescued lysosomal proteolytic activity and reduced the accumulation of pSer129-αSyn without evident alterations to the autophagic flux in G2019S LRRK2 cells, suggesting the involvement of a specific lysosomal pathway that is affected by G2019S mutation and/or Rit2 downregulation. To better characterize the role of lysosomal degradation in our model we analyzed the levels of other autophagy substrates.

p62/SQSTM1 (hereafter referred to as p62) acts as a receptor recognizing polyubiquitinated proteins and linking them to LC3 present at the membrane of forming autophagosomes. p62 is then internalized and degraded in the autolysosomes, therefore is used as a marker of autophagic degradation [156]. We assessed p62 protein distribution by immunofluorescence (**Fig.2.9A**). The analysis of p62 positive puncta revealed accumulation of p62 in G2019S LRRK2 cells with respect to naïve SH-SY5Y cells, consistent with defects in lysosomal activity (**Fig.2.9B**). We then wondered whether Rit2-mediated rescue of proteolytic activity could have an effect on accumulated p62 in G2019S cells. Surprisingly, by immunofluorescence we observed an even larger increase in the accumulation of p62 upon Rit2 overexpression (**Fig.2.9A-B**). We found that Rit2 inhibits LRRK2 kinase activity. To rule out whether the Rit2-mediated effect on p62 depended on LRRK2 kinase activity we treated G2019S LRRK2 cells with pharmacological LRRK2 kinase inhibitor (PF-475, 500 nM for 2h, which is effective in reducing pSer129-αSyn, promoting lysosomal function and inhibiting LRRK2 activity). In this condition we observed a rescue of the number of p62 positive puncta with respect to non-treated G2019S LRRK2 cells, indicating that Rit2 and PF-475 regulate levels of p62 through different mechanisms (**Fig.2.9A-B**). We further measured p62 protein expression by Western blotting (**Fig.2.9C**). According to immunofluorescence, we found an increased p62 level in G2019S LRRK2 cells, but this was not affected by Rit2

overexpression nor by pharmacological LRRK2 kinase inhibition (**Fig.2.9D**). This discrepancy between immunofluorescence and Western blotting might be due to differential sensitivity and final output of the two techniques, and we cannot rule out the existence of different pools of p62 protein that are differentially detected by the two techniques. We also analyzed p62 mRNA expression by ddPCR to assess whether the observed differences resulted from alterations in gene transcription (**Fig.2.9E**).

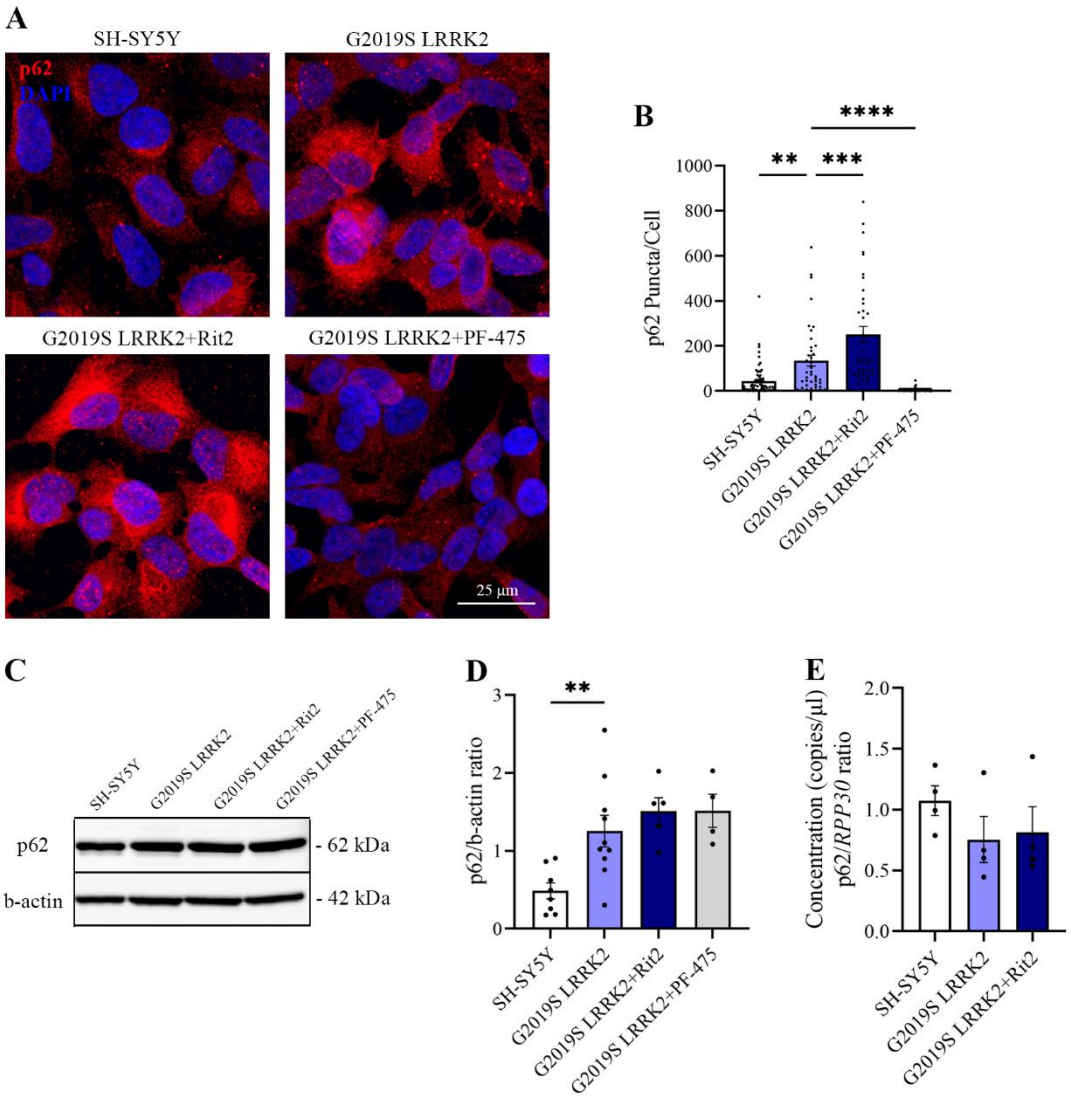

**Fig.2.9: p62 accumulates in G2019S LRRK2 cells and is possibly affected by Rit2 overexpression. A** Representative images of p62 immunofluorescence in naïve SH-SY5Y, G2019S LRRK2, G2019S LRRK2+Rit2, G2019S LRRK2+PF-475 (500 nM for 2h) cells. **B** Quantification of p62 positive puncta per cell. Data are shown as mean ± SEM (n=4). **p<0.01, ***p<0.001, ****p<0.0001 one-way ANOVA followed by Bonferroni's post-hoc test. **C** Representative images of Western blotting for p62 in naïve SH-SY5Y, G2019S LRRK2, G2019S LRRK2+Rit2, G2019S LRRK2+PF-475 cells. **D** Quantification of the levels of p62 normalized on b-actin. Data are shown as mean ± SEM (n=5). **p<0.01 one-way ANOVA followed by Bonferroni's post-hoc test. **E** Quantification of p62 mRNA levels by ddPCR normalized on *RPP30*. Data are shown as mean ± SEM (n=4). No significant differences were detected by one-way ANOVA followed by Bonferroni's post-hoc test.

We did not detect differences across all the conditions (**Fig.2.9E**), suggesting that the differences we observed in protein levels are linked to protein handling/processing, and not gene expression. It has been previously suggested that overexpression of G2019S LRRK2 in HEK293T cells led to increased levels of p62 in a protein synthesis-dependent manner [96]. Others reported protein synthesis-mediated upregulation of p62 upon prolonged but not short LRRK2 kinase inhibition in fibroblast expressing endogenous WT LRRK2 [98]. This kinetic difference might explain, at least partially, the differential effect we observe upon Rit2 overexpression (3 days) and acute pharmacological LRRK2 kinase inhibition (2 hours). Indeed, deeper examination of p62 handling is needed to understand its regulation in our model, and possibly, in a neuron-relevant setting. Caution is needed when interpreting autophagy status based on p62 levels, since its regulation is cell specific and could be affected by environmental conditions [156]. The role of LRRK2 and its kinase activity on p62 need better elucidation, especially when used to drive hypothesis on autophagic flux. p62 has been found to be accumulated in idiopathic PD patient brains, but not in G2019S LRRK2 patient brains [54]. In another report, p62 was found increased in LRRK2 kinase-dead mice, in G2019S LRRK2 knock-in mice upon kinase inhibition and in aged LRRK2 KO mice [157]. Moreover, p62 accumulation was found in the kidney of LRRK2 KO rodents [89, 155]. These data demonstrate a role for LRRK2 and its kinase activity in proteostasis and autophagy, however the direction of LRRK2-mediated regulation on these processes remain elusive and not unequivocally informed by p62 levels.

We also analyzed the levels of another autophagic marker, namely Paxillin. Paxillin is a focal adhesion protein, and its recycling by AMPK-induced autophagy is necessary to sustain cell migration. It has been shown that autophagy inhibition led to accumulation of

Paxillin and impaired cell migration [158, 159]. Here we assessed Paxillin protein levels by immunofluorescence (**Fig.2.10A-B**) and Western blotting (**Fig.2.10C-D**). With both approaches, we found decreased levels of Paxillin in G2019S LRRK2 cells, only partially restored by Rit2 overexpression, suggesting higher autophagic Paxillin turnover. However, confirmation of this result can be obtained only after evaluation of gene expression and protein synthesis. Paxillin is thought to act as a signal integrator, even though the precise signaling cascades in which it is involved are yet to be defined. Interestingly, active phosphorylated Paxillin was detected in dystrophic neurites surrounding beta-amyloid plaque cores, where they colocalize with hyperphosphorylated tau. Moreover, Paxillin activation and its consequent translocation to the cytoskeleton has been associated to beta-amyloid-induced neuronal dystrophy [160, 161]. To date, no reports exist connecting Paxillin to LRRK2. It would be interesting to explore whether an interplay between signaling cascades regulated by the two proteins exist, and whether it might be relevant in PD pathogenesis.

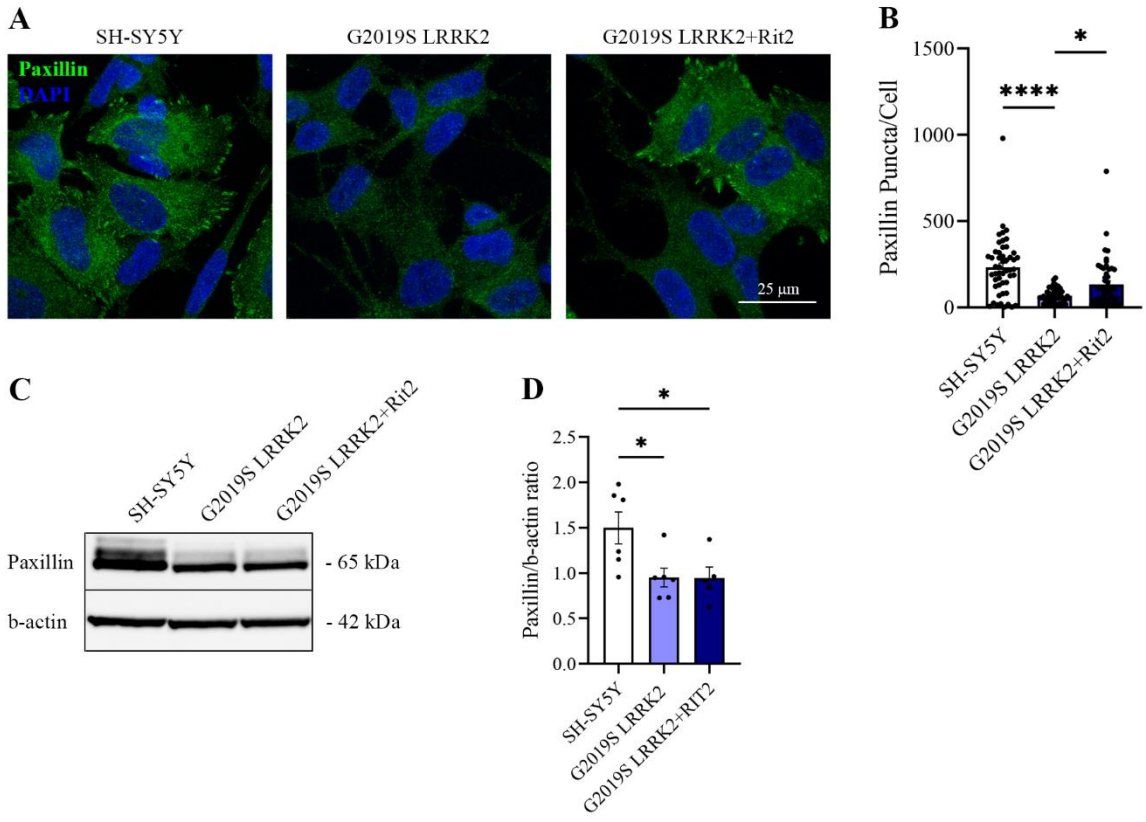

**Fig.2.10: Paxillin expression is reduced in G2019S LRRK2 and minimally affected by Rit2 overexpression. A** Representative images of Paxillin immunofluorescence in naïve SH-SY5Y, G2019S LRRK2, G2019S LRRK2+Rit2 cells. **B** Quantification of Paxillin positive puncta per cell. Data are shown as mean ± SEM (n=4). *p<0.05, ****p<0.0001 one-way ANOVA followed by Bonferroni's post-hoc test. **C** Representative images of Western blotting for Paxillin in naïve SH-SY5Y, G2019S LRRK2, G2019S LRRK2+Rit2 cells. **D** Quantification of the protein levels of Paxillin normalized on b-actin. Data are shown as mean ± SEM (n=6). *p<0.05 one-way ANOVA followed by Bonferroni's post-hoc test.

## 2.8 Rit2 is required for lysosomal function in cells

We showed that enhancing Rit2 expression in a pathological context, where Rit2 is downregulated, reduces accumulation of pSer129-αSyn (both *in vitro* and *in vivo*) and rescues lysosomal defects. This effect phenocopied pharmacological LRRK2 kinase inhibition in G2019S LRRK2 cells, and we found that Rit2 interacts with LRRK2 and limits its pathologic hyperactive kinase function, suggesting the participation of Rit2 and LRRK2 in the regulation of common processes. Of note, the role of Rit2 in ALP has never been investigated before and we hypothesized its physiological involvement in this process, which could also be LRRK2-indipendent. We directly addressed this point using SH-SY5Y Rit2-KO cells, generated, characterized and kindly provided by the group of Prof. Tatsushi Toda (Kobe University Graduate School of Medicine, Japan) [118]. We performed ddPCR for Rit2 mRNA to ensure correct ablation of Rit2 expression in our culture conditions, which indeed resulted completely silenced (**Fig2.11A-B**).

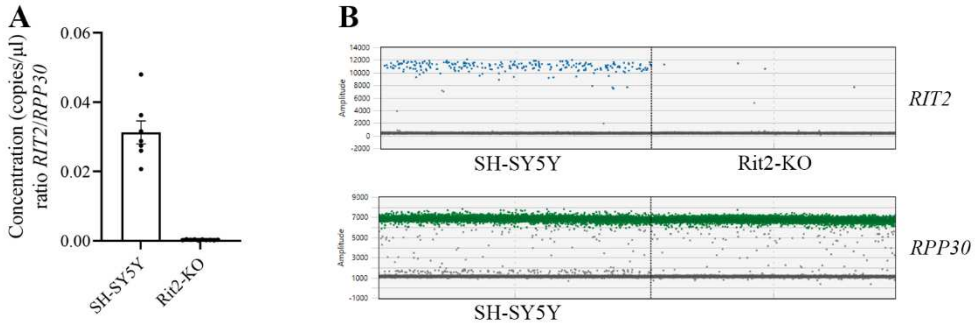


**Fig.2.11: Rit2 gene expression is effectively ablated in Rit2-KO cells. A** Graphical representation of the ratio between *RIT2* and *RPP30* mRNA concentrations. Data are shown as mean ± SEM (n=7). **B** 1D amplitude view of an example of ddPCR reaction for *RIT2* and *RPP30*.

We analyzed different steps of the ALP. First, we looked at LC3B levels by Western Blotting (**Fig2.12A**). We observed that both LC3B-II/LC3B-I ratio (**Fig.2.12B**) and LC3B-II/b-actin ratio (**Fig.2.12C**) were significantly increased in Rit2-KO cells with respect to naïve SH-SY5Y cells. This might indicate slowed autophagic flux and/or an accumulation of autophagosomes. We confirmed this observation using the Cyto-ID assay, to specifically visualize autophagosomes/autolysosomes (**Fig.2.12D**). Consistently, we found that Rit2-KO cells displayed an increased number of Cyto-ID-positive objects per cell (**Fig.2.12E**), confirming accumulation of autophagic vesicles in these cells with respect to naïve SH-SY5Y cells. This dataset *per se* does not provide unequivocal information on the status of the autophagic process, where increased autophagy induction or impairment in lysosomal degradation might be occurring. Therefore, we looked at lysosomal morphology with Lysotracker staining (**Fig.2.12F**). The quantitative analysis of Lysotracker positive objects revealed that Rit2-KO cells had fewer but enlarged lysosomes (**Fig2.12G-H**), which could possibly represent a condition associated to functional defects. To clarify this functional aspect, we assessed lysosomal proteolytic activity using the DQ-Red-BSA assay (**Fig.2.12I**), where the analysis of fluorescent puncta revealed a significantly reduced number of objects per cells, paralleled by a reduction of their signal intensity (**Fig.2.12J-K**). These indications support the existence of altered lysosomal proteolytic activity in Rit2-KO cells. Altogether, these data provide strong evidence supporting a physiological role for Rit2 in the regulation of lysosome biology and function. Interestingly, these phenotypes are consistently overlapping to those we observed in G2019S LRRK2 cells, where Rit2 expression is downregulated, supporting its requirement for correct lysosome activity.

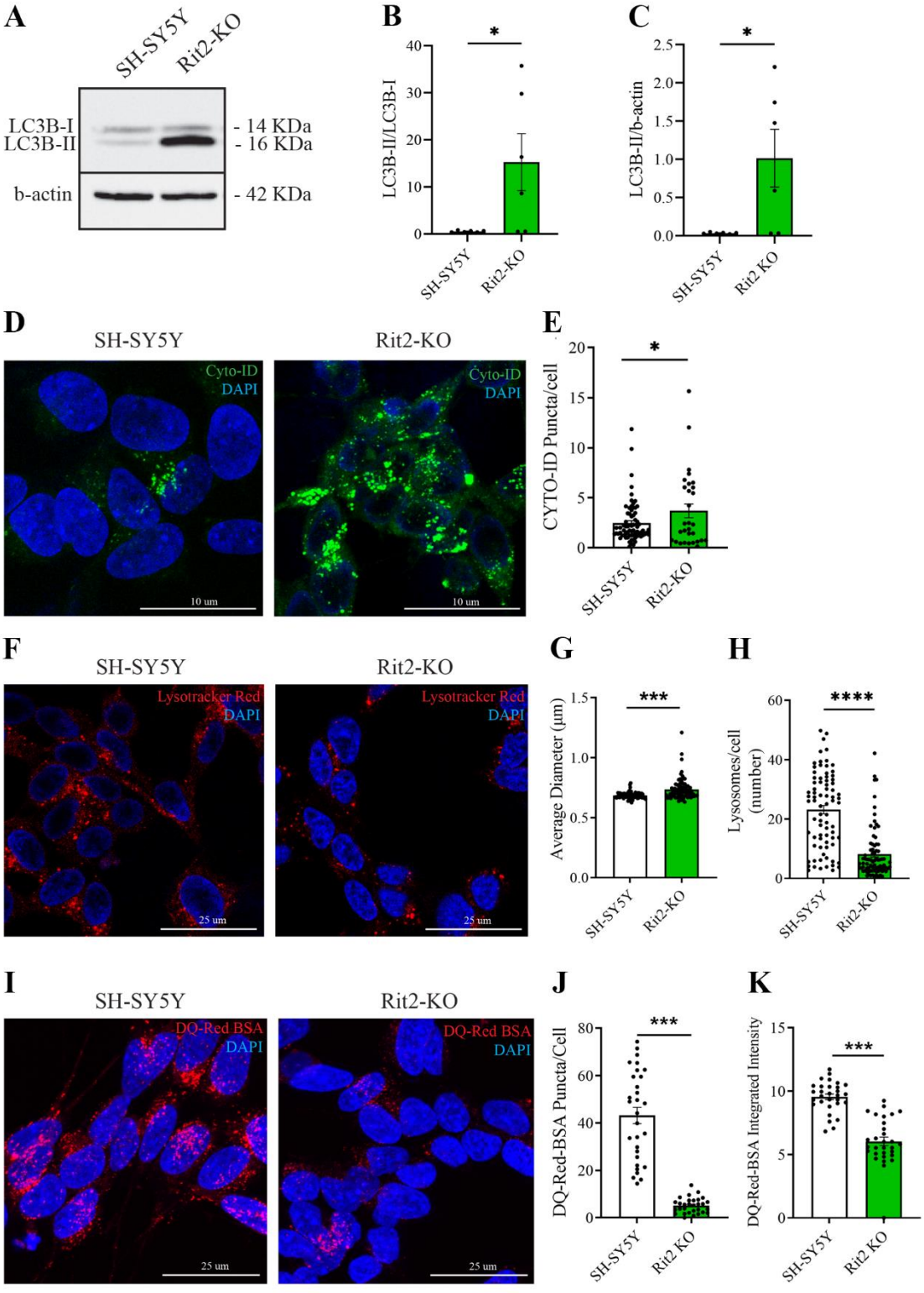
A
SH-SY5Y
Rit2-KO
LC3B-I
LC3B-II
- 14 KDa
- 16 KDa
b-actin
- 42 KDa
B
LC3B-II/LC3B-I
SH-SY5Y
Rit2-KO
C
LC3B-II/b-actin
SH-SY5Y
Rit2 KO
D
SH-SY5Y
Rit2-KO
Cyto-ID
DAPI
10 um
E
CYTO-ID Puncta/cell
SH-SY5Y
Rit2-KO
F
SH-SY5Y
Rit2-KO
Lysotracker Red
DAPI
25 um
G
Average Diameter (µm)
SH-SY5Y
Rit2-KO
H
Lysosomes/cell (number)
SH-SY5Y
Rit2-KO
I
SH-SY5Y
Rit2-KO
DQ-Red BSA
DAPI
25 um
J
DQ-Red-BSA Puncta/Cell
SH-SY5Y
Rit2 KO
K
DQ-Red-BSA Integrated Intensity
SH-SY5Y
Rit2 KO

**Fig.2.12: Rit2-KO cells display autophagosome accumulation and lysosomal defects: A** Representative images of Western blot for LC3B in naïve SH-SY5Y and Rit2-KO cells. **B-C** Quantification of LC3B-II/LC3B-I and LC3B-II/b-actin ratios. Data are shown as mean ± SEM (n=6). *p<0.05 two tailed Student's t-test. **D** Representative images of Cyto-ID staining for autophagosomes/autolysosomes in naïve SH-SY5Y and Rit2-KO cells. **E** Quantification of the number of fluorescent objects per cell. Data are shown as mean ± SEM (n=3). *p<0.05 two tailed Student's t-test. **F** Representative images of Lysotracker Deep Red staining in naïve SH-SY5Y and Rit2-KO cells. **G-H** Quantification of lysosomes number per cell and average lysosomal diameter. Data are shown as mean ± SEM (n=3). ***p<0.001, ****p<0.0001 two tailed Student's t-test. **I** Representative images of DQ-Red-BSA assay in naïve SH-SY5Y and Rit2-KO cells. **J-K** Quantification of DQ-Red-BSA puncta per cell and fluorescence intensity. Data are shown as mean ± SEM (n=3). ***p<0.001 two tailed Student's t-test.

Next, we wanted to ascertain the Rit2 dependance of the phenotypes observed in Rit2 KO cells and thus performed a series of "rescue" experiments based on Rit2 overexpression in this cell line. We verified that Rit2 was correctly overexpressed by both ddPCR (**Fig.2.13A**) and Western blotting (**Fig.2.13B**). Using Cyto-ID staining we did not detect changes in autophagosome/autolysosome number upon Rit2 overexpression (**Fig.2.13C-D**). However, lysosome number (assessed by Lysotracker staining, **Fig.2.13E-F**) and DQ-Red-BSA fluorescence signal (**Fig.2.13G-H**) were significantly enhanced by Rit2 overexpression, indicating that these phenotypes were specifically caused by Rit2 silencing. The reason why accumulation of autophagosomes is not rescued by the restoration of Rit2 expression is not clear and we speculate it could be due to a Rit2-independent mechanism that needs further specific exploration.

We also investigated the levels of the autophagic substrates p62 and Paxillin in these experimental settings. In analogy to what we determined in G2019S LRRK2 cells, we observed accumulation of p62-positive puncta in Rit2-KO cells by immunofluorescence (**Fig.2.14A-B**). Western blotting did not reveal an increase in protein levels (**Fig.2.14C-D**), nor ddPCR detected increased p62 gene expression (**Fig.2.14E**). A possible explanation of this apparently contradicting result could be that p62 tends to aggregate in discrete structures that are specifically detected by immunofluorescence, without an observable increase in total levels of the protein (which is denatured and linearized in Western blotting, thus losing the tertiary and quaternary structures). Evaluation of protein synthesis would provide a more complete assessment of p62 protein handling in these conditions. In addition, Rit2 re-expression in Rit2-KO cells would provide additional information on the Rit2-mediated

regulation of p62 proteostasis. Both these approaches will be the subject of future, more focused studies that are currently outside the aim of this thesis work. Similar to p62, Paxillin followed the same trend of decreased protein levels found in G2019S LRRK2 cells. Reduced Paxillin levels were found in Rit2-KO cells by both immunofluorescence (**Fig.2.14F-G**) and Western Blotting (**Fig.2.14H-I**), results that are in general accordance to an alteration in Paxillin metabolism that is affected by differential Rit2 levels.

As a whole, these data strongly indicate for the first time a role for Rit2 in the modulation of lysosomal function, even though the exact mechanism/s underlying this modulation remain to be untangled, and especially, the neuronal relevance. To partially address these issues, the lab of our collaborator Prof. Martin Lévesque performed Rit2 knock-down in mouse primary dopaminergic neurons, which were then subjected to assessment of lysosomal morphology and catabolic activity using Lysotracker staining and DQ-Red-BSA assay, respectively. Of note, Rit2 knock-down in primary neurons produced a decrease in the number of lysosomes and an increase in their size, paralleled by a reduction of proteolytic activity (***Appendix I***). These results correctly mirror the phenotypes we observed in Rit2-KO and G2019S LRRK2 SH-SY5Y cells. Altogether, these results functionally place Rit2 inside a neuron-relevant mechanism mediating lysosome biology, alterations of which could be causatively involved in PD pathogenesis.

**Fig.2.13: Rit2 overexpression in Rit2-KO cells rescues lysosomal defects: A** Quantification of Rit2 mRNA levels by ddPCR normalized on RPP30 in Rit2-KO and Rit2-KO+Rit2 cells. Data are shown as mean ± SEM (n=6). **B** Representative Western Blot for Rit2 in Rit2-KO and Rit2-KO+Rit2 cells. **C** Representative images of Cyto-ID staining for autophagosomes/autolysosomes in Rit2-KO and Rit2-KO+Rit2 cells. **D** Quantification of the number of fluorescent objects per cell. Data are shown as mean ± SEM (n=4). No differences were detected by Mann-Whitney test. **E** Representative images of Lysotracker Deep Red staining in Rit2-KO and Rit2-KO+Rit2 cells. **F** Quantification of lysosomes number per cell. Data are shown as mean ± SEM (n=4). *p<0.05 Mann-Whitney test. **G** Representative images of DQ-Red-BSA assay in Rit2-KO and Rit2-KO+Rit2 cells. **H** Quantification of DQ-Red-BSA fluorescence intensity. Data are shown as mean ± SEM (n=4). *p<0.05 Mann-Whitney test.

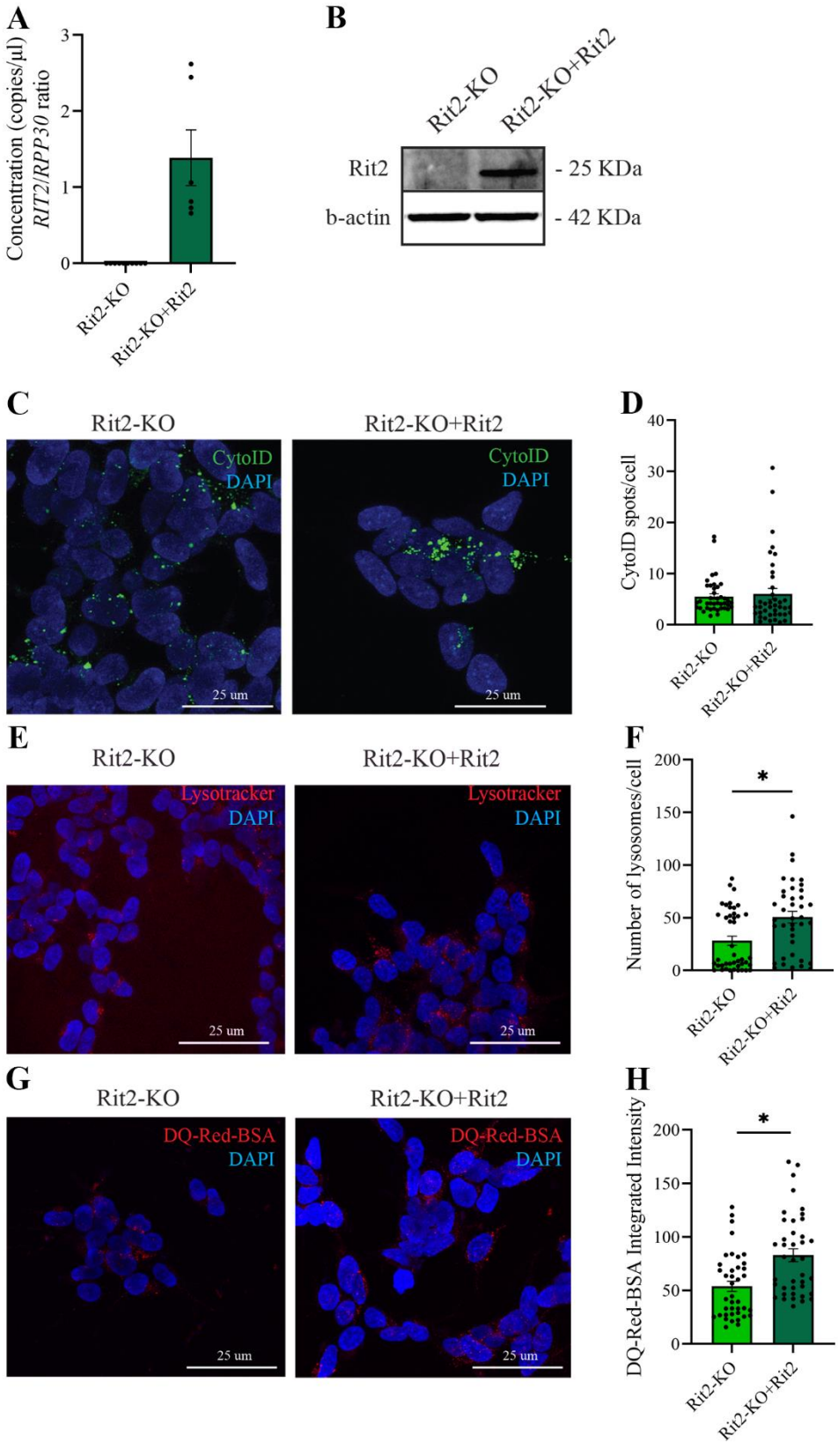
A
Concentration (copies/µl)
RIT2/RPP30 ratio
3
2
1
0
Rit2-KO
Rit2-KO+Rit2
B
Rit2-KO
Rit2-KO+Rit2
Rit2
- 25 KDa
b-actin
- 42 KDa
C
Rit2-KO
Rit2-KO+Rit2
CytoID
DAPI
25 um
D
CytoID spots/cell
40
30
20
10
0
Rit2-KO
Rit2-KO+Rit2
E
Rit2-KO
Rit2-KO+Rit2
Lysotracker
DAPI
25 um
F
Number of lysosomes/cell
200
150
100
50
0
*
Rit2-KO
Rit2-KO+Rit2
G
Rit2-KO
Rit2-KO+Rit2
DQ-Red-BSA
DAPI
25 um
H
DQ-Red-BSA Integrated Intensity
200
150
100
50
0
*
Rit2-KO
Rit2-KO+Rit2

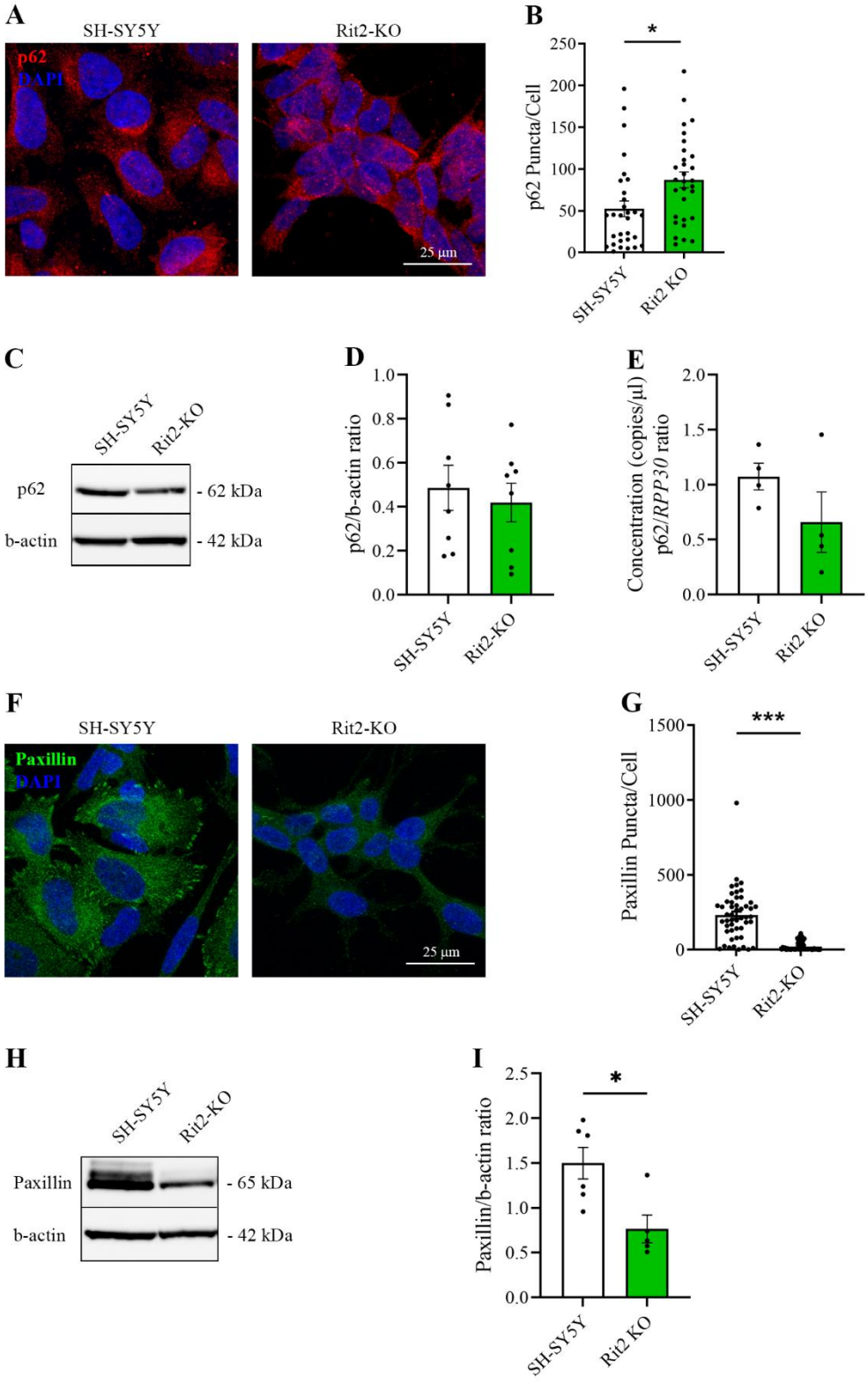
A
SH-SY5Y
Rit2-KO
p62
DAPI
25 µm
B
*
p62 Puncta/Cell
250
200
150
100
50
0
SH-SY5Y
Rit2 KO
C
SH-SY5Y
Rit2-KO
p62
- 62 kDa
b-actin
- 42 kDa
D
p62/b-actin ratio
1.0
0.8
0.6
0.4
0.2
0.0
SH-SY5Y
Rit2-KO
E
Concentration (copies/µl)
p62/RPP30 ratio
2.0
1.5
1.0
0.5
0.0
SH-SY5Y
Rit2 KO
F
SH-SY5Y
Rit2-KO
Paxillin
DAPI
25 µm
G
***
Paxillin Puncta/Cell
1500
1000
500
0
SH-SY5Y
Rit2-KO
H
SH-SY5Y
Rit2-KO
Paxillin
- 65 kDa
b-actin
- 42 kDa
I
*
Paxillin/b-actin ratio
2.5
2.0
1.5
1.0
0.5
0.0
SH-SY5Y
Rit2 KO

**Fig.2.14: The levels of autophagy substrates p62 and Paxillin are altered in Rit2-KO cells. A** Representative images of p62 immunofluorescence in naïve SH-SY5Y and Rit2-KO cells. **B** Quantification of p62 positive puncta per cell. Data are shown as mean ± SEM (n=4). *p<0.5 two tailed Student's t-test. **C** Representative images of Western blot for p62 in naïve SH-SY5Y and Rit2-KO cells. **D** Quantification of the levels of p62 normalized to b-actin. Data are shown as box plots (n=8). No differences were detected by two tailed Student's t-test. **E** Quantification of p62 mRNA levels by ddPCR normalized to RPP30 in naïve SH-SY5Y and Rit2-KO cells. Data are shown as mean ± SEM (n=4). No differences were detected by two tailed Student's t-test. **F** Representative images of Paxillin immunofluorescence in naïve SH-SY5Y and Rit2-KO cells. **G** Quantification of Paxillin positive puncta per cell. Data are shown as mean ± SEM (n=4). ***p<0.001 two tailed Student's t-test. **H** Representative images of Western blotting for Paxillin in naïve SH-SY5Y and Rit2-KO cells. **I** Quantification of the protein levels of Paxillin normalized on b-actin. Data are shown as mean ± SEM (n=6). *p<0.05 two tailed Student's t-test.

## 2.9 Rit2 is involved in TPC2-mediated calcium release from the lysosomes

The observation we made in Rit2-KO cells suggest an involvement of Rit2 in mechanism/s that regulate ALP, and specifically lysosomal function. Increasing evidence link calcium signaling to regulation of autophagy at different steps. Importantly, lysosomes have been recognized as important calcium stores, containing luminal concentrations that are up to 10 times those in the cytosol, depending on the cell type [162]. The efflux of calcium from endo-lysosomal calcium channels TRPML1 and TPCs has been demonstrated to affect lysosome biogenesis, homeostasis, and function (extensively reviewed in [45]). Of note, LRRK2 overexpression has been shown to induce autophagosome formation via the activation of the CaMKK-β/AMPK pathway, including the activation of the NAADP-sensitive TPC2 located on the lysosomal membrane. A specific antagonist of NAADP, Ned-19, was able to revert the increase in autophagosome number and lysosomal alkalinization elicited by LRRK2 overexpression [96]. In line with this work, G2019S LRRK2 patient-derived fibroblasts displayed lysosomal morphological defects and alkalinization, that were restored by TPC2 inhibition [107]. These works provide the evidence of LRRK2-dependent modulation of lysosomal calcium efflux from TPC2 and its relevance in regulating lysosomal function. On the other hand, Rit2 can bind calmodulin, therefore a role in calcium signaling has been proposed [116], even though never further dissected. Since we found a deep interplay between Rit2 and LRRK2, and we propose a specific role for Rit2 in regulating lysosomal function, we sought to investigate whether Rit2 could physiologically modulate calcium efflux from the TPC2 lysosomal calcium channel.

We measured calcium transients evoked by a selective TPC2 agonist, TPC2-A1-N, (which has been recently described and pharmacologically characterized [163]) in naïve SH-SY5Y and Rit2-KO cells. First of all, we monitored cytosolic calcium fluctuations upon TPC2-A1-N treatment by live imaging using the cell permeable Fura-2 calcium indicator (**Fig.2.15A**). We applied different concentrations of TPC2-A1-N to establish a dose/response curve in both naïve SH-SY5Y and Rit2-KO cells (**Fig.2.15B**; fitting: SH-SY5Y $R^2 = 0.70$, Rit2-KO $R^2 = 0.73$). We observed that the $EC_{50}$ was lower in Rit2-KO cells, indicating a higher responsiveness to TPC2 activation. Moreover, Fura-2 fluorescence was significantly higher in Rit2-KO cells with respect to naïve SH-SY5Y cells (**Fig.2.15B**), indicating a greater TPC2-mediated calcium efflux in these cells. This result strongly indicates that Rit2 may play a role in the modulation of calcium signaling upon the activation of the lysosomal calcium channel TPC2, possibly inhibiting it. We used a second, complementary approach to measure calcium transients upon TPC2 activation. Specifically, we nucleofected both naïve SH-SY5Y and Rit2-KO cells with a construct containing a green genetically encoded calcium indicator (G-GECO) fused to the TPC2 channel itself. This construct was kindly donated by the lab of Prof. Antony Galione (Department of Pharmacology, University of Oxford, Oxford, UK) [164]. The advantage of this methodology rests in the specific measurement of calcium upon its release from the channel, of interest since the indicator is located immediately close to the released calcium (**Fig.2.15C**). This makes it a reliable tool to specifically measure lysosomal calcium efflux from this specific channel, rather than measuring cytosolic calcium, that is also affected by release from other calcium stores, owning to better spatial specificity. Although still preliminary, the results obtained with this approach are in line with the Fura-2 experiments, indicating an increase in TPC2-A1-N-evoked calcium transients in Rit2-KO cells (**Fig.2.15D**). This consistency corroborates a physiological role for Rit2 in the modulation of lysosomal calcium release, through which it could regulate lysosome biology and function. Additional work is required to demonstrate whether the calcium transients that we measured are specifically evoked by TPC2 activation (albeit a strong indication exists as we reduced these signals using the Ned-19 antagonist) and whether they specifically come from calcium stored in the lysosomes. However, the results obtained in Rit2-KO cells are in line with those in the literature obtained in G20192 LRRK2 fibroblast, where the overactivation of TPC2 channel elicited by this LRRK2 mutation produced lysosomal

alkalinization and morphological defects [107]. We are currently looking at TPC2-mediated calcium release in our G2019S LRRK2 cells (where Rit2 is downregulated), in order to draw a parallel between these experimental paradigms. Our results further point to the involvement of Rit2 in the modulation of lysosomal function, possibly via the modulation of lysosomal calcium release in a mechanism which might be shared with LRRK2 (a detail that needs dedicated experimental address). The neuronal relevance of this mechanism also needs to be clarified. However, extensive evidence suggests that calcium homeostasis in dopaminergic neurons might be a valuable target for developing new drugs for PD patients. Rit2 has been found downregulated in PD patients, specifically in dopaminergic neurons of SNpc [143], where it regulates DAT endocytosis [140]. The endocytic and lysosomal pathways are strictly interconnected, therefore alterations of Rit2 expression or activity may underlie susceptibility towards pathological alterations. Additionally, it has been recently discovered that the G2019S LRRK2 mutation in immune cells exerts cytotoxicity by over-activating TFEB in a NAADP-TPC2 calcium signaling dependent manner [165], possibly extending the role of Rit2-LRRK2 axis in modulation of (neuro)inflammation.

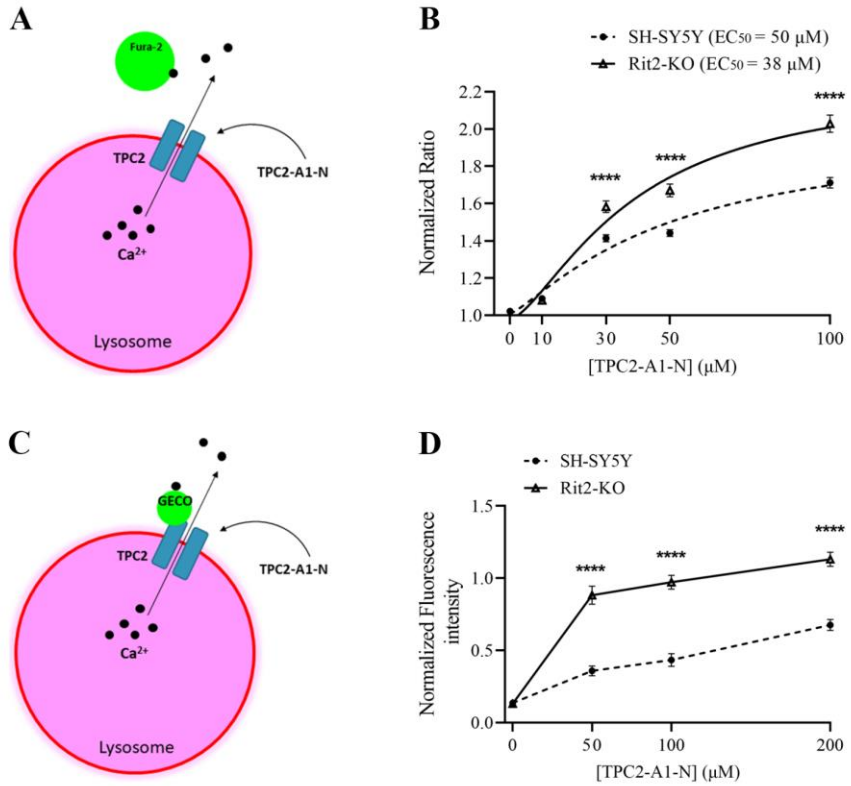

**Fig.2.15: Rit2 modulates TPC2-mediated lysosomal calcium release. A** Schematic overview of Fura-2 experiments, highlighting cytosolic localization of calcium indicator. **B** Concentration-effect response of Fura-2 fluorescence upon application of different concentrations of TPC2-A1-N (three independent experiments, 60 cells analyzed). ****$p<0.0001$ Multiple Mann-Whitney tests. **C** Schematic overview of TPC2-G-GECO1.2 experiments, highlighting lysosomal localization of calcium indicator. **D** Concentration-effect response of TPC2-G-GECO1.2 fluorescence upon application of different concentration of TPC2-A1-N (two independent experiments, 100 cells analyzed). ****$p<0.0001$ Multiple Mann-Whitney tests.

# 3. Conclusions and future perspectives

In this work we corroborate the view that variations in expression (and possibly activity) of the small neuronal GTPase Rit2 could underly PD pathogenesis. We further validated the neuroprotective role of Rit2, exploring for the first time its potential beneficial effect in complementary *in vitro* and *in vivo* models, and dissecting the molecular mechanism involved. We discovered a novel axis between the PD susceptibility genes LRRK2 and Rit2, that is involved in the regulation of lysosomal function, a hot-topic in LRRK2 biology and PD pathogenesis. Therefore, we propose the small GTPase Rit2, and the molecular mechanisms in which it is involved, as novel targets for the development of future, and hopefully, disease-modifying therapeutic approaches. Nevertheless, for this to be completely successful, further work will need to address a few outstanding questions. The regulation of *RIT2* gene expression requires attention, as it appears to be involved in PD pathogenesis. We found a nexus between Rit2 and LRRK2, and possibly its kinase activity, that needs further exploration. It is possible that differential regulation of Rit2 expression could modulate the penetrance of the disease, that has been found incomplete in LRRK2 PD patients. In this view, Rit2 would act as a modifier of the pathogenic process, modulating risk depending on its expression levels. Consistently, we found that Rit2 and LRRK2 interact, and that Rit2 is able to modulate LRRK2 kinase activity, even in a non-LRRK2-based mouse model. This is of particular interest in the view of finding a therapeutic approach that is applicable to not only familial PD, but also to the more common idiopathic form. However, the properties of this Rit2-LRRK2 interaction and the mechanism through which Rit2 modulates LRRK2 kinase activity require specific dissection at the molecular level. We found a neuroprotective role of Rit2, and we propose to be exerted, at least partially, via containment of pathologic hyperactivation of the LRRK2 kinase and subsequent promotion of lysosomal function. Of note, lysosome-mediated protein degradation via the CMA pathway is deeply implicated in LRRK2 biology and αSyn pathology, and it would be interesting to evaluate whether Rit2 might be implicated in this process as well. Our results demonstrate a neuron-relevant physiological role of Rit2 in the regulation of lysosomal function. Additionally, we propose the involvement of Rit2 in the modulation of lysosomal calcium signaling, a mechanism in which LRRK2 plays an established role and that is involved in the regulation of lysosomal

function itself. A better dissection of the molecular mechanism mediating these processes is needed: for example, future work would address whether Rit2 and LRRK2 act in synergy and/or have independent roles; dissect the role of LRRK2 kinase activity; explore whether Rit2 could directly modulate lysosomal calcium channels activity, and conversely whether this putative interaction might be affected by lysosomal channels modulation. To conclude, the physiological role of Rit2 appears deeply related to the physiology of dopaminergic neurons, which are highly susceptible to neurodegeneration in PD. Of note, a single-cell transcriptomic analysis revealed a subtype of nigral dopaminergic neurons that lose Rit2 expression in PD patients, and is particularly susceptible to PD pathology and neurodegeneration [143]. This evidence will contribute to the molecular delineation of neuronal subpopulations that are more sensitive to pathology and to identify specific sensitivity factors. However, the precise mapping of Rit2 gene and protein expression in human brain is still to be defined. Also, the indication of Rit2 expression inside putative susceptible neuronal subtypes that have been recently identified [166] is missing. On the other hand, LRRK2 expression is particularly enriched in the brain regions receiving dopaminergic input (i.e. cortex and striatum), but relatively low in the midbrain [167]. Therefore, LRRK2 neurotoxicity in PD can be explained by a non-cell autonomous manner, retrogradely propagating from the nigral-striatal terminals, or by a cell-specific function of LRRK2 that is altered during pathology, possibly hampering compensatory mechanisms, or even a combination of the two. In all these possible cases, effectors and interactors that could modulate LRRK2 toxicity need to be defined, and we propose that Rit2 would be a candidate target for future studies. The generation of novel Rit2-based animal and human-relevant models would be key in broadening the view on pathophysiology of PD and to unequivocally determine the role played by Rit2.

# 4. Materials and Methods

## 4.1 Cell cultures

Naïve SH-SY5Y cells were obtained from Cell bank IRCCS AOU San Martino IST [168]. They were maintained in DMEM High Glucose (Biowest, L0103), supplemented with 10% fetal bovine serum (FBS; Sigma-Aldrich F2442) and 1% penicillin/streptomycin (Biowest, L0022).

SH-SY5Y cells stably overexpressing WT LRRK2 and G2019S LRRK2 were obtained from the Department of Neurosciences KU Leuven [169]. They were maintained in DMEM High Glucose, supplemented with 15% FBS, 1% MEM non-essential amino acids (Sigma-Aldrich, M7145), 50 µg/ml gentamicin sulphate (Sigma-Aldrich, G-1397) 200 or 400 µg/ml hygromycin B (Invitrogen, 10687010) for WT LRRK2 or G2019S LRRK2 cells respectively.

SH-SY5Y Rit2-KO cells were obtained from Division of Neurology/Molecular Brain Science, Kobe University Graduate School of Medicine, Kobe, Hyogo, Japan [118]. They were maintained in DMEM High Glucose, supplemented with 20% FBS and 1% penicillin/streptomycin.

HEK293T cells were maintained in MEM (Biowest, L0440), supplemented with 10% FBS, 1% non-essential amino acids, 1% L-Glutamine (Biowest, X0550), and 1% penicillin/streptomycin.

All cells were incubated at 37°C with 5% $CO_2$ and passaged two or three times a week depending on confluency using 0.05% trypsin-EDTA (Gibco, 25300-054).

## 4.2 Pharmacological treatments

The LRRK2 kinase inhibitor PF-06447475 (Pfizer; referred as PF-475,) was dissolved in DMSO at a concentration of 10mM under sterile conditions. PF-475 was diluted in complete medium and applied to cultured cells for 2 or 6 hours at concentration of 500 nM.

Chloroquine (CQ; Thermo Fisher L10382) was prepared as aqueous solution at a stock concentration of 50mM CQ was applied for 3 hours at a concentration of 100 µM in complete medium to block the fusion of autophagosomes with lysosomes and to evaluate the autophagic flux in cells.

## 4.3 Nucleofection and plasmids

Cells were transfected using the SF Cell Line 4D-Nucleofector X kit L (Lonza, V4XC-2024). Nucleofection was carried out according to the manufacturer's protocol. Briefly, $2x10^6$ cells were gently resuspended in 100 µl of nucleofection solution mix (82 µl SF Cell Line Solution + 18 µl Supplement) containing 2 µg of plasmid DNA,and nucleofected in the 4D Nucleofector X unit applying the CA-137 program. The reaction was incubated 10 minutes at RT and then 500 µl of complete plating medium were added. Cells were plated on appropriate culture vessel and processed after 48h (for CO-IP) or 72h (restoration of *RIT2* expression).

h*RIT2* coding sequence was amplified by PCR from the SC118279 plasmid (Origene) using the following pair of primers (fw: CGGATATCAAGATGGAGGTAGAAAATGAA; rev: CCGCTCGAGCGGTCATGTCATATTTTCTCTC). The PCR product was cloned inside pcDNA3.1/Hygro$^+$ vector (Thermo Fisher, V87020) into EcoRV and XhoI cloning sites. WT and G2019S LRRK2 tagged with 2xMyc constructs, cloned into pCMV vector, were used in HEK293T cells for Rit2-LRRK2 CO-IP and PLA experiments. For Rit2-LRRK2 PLA, RIT2-TurboGFP cloned in pCMV vector (Origene, RG205367) was used. TPC2-G-GECO1.2 cloned in pCMV vector was kindly donated by the lab of Prof. Antony Galione (Department of Pharmacology, University of Oxford, Oxford, UK) [164].

## 4.4 RNA extraction, reverse transcription, ddPCR

Total RNA was extracted using RNeasy Plus Mini Kit (Qiagen, 74104) following manufacturer's protocol. DNase treatment for 15 minutes at RT, was carried out to remove DNA contamination. RNA concentration was determined using Qubit RNA High Sensitivity Kit (Invitrogen, Q32855) following manufacturer's instructions. RNA quality was assessed by 1% agarose gel electrophoresis.

cDNA was synthesized using the SuperScript VILO cDNA Synthesis Kit (Invitrogen, 11754250) following manufacturer's protocol. Briefly, 1 µg of RNA was retrotranscribed in 20 µl of total volume reaction. As negative control, the reaction mix was prepared without the 10x Superscript enzyme mix. Reverse transcription cycling conditions were 25°C for 10 minutes, 42°C for 60 minutes, 85°C for 5 minutes.

To quantify *RIT2* and p62/*SQSTM1* expression, 7ng and 1 ng of cDNA, were used in ddPCR experiments and mixed to ddPCR Supermix for Probes (no dUTPs; Biorad, 1863025) following manufacturer's instructions. Predesigned assays were selected to specifically amplify *RIT2* (IDT, HsPT58196183 FAM) and p62/*SQSTM1* (IDT, HsPT584078835.gs FAM). Assays for genes of interest were multiplexed with the gene expression assay of the housekeeping gene *RPP30* (Biorad, dHsaCPE5038241 HEX). Negative template control (NTC) was prepared by omitting sample cDNA in the reaction mix. Droplets were generated inside the QX200 Droplet Generator (Biorad) using the Droplet Generation Oil for Probes (Biorad, 1863005). Droplets were transferred in an appropriate plate (Biorad, 17005224) and subjected to PCR amplification following the protocol: 95°C for 10 minutes, 39 cycles of 94°C for 30 seconds and 57°C for 2 minutes, 98°C for 10 minutes. After PCR amplification, the content was measured using the QX200 Droplet Reader (Biorad), setting direct quantification as type of experiment. Data were analyzed using QuantaSoft software from Biorad. Amplitude threshold in FAM and HEX channels was set individually for each channel. Results are reported as a ratio between concentration (number of copies/ µl) of the gene of interest and concentration of the housekeeping gene.

## 4.5 Western blotting

Western blotting was used to investigate protein levels. Cells were lysed in Pierce RIPA lysis buffer (Thermo Fisher, 89900) containing protease inhibitors (cOmplete tablets; Roche, 04693124001) and phosphatase inhibitors (PhosSTOP; Roche, 4906837001) and incubated on ice for 30 minutes. Then, lysates were sonicated for 10 seconds at 10% intensity, centrifuged at 10000 rcf for 10 minutes at 4°C and the supernatant transferred to a new tube. Protein concentration of the lysates was determined against a bovine serum albumin (BSA) standard curve using the Pierce bicinchoninic acid (BCA) Protein Assay Kit (Thermo Fisher, 23225). Absorbance was read using the Envision plate reader (Perkin Elmer) at 562 nm. Protein concentration was extrapolated using a linear regression of the standard curve. Same amount of total proteins (15-25 µg, 50 µg for Rit2) for each sample were mixed to LDS sample buffer (Invitrogen; NuPAGE, NP0007) and reducing agent (containing 50 mM dithiothreitol; Invitrogen; NuPAGE, NP0009), and further denatured at 95°C for 5 minutes. Denatured samples were immediately loaded onto 4-12% Bis-Tris Protein Gels (Invitrogen;

NuPAGE). MOPS running buffer (Invitrogen; NuPAGE, NP0001-02) was used during gel electrophoresis. MES running buffer (Invitrogen; NuPAGE, NP0002-02) was used to resolve LC3B double band. Proteins were separated applying constant voltage (120V) for about 1 hour and 30 minutes. After gel electrophoresis the proteins were transferred onto polyvinylidene difluoride (PVDF) membrane (Biorad, 1620177) applying constant current (100mA) overnight (16 hours) at 4°C in transfer buffer (Invitrogen; NuPAGE, NP00061) plus 20% methanol. For Rit2 detection, transfer conditions were 2 hours and 30 minutes at 300mA at 4°C. Transfer efficiency was controlled with Ponceau S staining and washed in dd$H_2O$ and finally in 1X Tris-buffered saline (TBS; Thermo Fisher, 28358). Membranes were then blocked with appropriate blocking solution for 1 hour at RT. Primary antibodies (**Table 4.1**) were diluted in appropriate solution and incubated overnight at 4°C. After three washing steps in TBS-0.1% Tween 20 (Biorad, 161-0781; TBS-T), secondary antibody (**Table 4.1**) was diluted in 5% milk (Sigma Aldrich, 70166) and incubated for 1 hour and 30 minutes at RT. Then membranes were washed three times with TBS-T, incubated 5 minutes in Clarity Wester ECL substrate solution (Biorad, 1705060) in the dark, and chemiluminescence images were acquired using Chemidoc Touch (Biorad). Relative band intensity levels were calculated using ImageLab software (Biorad).

**Table 4.1: Primary and secondary antibodies used for Western blotting**

| **Primary antibodies** | | | | |
|---|---|---|---|---|
| **Target** | **Species** | **Product code** | **Dilution factor** | **Blocking/antibody solution** |
| Rit2 | Mouse | Origene, TA501704 | 1:1000 | 5% milk in TBS-T |
| LRRK2 | Rabbit | Abcam, ab133474 | 1:10000 | 5% milk in TBS-T |
| pSer1292-LRRK2 | Rabbit | Abcam, ab203181 | 1:1000 | 5% BSA in TBS-T |
| pSer935-LRRK2 | Rabbit | Abcam, ab133450 | 1:1000 | 5% BSA in TBS-T |
| αSyn | Mouse | Abnova, MAB5383 | 1:2000 | 5% milk in TBS-T |
| p62 | Rabbit | Novus Biologicals, NBP1-48320 | 1:4000 | 5% milk in TBS-T |
| LC3B | Rabbit | CST, 3868 | 1:2000 | 5% milk in TBS-T |
| Paxillin | Mouse | BD Biosciences, 610051 | 1:1000 | 5% milk in TBS-T |
| b-actin | Mouse | Sigma-Aldrich, A2228 | 1:12000 | 5% milk in TBS-T |
| **Secondary antibodies** | | | | |
| Mouse IgG, HRP conjugated | Rabbit | Millipore, AP160P | 1:10000 | 5% milk in TBS-T |
| Rabbit IgG, HRP conjugated | Mouse | Millipore, AP188P | 1:10000 | 5% milk in TBS-T |

## 4.6 Cyto-ID live staining

CYTO-ID Autophagy Detection Kit (Enzo Lifesciences, ENZ-51031-K200) was used to specifically stain autophagic vesicles (mainly autophagosomes and autolysosomes) in living cells. The assay was carried out following manufacturer's instructions. Briefly, Cyto-ID Green detection reagent was diluted in 1X assay buffer, supplemented with 10% FBS, and incubated for 30 minutes in incubator. After three washes in assay buffer, complete medium containing DAPI for live imaging (Invitrogen, R37605) was added on cells prior to imaging processing. Live imaging was carried out under controlled temperature (37°C) and $CO_2$ (5%) conditions at the Leica SP8-X laser scanning confocal microscope at 63X magnification. Images were analyzed using CellProfiler software to count the number of fluorescent objects per cell, indicative of the number of autophagic vesicles.

## 4.7 Lysotracker Deep Red staining

To investigate lysosomes morphology and number Lysotracker Deep Red dye (Invitrogen, L12492) was used. On the day of experimentation cells were washed twice with HBSS (Gibco, 14025-050) and then incubated with Lysotracker dye at a final concentration of 50nM in HBSS for 20 minutes in incubator. After the incubation cells were washed twice with HBSS and then imaged in complete medium containing DAPI for live imaging. Cells were visualized live, under controlled temperature (37°C) and $CO_2$ (5%) conditions, on the Leica SP8-X laser scanning confocal microscope at 63X magnification, using the *resonant* function. Single stacks were reconstructed in Imaris software (Oxford Instruments, BitPlane) to a 3D structure and number and diameter of lysosomes quantified by the software.

## 4.8 DQ-Red-BSA assay

To study the proteolytic activity of lysosomes, the fluorescent DQ-Red-BSA dye (Invitrogen, D12051) was used. DQ-Red-BSA powder was dissolved at a concentration of 1 mg/ml in sterile PBS (Biowest, L0615). The day of experimentation cells were incubated with the dye in complete medium for 120 minutes in incubator. After the incubation cells were washed three times with PBS and then imaged in complete medium containing DAPI for live imaging. Cells were visualized live, under controlled temperature (37°C) and $CO_2$ (5%) conditions, on the Leica SP8-X laser scanning confocal microscope at 63X magnification.

Projected stack images were then analyzed with CellProfiler to quantify the number and intensity of fluorescent spots per cell, indicative of the number of active lysosomes.

## 4.9 Immunofluorescence

Cells, plated on glass coverslips (12 mm), were fixed in 4% paraformaldehyde (PFA; Santa Cruz, sc-281692) for 20 minutes at RT and then washed three times in 1x phosphate buffered saline (PBS). Cells were then permeabilized for 5 minutes with 0.5% Triton X-100 (Sigma-Aldrich, T8787) in PBS at RT and subsequently blocked in 3% BSA (Sigma-Aldrich, A9418) in PBS for 30 minutes at RT. After blocking cells were incubated with primary antibodies (**Table 4.2**) diluted in 0.05% Triton X-100 in PBS shaking overnight at 4°C. The following day, after three washing with PBS, cells were incubated with secondary fluorescent antibodies (**Table 4.2**) in 0.05% Triton X-100 in PBS for 2h at RT. Cells were washed three times in PBS and in the last wash step NucBlue Fixed Cell ReadyProbes Reagent (Invitrogen, R37606) was added to stain nuclei. Coverslips were mounted using fluorescent mounting medium (Agilent; Dako, S3023) and then sealed with nail polish. Visualization of stained coverslips was performed using a Leica SP8-X confocal laser scanning microscope system equipped with a 63X oil immersion objective. Images were analyzed as projected stacks with custom pipelines in CellProfiler.

**Table 4.2: Primary and secondary antibodies used for immunofluorescence.**

| **Primary antibodies** | | | |
|---|---|---|---|
| **Target** | **Species** | **Product code** | **Dilution factor** |
| pSer129-αSyn | Mouse | Abcam, ab184674 | 1:2000 |
| Paxillin | Mouse | BD Biosciences, 610051 | 1:1000 |
| p62 | Rabbit | Novus Biologicals, NBP1-48320 | 1:2000 |
| **Secondary antibodies** | | | |
| Mouse IgG, Alexa Fluor 555 conjugated | Donkey | Invitrogen, A31570 | 1:1000 |
| Mouse IgG, Alexa Fluor 488 conjugated | Donkey | Invitrogen, A21202 | 1:1000 |
| Rabbit IgG, Alexa Fluor 555 conjugated | Donkey | Invitrogen, A31572 | 1:1000 |

## 4.10 Proximity ligation assay

Cells for PLA were processed as for immunofluorescence experiments. After fixation, coverslips were washed three times in PBS and then blocked for 30 minutes in Duolink Blocking Solution at RT. Primary antibodies (pS1292 LRRK2, Abcam ab203181 combined to

total LRRK2, UC Davis #75-36253 for pS1292-LRRK2; total LRRK2, Abcam ab133474 combined to Rit2, Origene TA501704 for Rit2-LRRK2 PLA) were diluted 1:500 in Duolink Antibody Diluent and incubated overnight at 4°C with gentle shaking. After 2x5 minutes washes in PBS + 0.1% Triton-X100, coverslips were incubated with 1:5 PLA probes (Duolink in situ PLA Probe anti-Mouse MINUS, Sigma-Aldrich DUO92004, and Duolink in situ PLA Probe anti-Rabbit PLUS, Sigma-Aldrich, DUO92002) in Duolink Antibody Diluent and incubated for 90 minutes at 37°C. After 3x5 minutes washes in 1x PBS + 0.1% Triton-X100 coverslips were incubated in ligation solution (1:5 Duolink Ligation stock + 1:40 Ligase in $ddH_2O$) for 45 min at 37°C. After ligation coverslips were washed 2x5 minutes in PBS and then incubated with an amplification solution (1:5 Duolink Amplification stock + 1:80 Polymerase in $ddH_2O$) for 100 minutes at 37°C. After the amplification step coverslips were washed twice in PBS for 10 minutes and in the last wash step NucBlue Fixed Cell ReadyProbes Reagent was added to stain nuclei. Coverslips were mounted using fluorescent mounting medium (Agilent; Dako, S3023) and then sealed with nail polish. Visualization of stained coverslips was performed using a Leica SP8-X confocal laser scanning microscope system equipped with a 63X oil immersion objective and analysis of PLA spots was carried out using the "Particle Analysis" function in Fiji (ImageJ, NIH)

### 4.11 Co-immunoprecipitation

Cells were mechanically lysed in lysis buffer composed of 50 mM Tris-HCl (pH=7.6), 150 mM NaCl, 1% IGEPAL CA-630, 0.1% SDS (Sodium Dodecyl Sulfate), protease/phosphatase inhibitors cocktail, and incubated 30 minutes on ice. Total lysates were cleared by centrifugation for 10 minutes at 13000 rcf, at 4°C. Protein concentration was assessed by BCA assay and samples volume was adjusted so that all samples were at same concentration of 1 mg/ml. Pre-clearing was performed incubating samples with protein G-agarose (Roche, 11719416001) with gentle agitation for 30 minutes at 4°C. After pre-clearing, 0.5 mg of protein extracts were incubated overnight at 4°C with 5 µg of rabbit anti-LRRK2 antibody (Abcam, ab133474), or with same species IgG (Sigma-Aldrich, 12-370) as negative control. The day after, samples were incubated with 100 µl of protein G-agarose for 2 hours at 4°C. After centrifugation, supernatants were conserved for Western-blotting analysis (~ 40 µg), and protein G-agarose pellets were washed three times and resuspended in 2X LDS

sample buffer and processed for SDS-PAGE following the procedure described above. Primary antibodies used for membrane immunolabelling were anti-Rit2 mouse (Origene, TA501704), and anti-LRRK2 rabbit (Abcam, ab133474). Three independent experiments were performed.

## 4.12 Intracellular calcium imaging

### *4.12.1 Fura2-AM calcium imaging*

SH-SY5Y WT and/or Rit2-KO cells were plated on poli-D-lysine-coated glass dishes and grown for 48 hours in complete media. TPC2-A1-N-evoked cytosolic calcium dynamics were evaluated in Fura2-AM loaded cells. Briefly, cells were loaded with 2.5 µM of Fura2-AM (Invitrogen, F1221) for 30 min at 37 °C and washed using a calcium-free Krebs solution containing in mM: 140 NaCl, 5,4 KCl, 2.9 $MgCl_2$, 5.0 HEPES, 10 D-(+) glucose and 0.1 EGTA; pH adjusted to 7.3 with NaOH. Dishes were then placed on the stage of an epifluorescence Eclipse-Ti microscope (Nikon) equipped with a 75 W Xenon lamp, associated to a monochromator commanded by the Optoscan system (CAIRN research, Faversham, Kent, UK) and connected to the Evolve 512 Delta CCD camera (Photometrics, Tucson, AZ, USA). Cells were excited at 340 nm and 380 nm wavelengths alternatively, and the fluorescence emission was recorded using the MetaFluor Software (Molecular Devices, Sunnyvale, CA, USA) by sampling the signal at 0.5 Hz for a total of 900 frames. Calcium transients were evoked by the application of the vehicle (1% DMSO) or different concentrations of TPC2-A1-N (MedChemExpress, HY-131614; 10-100 µM in calcium-free Krebs solution) directly to the dish (400 µl). At the end of each experiment, the proper loading of the cells was checked by applying 5 seconds pulse of 2 µM ionomycin (Sigma-Aldrich, I3909) dissolved in a high-calcium Krebs solution (10mM $CaCl_2$). All the experiments were performed at room temperature (23-25°C). Data analysis was performed off-line using the Excel software (Office suite). The background fluorescence signal was acquired during each experiment and then subtracted from each fluorescence value at each experimental wavelength (i.e., 340 and 380 nm). After that, the 340/380 ratio was calculated and normalized to each cell-baseline value computed as the average of the first 90 acquired episodes. The highest value of fluorescence (peak or plateau) obtained, for each cell, after agonist (or vehicle) application was determined and used to obtain the concentration/response

curves. the data fitting (nonlinear agonist vs. response equation) as well as the statistical analyses (multiple Mann-Whitney tests) were performed using GraphPad Prism 9. Three independent experiments were carried out, and a total of at least 60 cells per conditions were analyzed.

### *4.12.2 TPC2-G-GECO1.2 calcium imaging*

SH-SY5Y WT and Rit2-KO cells were nucleofected with TPC2-G-GECO1.2, plated on imaging chamber slides (Ibidi, 80426), and processed after 48 hours for evaluation of TPC2-A1-N-evoked lysosomal calcium release. Briefly, cells were washed using a calcium-free Krebs solution. DAPI for live imaging was added in the last washing step. Live cell imaging was performed at RT on an Eclipse Ti2 fluorescence microscope equipped with a DS-Qi2 camera (Nikon) using 20X dry objective. Cells were exited with 488 nm wavelength and fluorescence emission was followed in time-lapse acquisition (frames acquired with an interval of 0,5 seconds for the duration of 5 minutes). Calcium transients were evoked by the application of the vehicle (1% DMSO) or different concentrations of TPC2-A1-N (50-200 µM in calcium-free Krebs solution) directly to the well (300 µl). At the end of each experiment, the proper transfection of the cells was checked by applying 2 µM ionomycin in high-calcium Krebs solution. Fluorescence intensity of each cell was analyzed inside manually drawn ROIs with Fiji software. Data handling was performed using the Excel software (Office suite). The background fluorescence signal was acquired during each experiment and then subtracted from each fluorescence value. Fluorescence signal was then normalized to each cell-baseline value. The highest value of fluorescence (peak or plateau) obtained for each cell after agonist (or vehicle) application was determined and used to obtain the concentration/response curves. Statistical analyses (multiple nonparametric Mann-Whitney tests) were performed using GraphPad Prism 9. Two independent experiments were carried out, and a total of at least 100 cells per conditions were analyzed.

## 4.13 Statistical analysis

Statistical analyses were performed using GraphPad Prism 9. Data distribution was assessed using the D`Agostino-Pearson test for normal distribution. One-way ANOVA followed by Bonferroni´s post-hoc test, or Kruskal-Wallis followed by Dunn’s post-hoc test

were used in experiments comparing 3 or more groups. Unpaired two-tailed Student´s t-test or two-tailed Mann-Whitney test was utilized when comparing 2 experimental groups. Threshold for significance was set at $p<0.05$. Details of statistical analysis are present in figure legends.

# References


1. Rocca, W.A., *The burden of Parkinson's disease: a worldwide perspective.* Lancet Neurol, 2018. **17**(11): p. 928-929.
2. Poewe, W., et al., *Parkinson disease.* Nat Rev Dis Primers, 2017. **3**: p. 17013.
3. Thomsen, T.R. and R.L. Rodnitzky, *Juvenile parkinsonism: epidemiology, diagnosis and treatment.* CNS Drugs, 2010. **24**(6): p. 467-77.
4. Bloem, B.R., M.S. Okun, and C. Klein, *Parkinson's disease.* Lancet, 2021. **397**(10291): p. 2284-2303.
5. Parkinson, J., *An essay on the shaking palsy. 1817.* J Neuropsychiatry Clin Neurosci, 2002. **14**(2): p. 223-36; discussion 222.
6. Frank, C., G. Pari, and J.P. Rossiter, *Approach to diagnosis of Parkinson disease.* Can Fam Physician, 2006. **52**: p. 862-8.
7. Gibb, W.R. and A.J. Lees, *The relevance of the Lewy body to the pathogenesis of idiopathic Parkinson's disease.* J Neurol Neurosurg Psychiatry, 1988. **51**(6): p. 745-52.
8. Postuma, R.B., et al., *MDS clinical diagnostic criteria for Parkinson's disease.* Mov Disord, 2015. **30**(12): p. 1591-601.
9. Postuma, R.B. and D. Berg, *Prodromal Parkinson's Disease: The Decade Past, the Decade to Come.* Mov Disord, 2019. **34**(5): p. 665-675.
10. Braak, H. and K. Del Tredici, *Neuropathological Staging of Brain Pathology in Sporadic Parkinson's disease: Separating the Wheat from the Chaff.* J Parkinsons Dis, 2017. **7**(s1): p. S71-S85.
11. Postuma, R.B. and D. Berg, *Advances in markers of prodromal Parkinson disease.* Nat Rev Neurol, 2016. **12**(11): p. 622-634.
12. Berg, D., et al., *MDS research criteria for prodromal Parkinson's disease.* Mov Disord, 2015. **30**(12): p. 1600-11.
13. Postuma, R.B., et al., *Validation of the MDS clinical diagnostic criteria for Parkinson's disease.* Mov Disord, 2018. **33**(10): p. 1601-1608.
14. Kwon, E.H., et al., *Update on CSF Biomarkers in Parkinson's Disease.* Biomolecules, 2022. **12**(2).
15. Tolosa, E., et al., *Challenges in the diagnosis of Parkinson's disease.* Lancet Neurol, 2021. **20**(5): p. 385-397.
16. Galvan, A. and T. Wichmann, *Pathophysiology of parkinsonism.* Clin Neurophysiol, 2008. **119**(7): p. 1459-74.

17. Armstrong, M.J. and M.S. Okun, *Diagnosis and Treatment of Parkinson Disease: A Review.* JAMA, 2020. **323**(6): p. 548-560.
18. Vijiaratnam, N., et al., *Progress towards therapies for disease modification in Parkinson's disease.* Lancet Neurol, 2021. **20**(7): p. 559-572.
19. Goedert, M., et al., *100 years of Lewy pathology.* Nat Rev Neurol, 2013. **9**(1): p. 13-24.
20. Breydo, L., J.W. Wu, and V.N. Uversky, *Alpha-synuclein misfolding and Parkinson's disease.* Biochim Biophys Acta, 2012. **1822**(2): p. 261-85.
21. Braak, H., et al., *Staging of brain pathology related to sporadic Parkinson's disease.* Neurobiol Aging, 2003. **24**(2): p. 197-211.
22. Kordower, J.H., et al., *Lewy body-like pathology in long-term embryonic nigral transplants in Parkinson's disease.* Nat Med, 2008. **14**(5): p. 504-6.
23. Li, J.Y., et al., *Lewy bodies in grafted neurons in subjects with Parkinson's disease suggest host-to-graft disease propagation.* Nat Med, 2008. **14**(5): p. 501-3.
24. Guo, J.L. and V.M. Lee, *Cell-to-cell transmission of pathogenic proteins in neurodegenerative diseases.* Nat Med, 2014. **20**(2): p. 130-8.
25. Peng, C., J.Q. Trojanowski, and V.M. Lee, *Protein transmission in neurodegenerative disease.* Nat Rev Neurol, 2020. **16**(4): p. 199-212.
26. Recasens, A., et al., *In vivo models of alpha-synuclein transmission and propagation.* Cell Tissue Res, 2018. **373**(1): p. 183-193.
27. Goedert, M., R. Jakes, and M.G. Spillantini, *The Synucleinopathies: Twenty Years On.* J Parkinsons Dis, 2017. **7**(s1): p. S51-S69.
28. Nussbaum, R.L. and M.H. Polymeropoulos, *Genetics of Parkinson's disease.* Hum Mol Genet, 1997. **6**(10): p. 1687-91.
29. Day, J.O. and S. Mullin, *The Genetics of Parkinson's Disease and Implications for Clinical Practice.* Genes (Basel), 2021. **12**(7).
30. Ascherio, A. and M.A. Schwarzschild, *The epidemiology of Parkinson's disease: risk factors and prevention.* Lancet Neurol, 2016. **15**(12): p. 1257-1272.
31. Nalls, M.A., et al., *Identification of novel risk loci, causal insights, and heritable risk for Parkinson's disease: a meta-analysis of genome-wide association studies.* Lancet Neurol, 2019. **18**(12): p. 1091-1102.
32. Trinh, J. and M. Farrer, *Advances in the genetics of Parkinson disease.* Nat Rev Neurol, 2013. **9**(8): p. 445-54.
33. Kalia, L.V. and A.E. Lang, *Parkinson's disease.* Lancet, 2015. **386**(9996): p. 896-912.

34. Ho, M., et al., *Exploiting autophagy in multiple myeloma.* Journal of Cancer Metastasis and Treatment, 2019. **5**: p. 70.
35. Oku, M. and Y. Sakai, *Three Distinct Types of Microautophagy Based on Membrane Dynamics and Molecular Machineries.* Bioessays, 2018. **40**(6): p. e1800008.
36. Bejarano, E. and A.M. Cuervo, *Chaperone-mediated autophagy.* Proc Am Thorac Soc, 2010. **7**(1): p. 29-39.
37. Kirkin, V., *History of the Selective Autophagy Research: How Did It Begin and Where Does It Stand Today?* J Mol Biol, 2020. **432**(1): p. 3-27.
38. Mizushima, N., *A brief history of autophagy from cell biology to physiology and disease.* Nat Cell Biol, 2018. **20**(5): p. 521-527.
39. Mizushima, N., T. Yoshimori, and Y. Ohsumi, *The role of Atg proteins in autophagosome formation.* Annu Rev Cell Dev Biol, 2011. **27**: p. 107-32.
40. Yang, Z. and D.J. Klionsky, *Mammalian autophagy: core molecular machinery and signaling regulation.* Curr Opin Cell Biol, 2010. **22**(2): p. 124-31.
41. Takahashi, Y., et al., *An autophagy assay reveals the ESCRT-III component CHMP2A as a regulator of phagophore closure.* Nat Commun, 2018. **9**(1): p. 2855.
42. Tian, X., J. Teng, and J. Chen, *New insights regarding SNARE proteins in autophagosome-lysosome fusion.* Autophagy, 2021. **17**(10): p. 2680-2688.
43. Zhao, Y.G. and H. Zhang, *Autophagosome maturation: An epic journey from the ER to lysosomes.* J Cell Biol, 2019. **218**(3): p. 757-770.
44. He, C. and D.J. Klionsky, *Regulation mechanisms and signaling pathways of autophagy.* Annu Rev Genet, 2009. **43**: p. 67-93.
45. Medina, D.L., *Lysosomal calcium and autophagy.* Int Rev Cell Mol Biol, 2021. **362**: p. 141-170.
46. Settembre, C., et al., *A lysosome-to-nucleus signalling mechanism senses and regulates the lysosome via mTOR and TFEB.* EMBO J, 2012. **31**(5): p. 1095-108.
47. Medina, D.L., et al., *Lysosomal calcium signalling regulates autophagy through calcineurin and TFEB.* Nat Cell Biol, 2015. **17**(3): p. 288-99.
48. Levine, B. and G. Kroemer, *Biological Functions of Autophagy Genes: A Disease Perspective.* Cell, 2019. **176**(1-2): p. 11-42.
49. Saha, S., et al., *Autophagy in health and disease: A comprehensive review.* Biomed Pharmacother, 2018. **104**: p. 485-495.
50. Komatsu, M., et al., *Loss of autophagy in the central nervous system causes neurodegeneration in mice.* Nature, 2006. **441**(7095): p. 880-4.

51. Sato, S., et al., *Loss of autophagy in dopaminergic neurons causes Lewy pathology and motor dysfunction in aged mice.* Sci Rep, 2018. **8**(1): p. 2813.
52. Anglade, P., et al., *Apoptosis and autophagy in nigral neurons of patients with Parkinson's disease.* Histol Histopathol, 1997. **12**(1): p. 25-31.
53. Chu, Y., et al., *Alterations in lysosomal and proteasomal markers in Parkinson's disease: relationship to alpha-synuclein inclusions.* Neurobiol Dis, 2009. **35**(3): p. 385-98.
54. Mamais, A., et al., *Analysis of macroautophagy related proteins in G2019S LRRK2 Parkinson's disease brains with Lewy body pathology.* Brain Res, 2018. **1701**: p. 75-84.
55. Menzies, F.M., et al., *Autophagy and Neurodegeneration: Pathogenic Mechanisms and Therapeutic Opportunities.* Neuron, 2017. **93**(5): p. 1015-1034.
56. Senkevich, K. and Z. Gan-Or, *Autophagy lysosomal pathway dysfunction in Parkinson's disease; evidence from human genetics.* Parkinsonism Relat Disord, 2020. **73**: p. 60-71.
57. Cuervo, A.M., et al., *Impaired degradation of mutant alpha-synuclein by chaperone-mediated autophagy.* Science, 2004. **305**(5688): p. 1292-5.
58. Martinez-Vicente, M. and M. Vila, *Alpha-synuclein and protein degradation pathways in Parkinson's disease: a pathological feed-back loop.* Exp Neurol, 2013. **247**: p. 308-13.
59. Sepulveda, D., et al., *Contribution of Autophagy-Lysosomal Pathway in the Exosomal Secretion of Alpha-Synuclein and Its Impact in the Progression of Parkinson's Disease.* Front Mol Neurosci, 2022. **15**: p. 805087.
60. Sidransky, E., et al., *Multicenter analysis of glucocerebrosidase mutations in Parkinson's disease.* N Engl J Med, 2009. **361**(17): p. 1651-61.
61. Xilouri, M., O.R. Brekk, and L. Stefanis, *Autophagy and Alpha-Synuclein: Relevance to Parkinson's Disease and Related Synucleopathies.* Mov Disord, 2016. **31**(2): p. 178-92.
62. Volta, M., *Lysosomal Pathogenesis of Parkinson's Disease: Insights From LRRK2 and GBA1 Rodent Models.* Neurotherapeutics, 2022.
63. Sassone, J., et al., *The Role of VPS35 in the Pathobiology of Parkinson's Disease.* Cell Mol Neurobiol, 2021. **41**(2): p. 199-227.
64. Zhang, F., et al., *The Roles of ATP13A2 Gene Mutations Leading to Abnormal Aggregation of alpha-Synuclein in Parkinson's Disease.* Front Cell Neurosci, 2022. **16**: p. 927682.
65. Tanaka, K., *The PINK1-Parkin axis: An Overview.* Neurosci Res, 2020. **159**: p. 9-15.
66. van der Merwe, C., et al., *Evidence for a common biological pathway linking three Parkinson's disease-causing genes: parkin, PINK1 and DJ-1.* Eur J Neurosci, 2015. **41**(9): p. 1113-25.
67. Correia Guedes, L., et al., *Worldwide frequency of G2019S LRRK2 mutation in Parkinson's disease: a systematic review.* Parkinsonism Relat Disord, 2010. **16**(4): p. 237-42.

68. Kalia, L.V., et al., *Clinical correlations with Lewy body pathology in LRRK2-related Parkinson disease.* JAMA Neurol, 2015. **72**(1): p. 100-5.
69. Bonet-Ponce, L. and M.R. Cookson, *LRRK2 recruitment, activity, and function in organelles.* FEBS J, 2022. **289**(22): p. 6871-6890.
70. Sheng, Z., et al., *Ser1292 autophosphorylation is an indicator of LRRK2 kinase activity and contributes to the cellular effects of PD mutations.* Sci Transl Med, 2012. **4**(164): p. 164ra161.
71. Steger, M., et al., *Phosphoproteomics reveals that Parkinson's disease kinase LRRK2 regulates a subset of Rab GTPases.* Elife, 2016. **5**.
72. West, A.B., et al., *Parkinson's disease-associated mutations in leucine-rich repeat kinase 2 augment kinase activity.* Proc Natl Acad Sci U S A, 2005. **102**(46): p. 16842-7.
73. West, A.B., et al., *Parkinson's disease-associated mutations in LRRK2 link enhanced GTP-binding and kinase activities to neuronal toxicity.* Hum Mol Genet, 2007. **16**(2): p. 223-32.
74. Biosa, A., et al., *GTPase activity regulates kinase activity and cellular phenotypes of Parkinson's disease-associated LRRK2.* Hum Mol Genet, 2013. **22**(6): p. 1140-56.
75. Di Maio, R., et al., *LRRK2 activation in idiopathic Parkinson's disease.* Sci Transl Med, 2018. **10**(451).
76. Greggio, E., et al., *Kinase activity is required for the toxic effects of mutant LRRK2/dardarin.* Neurobiol Dis, 2006. **23**(2): p. 329-41.
77. Lee, B.D., et al., *Inhibitors of leucine-rich repeat kinase-2 protect against models of Parkinson's disease.* Nat Med, 2010. **16**(9): p. 998-1000.
78. Smith, W.W., et al., *Kinase activity of mutant LRRK2 mediates neuronal toxicity.* Nat Neurosci, 2006. **9**(10): p. 1231-3.
79. Daher, J.P., et al., *Leucine-rich Repeat Kinase 2 (LRRK2) Pharmacological Inhibition Abates alpha-Synuclein Gene-induced Neurodegeneration.* J Biol Chem, 2015. **290**(32): p. 19433-44.
80. Jennings, D., et al., *Preclinical and clinical evaluation of the LRRK2 inhibitor DNL201 for Parkinson's disease.* Sci Transl Med, 2022. **14**(648): p. eabj2658.
81. Azeggagh, S. and D.C. Berwick, *The development of inhibitors of leucine-rich repeat kinase 2 (LRRK2) as a therapeutic strategy for Parkinson's disease: the current state of play.* Br J Pharmacol, 2022. **179**(8): p. 1478-1495.
82. Cookson, M.R., *LRRK2 Pathways Leading to Neurodegeneration.* Curr Neurol Neurosci Rep, 2015. **15**(7): p. 42.
83. Dzamko, N., et al., *Inhibition of LRRK2 kinase activity leads to dephosphorylation of Ser(910)/Ser(935), disruption of 14-3-3 binding and altered cytoplasmic localization.* Biochem J, 2010. **430**(3): p. 405-13.

84. Nichols, R.J., et al., *14-3-3 binding to LRRK2 is disrupted by multiple Parkinson's disease-associated mutations and regulates cytoplasmic localization.* Biochem J, 2010. **430**(3): p. 393-404.
85. Lobbestael, E., et al., *Pharmacological LRRK2 kinase inhibition induces LRRK2 protein destabilization and proteasomal degradation.* Sci Rep, 2016. **6**: p. 33897.
86. Manzoni, C., *The LRRK2-macroautophagy axis and its relevance to Parkinson's disease.* Biochem Soc Trans, 2017. **45**(1): p. 155-162.
87. Manzoni, C. and P.A. Lewis, *LRRK2 and Autophagy.* Adv Neurobiol, 2017. **14**: p. 89-105.
88. Albanese, F., S. Novello, and M. Morari, *Autophagy and LRRK2 in the Aging Brain.* Front Neurosci, 2019. **13**: p. 1352.
89. Herzig, M.C., et al., *LRRK2 protein levels are determined by kinase function and are crucial for kidney and lung homeostasis in mice.* Hum Mol Genet, 2011. **20**(21): p. 4209-23.
90. Hinkle, K.M., et al., *LRRK2 knockout mice have an intact dopaminergic system but display alterations in exploratory and motor co-ordination behaviors.* Mol Neurodegener, 2012. **7**: p. 25.
91. Tong, Y., et al., *Loss of leucine-rich repeat kinase 2 causes impairment of protein degradation pathways, accumulation of alpha-synuclein, and apoptotic cell death in aged mice.* Proc Natl Acad Sci U S A, 2010. **107**(21): p. 9879-84.
92. Giaime, E., et al., *Age-Dependent Dopaminergic Neurodegeneration and Impairment of the Autophagy-Lysosomal Pathway in LRRK-Deficient Mice.* Neuron, 2017. **96**(4): p. 796-807 e6.
93. Hartlova, A., et al., *LRRK2 is a negative regulator of Mycobacterium tuberculosis phagosome maturation in macrophages.* EMBO J, 2018. **37**(12).
94. Manzoni, C., et al., *mTOR independent regulation of macroautophagy by Leucine Rich Repeat Kinase 2 via Beclin-1.* Sci Rep, 2016. **6**: p. 35106.
95. Wallings, R., N. Connor-Robson, and R. Wade-Martins, *LRRK2 interacts with the vacuolar-type H+-ATPase pump a1 subunit to regulate lysosomal function.* Hum Mol Genet, 2019. **28**(16): p. 2696-2710.
96. Gomez-Suaga, P., et al., *Leucine-rich repeat kinase 2 regulates autophagy through a calcium-dependent pathway involving NAADP.* Hum Mol Genet, 2012. **21**(3): p. 511-25.
97. Orenstein, S.J., et al., *Interplay of LRRK2 with chaperone-mediated autophagy.* Nat Neurosci, 2013. **16**(4): p. 394-406.
98. Manzoni, C., et al., *Inhibition of LRRK2 kinase activity stimulates macroautophagy.* Biochim Biophys Acta, 2013. **1833**(12): p. 2900-2910.

99. Saez-Atienzar, S., et al., *The LRRK2 inhibitor GSK2578215A induces protective autophagy in SH-SY5Y cells: involvement of Drp-1-mediated mitochondrial fission and mitochondrial-derived ROS signaling.* Cell Death Dis, 2014. **5**(8): p. e1368.

100. Schapansky, J., et al., *Membrane recruitment of endogenous LRRK2 precedes its potent regulation of autophagy.* Hum Mol Genet, 2014. **23**(16): p. 4201-14.

101. Li, Y., et al., *Mutant LRRK2(R1441G) BAC transgenic mice recapitulate cardinal features of Parkinson's disease.* Nat Neurosci, 2009. **12**(7): p. 826-8.

102. Ramonet, D., et al., *Dopaminergic neuronal loss, reduced neurite complexity and autophagic abnormalities in transgenic mice expressing G2019S mutant LRRK2.* PLoS One, 2011. **6**(4): p. e18568.

103. Schapansky, J., et al., *Familial knockin mutation of LRRK2 causes lysosomal dysfunction and accumulation of endogenous insoluble alpha-synuclein in neurons.* Neurobiol Dis, 2018. **111**: p. 26-35.

104. Yue, M., et al., *Progressive dopaminergic alterations and mitochondrial abnormalities in LRRK2 G2019S knock-in mice.* Neurobiol Dis, 2015. **78**: p. 172-95.

105. Bravo-San Pedro, J.M., et al., *The LRRK2 G2019S mutant exacerbates basal autophagy through activation of the MEK/ERK pathway.* Cell Mol Life Sci, 2013. **70**(1): p. 121-36.

106. Plowey, E.D., et al., *Role of autophagy in G2019S-LRRK2-associated neurite shortening in differentiated SH-SY5Y cells.* J Neurochem, 2008. **105**(3): p. 1048-56.

107. Hockey, L.N., et al., *Dysregulation of lysosomal morphology by pathogenic LRRK2 is corrected by TPC2 inhibition.* J Cell Sci, 2015. **128**(2): p. 232-8.

108. Beilina, A., et al., *Unbiased screen for interactors of leucine-rich repeat kinase 2 supports a common pathway for sporadic and familial Parkinson disease.* Proc Natl Acad Sci U S A, 2014. **111**(7): p. 2626-31.

109. Gomez, R.C., et al., *Membrane association but not identity is required for LRRK2 activation and phosphorylation of Rab GTPases.* J Cell Biol, 2019. **218**(12): p. 4157-4170.

110. Liu, Z., et al., *LRRK2 phosphorylates membrane-bound Rabs and is activated by GTP-bound Rab7L1 to promote recruitment to the trans-Golgi network.* Hum Mol Genet, 2018. **27**(2): p. 385-395.

111. MacLeod, D.A., et al., *RAB7L1 interacts with LRRK2 to modify intraneuronal protein sorting and Parkinson's disease risk.* Neuron, 2013. **77**(3): p. 425-39.

112. Eguchi, T., et al., *LRRK2 and its substrate Rab GTPases are sequentially targeted onto stressed lysosomes and maintain their homeostasis.* Proc Natl Acad Sci U S A, 2018. **115**(39): p. E9115-E9124.

113. Herbst, S., et al., *LRRK2 activation controls the repair of damaged endomembranes in macrophages.* EMBO J, 2020. **39**(18): p. e104494.
114. Bonet-Ponce, L., et al., *LRRK2 mediates tubulation and vesicle sorting from lysosomes.* Sci Adv, 2020. **6**(46).
115. Lee, C.H., et al., *Rin, a neuron-specific and calmodulin-binding small G-protein, and Rit define a novel subfamily of ras proteins.* J Neurosci, 1996. **16**(21): p. 6784-94.
116. Shao, H., et al., *Biochemical characterization of the Ras-related GTPases Rit and Rin.* Arch Biochem Biophys, 1999. **371**(2): p. 207-19.
117. Shi, G.X., W. Cai, and D.A. Andres, *Rit subfamily small GTPases: regulators in neuronal differentiation and survival.* Cell Signal, 2013. **25**(10): p. 2060-8.
118. Uenaka, T., et al., *In silico drug screening by using genome-wide association study data repurposed dabrafenib, an anti-melanoma drug, for Parkinson's disease.* Hum Mol Genet, 2018. **27**(22): p. 3974-3985.
119. Cai, W., et al., *Rit GTPase signaling promotes immature hippocampal neuronal survival.* J Neurosci, 2012. **32**(29): p. 9887-97.
120. Cai, W., et al., *An evolutionarily conserved Rit GTPase-p38 MAPK signaling pathway mediates oxidative stress resistance.* Mol Biol Cell, 2011. **22**(17): p. 3231-41.
121. Cai, W., et al., *Rit GTPase regulates a p38 MAPK-dependent neuronal survival pathway.* Neurosci Lett, 2012. **531**(2): p. 125-30.
122. Glessner, J.T., et al., *Strong synaptic transmission impact by copy number variations in schizophrenia.* Proc Natl Acad Sci U S A, 2010. **107**(23): p. 10584-9.
123. Emamalizadeh, B., et al., *The human RIT2 core promoter short tandem repeat predominant allele is species-specific in length: a selective advantage for human evolution?* Mol Genet Genomics, 2017. **292**(3): p. 611-617.
124. Emamalizadeh, B., et al., *RIT2 Polymorphisms: Is There a Differential Association?* Mol Neurobiol, 2017. **54**(3): p. 2234-2240.
125. Liu, X., et al., *Genome-wide Association Study of Autism Spectrum Disorder in the East Asian Populations.* Autism Res, 2016. **9**(3): p. 340-9.
126. Hamedani, S.Y., et al., *Ras-like without CAAX 2 (RIT2): a susceptibility gene for autism spectrum disorder.* Metab Brain Dis, 2017. **32**(3): p. 751-755.
127. Pankratz, N., et al., *Meta-analysis of Parkinson's disease: identification of a novel locus, RIT2.* Ann Neurol, 2012. **71**(3): p. 370-84.
128. Emamalizadeh, B., et al., *RIT2, a susceptibility gene for Parkinson's disease in Iranian population.* Neurobiol Aging, 2014. **35**(12): p. e27-e28.

129. Liu, Z.H., et al., *Assessment of RIT2 rs12456492 association with Parkinson's disease in Mainland China.* Neurobiol Aging, 2015. **36**(3): p. 1600 e9-11.
130. Lu, Y., et al., *Genetic association of RIT2 rs12456492 polymorphism and Parkinson's disease susceptibility in Asian populations: a meta-analysis.* Sci Rep, 2015. **5**: p. 13805.
131. Nie, K., et al., *RIT2 polymorphism is associated with Parkinson's disease in a Han Chinese population.* Neurobiol Aging, 2015. **36**(3): p. 1603 e15-7.
132. Wang, J.Y., et al., *The RIT2 and STX1B polymorphisms are associated with Parkinson's disease.* Parkinsonism Relat Disord, 2015. **21**(3): p. 300-2.
133. Nalls, M.A., et al., *Large-scale meta-analysis of genome-wide association data identifies six new risk loci for Parkinson's disease.* Nat Genet, 2014. **46**(9): p. 989-93.
134. Zhang, X., et al., *RIT2 rs12456492 polymorphism and the risk of Parkinson's disease: A meta-analysis.* Neurosci Lett, 2015. **602**: p. 167-71.
135. Lin, C.H., et al., *RIT2 variant is not associated with Parkinson's disease in a Taiwanese population.* Neurobiol Aging, 2013. **34**(9): p. 2236 e1-3.
136. Liu, T.W., et al., *Association of RIT2 and RAB7L1 with Parkinson's disease: a case-control study in a Taiwanese cohort and a meta-analysis in Asian populations.* Neurobiol Aging, 2020. **87**: p. 140 e5-140 e11.
137. Zhou, Q., et al., *Identification of nigral dopaminergic neuron-enriched genes in adult rats.* Neurobiol Aging, 2011. **32**(2): p. 313-26.
138. Bossers, K., et al., *Analysis of gene expression in Parkinson's disease: possible involvement of neurotrophic support and axon guidance in dopaminergic cell death.* Brain Pathol, 2009. **19**(1): p. 91-107.
139. Navaroli, D.M., et al., *The plasma membrane-associated GTPase Rin interacts with the dopamine transporter and is required for protein kinase C-regulated dopamine transporter trafficking.* J Neurosci, 2011. **31**(39): p. 13758-70.
140. Fagan, R.R., et al., *Dopamine transporter trafficking and Rit2 GTPase: Mechanism of action and in vivo impact.* J Biol Chem, 2020. **295**(16): p. 5229-5244.
141. Sweeney, C.G., et al., *Conditional, inducible gene silencing in dopamine neurons reveals a sex-specific role for Rit2 GTPase in acute cocaine response and striatal function.* Neuropsychopharmacology, 2020. **45**(2): p. 384-393.
142. Fagan, R.R., et al., *Dopaminergic Ric GTPase activity impacts amphetamine sensitivity and sleep quality in a dopamine transporter-dependent manner in Drosophila melanogaster.* Mol Psychiatry, 2021. **26**(12): p. 7793-7802.

143. Wang, Q., et al., *Single-cell transcriptomic atlas of the human substantia nigra in Parkinson's disease.* bioRxiv, 2022: p. 2022.03.25.485846.
144. Obergasteiger, J., et al., *Kinase inhibition of G2019S-LRRK2 enhances autolysosome formation and function to reduce endogenous alpha-synuclein intracellular inclusions.* Cell Death Discov, 2020. **6**: p. 45.
145. Mauthe, M., et al., *Chloroquine inhibits autophagic flux by decreasing autophagosome-lysosome fusion.* Autophagy, 2018. **14**(8): p. 1435-1455.
146. Kimura, S., T. Noda, and T. Yoshimori, *Dissection of the autophagosome maturation process by a novel reporter protein, tandem fluorescent-tagged LC3.* Autophagy, 2007. **3**(5): p. 452-60.
147. Frost, L.S., et al., *The Use of DQ-BSA to Monitor the Turnover of Autophagy-Associated Cargo.* Methods Enzymol, 2017. **587**: p. 43-54.
148. Kluss, J.H., et al., *Detection of endogenous S1292 LRRK2 autophosphorylation in mouse tissue as a readout for kinase activity.* NPJ Parkinsons Dis, 2018. **4**: p. 13.
149. Lynch-Day, M.A., et al., *The role of autophagy in Parkinson's disease.* Cold Spring Harb Perspect Med, 2012. **2**(4): p. a009357.
150. Oueslati, A., *Implication of Alpha-Synuclein Phosphorylation at S129 in Synucleinopathies: What Have We Learned in the Last Decade?* J Parkinsons Dis, 2016. **6**(1): p. 39-51.
151. Volpicelli-Daley, L.A., et al., *G2019S-LRRK2 Expression Augments alpha-Synuclein Sequestration into Inclusions in Neurons.* J Neurosci, 2016. **36**(28): p. 7415-27.
152. Longo, F., et al., *Age-dependent dopamine transporter dysfunction and Serine129 phospho-alpha-synuclein overload in G2019S LRRK2 mice.* Acta Neuropathol Commun, 2017. **5**(1): p. 22.
153. Gloeckner, C.J. and P. Porras, *Guilt-by-Association - Functional Insights Gained From Studying the LRRK2 Interactome.* Front Neurosci, 2020. **14**: p. 485.
154. Deng, X., et al., *Characterization of a selective inhibitor of the Parkinson's disease kinase LRRK2.* Nat Chem Biol, 2011. **7**(4): p. 203-5.
155. Fuji, R.N., et al., *Effect of selective LRRK2 kinase inhibition on nonhuman primate lung.* Sci Transl Med, 2015. **7**(273): p. 273ra15.
156. Klionsky, D.J., et al., *Guidelines for the use and interpretation of assays for monitoring autophagy (4th edition)(1).* Autophagy, 2021. **17**(1): p. 1-382.
157. Albanese, F., et al., *Constitutive silencing of LRRK2 kinase activity leads to early glucocerebrosidase deregulation and late impairment of autophagy in vivo.* Neurobiol Dis, 2021. **159**: p. 105487.

158. Sharifi, M.N., et al., *Autophagy Promotes Focal Adhesion Disassembly and Cell Motility of Metastatic Tumor Cells through the Direct Interaction of Paxillin with LC3.* Cell Rep, 2016. **15**(8): p. 1660-72.

159. Bressan, C., et al., *The dynamic interplay between ATP/ADP levels and autophagy sustain neuronal migration in vivo.* Elife, 2020. **9**.

160. Berg, M.M., G.A. Krafft, and W.L. Klein, *Rapid impact of beta-amyloid on paxillin in a neural cell line.* J Neurosci Res, 1997. **50**(6): p. 979-89.

161. Grace, E.A. and J. Busciglio, *Aberrant activation of focal adhesion proteins mediates fibrillar amyloid beta-induced neuronal dystrophy.* J Neurosci, 2003. **23**(2): p. 493-502.

162. Raffaello, A., et al., *Calcium at the Center of Cell Signaling: Interplay between Endoplasmic Reticulum, Mitochondria, and Lysosomes.* Trends Biochem Sci, 2016. **41**(12): p. 1035-1049.

163. Gerndt, S., et al., *Agonist-mediated switching of ion selectivity in TPC2 differentially promotes lysosomal function.* Elife, 2020. **9**.

164. Davis, L.C., A.J. Morgan, and A. Galione, *NAADP-regulated two-pore channels drive phagocytosis through endo-lysosomal Ca(2+) nanodomains, calcineurin and dynamin.* EMBO J, 2020. **39**(14): p. e104058.

165. Nabar, N.R., et al., *LRRK2 is required for CD38-mediated NAADP-Ca(2+) signaling and the downstream activation of TFEB (transcription factor EB) in immune cells.* Autophagy, 2022. **18**(1): p. 204-222.

166. Gaertner, Z., et al., *Molecular heterogeneity in the substantia nigra: A roadmap for understanding PD motor pathophysiology.* Neurobiol Dis, 2022. **175**: p. 105925.

167. Skelton, P.D., V. Tokars, and L. Parisiadou, *LRRK2 at Striatal Synapses: Cell-Type Specificity and Mechanistic Insights.* Cells, 2022. **11**(1).

168. Biedler, J.L., L. Helson, and B.A. Spengler, *Morphology and growth, tumorigenicity, and cytogenetics of human neuroblastoma cells in continuous culture.* Cancer Res, 1973. **33**(11): p. 2643-52.

169. Vancraenenbroeck, R., et al., *In silico, in vitro and cellular analysis with a kinome-wide inhibitor panel correlates cellular LRRK2 dephosphorylation to inhibitor activity on LRRK2.* Front Mol Neurosci, 2014. **7**: p. 51.

# Appendix I

# The small GTPase Rit2 modulates LRRK2 kinase activity, is required for lysosomal function and protects against alpha-synuclein neuropathology

Julia Obergasteiger[2+#], Anne-Marie Castonguay[2,#], Sara Pizzi[1], Stefano Magnabosco[1], Giulia Frapporti[1,|], Evy Lobbestael[3], Veerle Baekelandt[3], Andrew A. Hicks[1], Peter P. Pramstaller[1], Claude Gravel[2], Corrado Corti[1], Martin Lévesque[2,*], Mattia Volta[1,*]

[1]*Institute for Biomedicine, Eurac Research, via Volta 21, 39100, Bolzano (Italy).*

[2]*Department of Psychiatry and Neurosciences, Faculty of Medicine, Université Laval; CERVO Brain Research Centre, 2601 chemin de la Canardiere, Quebec (QC, Canada).*

[3]*Department of Neurosciences, KU Leuven, Herestraat 49 bus 1023, 3000, Leuven, Belgium*

[|]*Current affiliation: Department of Cellular, Computational and Integrative Biology-CIBO, University of Trento (Italy).*

[+]*Current affiliation: [2]Department of Psychiatry and Neurosciences, Faculty of Medicine, Université Laval; CERVO Brain Research Centre, 2601 chemin de la Canardiere, Quebec (QC, Canada).*

[#]These authors contributed equally

[*]These authors contributed equally and are co-corresponding authors at: martin.levesque@cervo.ulaval.ca or mattia.volta@eurac.edu

**Abstract**

In Parkinson's disease (PD) misfolded alpha-synuclein (aSyn) accumulates in the substantia nigra, where dopaminergic neurons are progressively lost. The mechanisms underlying aSyn pathology are still unclear, but they are hypothesized to involve the autophagy lysosome pathway (ALP). LRRK2 mutations are a major cause of familial and sporadic PD, and LRRK2 kinase activity has been shown to be involved in pS129-aSyn inclusion modulation. We observed selective downregulation of the novel PD risk factor *RIT2 in vitro* and *in vivo*. Rit2 overexpression in G2019S-LRRK2 cells rescued ALP abnormalities and diminished aSyn inclusions. *In vivo*, viral mediated overexpression of Rit2 operated neuroprotection against AAV-A53T-aSyn. Furthermore, Rit2 overexpression prevented the A53T-aSyn-dependent increase of LRRK2 kinase activity *in vivo*. On the other hand, reduction of Rit2 levels leads to defects in the ALP, similar to those induced by the G2019S LRRK2 mutation. Our data indicate that Rit2 is required for correct lysosome function, inhibits overactive LRRK2 to ameliorate ALP impairment, and counteracts aSyn aggregation and related deficits. Targeting Rit2 could represent a novel strategy to combat neuropathology in familial and idiopathic PD.

## Introduction

Parkinson's disease (PD) is the second most common neurodegenerative disorder affecting 2-3% of people over the age of 65. The disease is characterized by motor symptoms including resting tremor, rigidity, bradykinesia, and postural instability, which originate from the loss of dopaminergic (DA) neurons in the substantia nigra pars compacta (SNc)[1, 2]. Around 15% of PD patients have a family history and 5-10% of cases are caused by mutations and alterations in specific genes (e.g. SNCA, LRRK2, Parkin, VPS35)[3]. The vast majority of cases are sporadic and are thought to be caused by a combination of genetic and environmental factors[4, 5]. Gene variants in alpha-synuclein (aSyn) and leucine-rich repeat kinase 2 (LRRK2) lead to autosomal dominant PD, mostly presenting intracytoplasmic protein aggregates called Lewy bodies (LBs). LBs are one of the main neuropathological hallmarks of PD and a group of other neurological disorders termed synucleinopathies, and they are mainly composed of oligomeric and fibrillar aSyn [6, 7]. Mechanisms underlying the formation and clearance of these inclusions are still under intense investigation. The autophagy-lysosome pathway (ALP) is a conserved and tightly regulated cellular process that is dysregulated in PD and, amongst other cellular processes, likely contributes to the defective clearance of aSyn[10, 11, 12]. The ALP leads to lysosomal degradation of long-lived proteins, defective organelles and protein aggregates. Cargo delivery to the lysosome can be achieved by three main pathways: microautophagy, chaperone-mediated autophagy (CMA) and macroautophagy. Macroautophagy, named autophagy herein, involves the formation of double-membrane vesicles, termed autophagosomes that engulf the cargo and finally fuse with the lysosome, where final degradation takes place [8, 9].

Leucine-rich repeat kinase 2 (LRRK2) is a multifunctional protein composed of a catalytic GTPase and kinase core and several protein binding domains[13]. LRRK2 is expressed in different tissues with high expression levels in the lungs, kidneys and white blood cells[14]. In

the brain, LRRK2 is expressed ubiquitously and not restricted to neurons[15]. Mutations in the catalytic core have been associated with late-onset familial PD, with the G2019S substitution leading to a 3-4-fold increase in kinase activity and being the most common genetic cause of PD [16]. Cellular roles of LRRK2 are varied and include synaptic transmission, vesicle trafficking and autophagy[17, 18, 19, 20]. Numerous studies have reported that mutant LRRK2 alters the ALP, but a common consensus on the specific effects and the impact of LRRK2 mutations on the ALP is currently lacking[21, 22, 23, 24]. Moreover, LRRK2 kinase inhibition is beneficial against aSyn neuropathology, suggesting that LRRK2 activity mediates accumulation of pathologic aSyn [25].

Recent genome-wide association studies (GWAS) identified the locus containing the *RIT2* gene to be associated with increased risk for PD[26, 27, 28]. This gene encodes for the small GTPase Rit2, which is mainly expressed in neural tissue[29]. Rit2 belongs to the Ras superfamily of GTPases and is implicated in MAPK-mediated neurite outgrowth[30, 31, 32], calcium signaling[29, 30] and dopamine transporter (DAT) trafficking [33, 34]. Furthermore, the knock-down (KD) of Rit2 in male mice altered DAT levels and produced alterations in DA-dependent behaviors[35]. Recently, we reviewed the possible regulation of autophagy by GTPase-MAPK pathways. Since Rit2 modulates the activity of MAPKs (including p38 and ERK1/2), we hypothesized that it could contribute to the regulation of the ALP[36]. Notably, LRRK2 participates to MAPK signaling[37].

Here, we investigate the effects of altered Rit2 expression on ALP regulation and aSyn pathology and the underlying molecular mechanism using preclinical *in vitro* and *in vivo* PD models. Overexpression of Rit2 in G2019S-LRRK2 neuroblastoma cells restored ALP deficits and reduced accumulation of phosphorylated aSyn (pS129-aSyn), phenocopying the effects of pharmacological LRRK2 kinase inhibition that we recently reported[38]. The selective overexpression of Rit2 in DA neurons in the mouse SNc attenuated nigrostriatal

neurodegeneration and pS129-aSyn neuropathology induced by virally expressed aSyn. Importantly, we found that Rit2 interacts with LRRK2 and its enhanced expression inhibits both recombinant (*in vitro*) and endogenous (*in vivo*) LRRK2 kinase activity. On the other hand, reduced Rit2 levels lead to lysosome alteratrions, indicating its requirement for correctly functional ALP.

**Results**

*RIT2 gene expression is reduced in recombinant LRRK2 cells and in dopamine neurons from idiopathic PD patients*

Genetic alterations in the *RIT2* promoter region have been associated to PD and are hypothesized to alter expression levels[39]. Accordingly, *RIT2* expression was reduced in the SNc of PD patients[40]. Using publicly available datasets, we analyzed *RIT2* mRNA expression in human and rodent samples. The Geo dataset GSE20141 reports microarray data obtained from laser-capture microdissected SNc DA neurons from idiopathic PD patients and controls[41]. Consistent with literature, we found that *RIT2* expression is downregulated by about 2.2-fold in DA neurons from idiopathic PD patients, when compared to controls (Fig 1A). Interestingly, *RIT2* mRNA levels in total brain tissue were not changed (GSE7621[42]) (Fig S1A), indicating a specific downregulation of *RIT2* in DA neurons of the SNc. *In vitro*, *RIT2* mRNA levels were also reduced in DA neurons generated from induced pluripotent stem cells (iPSCs) carrying the A53T mutation in aSyn, when compared to isogenic control cells (published in dataset GSE46798[43]) (Fig 1B) and in SK-N-SH neuroblastoma cells overexpressing A53T-aSyn (Fig S1B) when compared to naïve SK-N-SH.

To complement these analyses, we measured *RIT2* mRNA levels in WT- and G2019S-LRRK2 overexpressing SH-SY5Y cells using droplet digital PCR (ddPCR). These cell lines have been previously characterised extensively by our group, for LRRK2 expression levels, lysosomal

alterations and pS129-aSyn accumulation in G2019S-LRRK2 cells. These phenotypes proved to be dependent on LRRK2 kinase activity as they were ameliorated by the selective LRRK2 kinase inhibitor PF-06447475[38]. Here, we found reduced gene expression in both cell lines, when compared to naïve SH-SY5Y cells (Fig 1C). In rodents, *Rit2* was reported to be expressed in the brain[44]. The analysis of Geo dataset GSE17542[45], comparing *Rit2* mRNA levels from laser capture microdissected mouse SNc and VTA did not reveal significant regional differences in *Rit2* mRNA expression (Fig. 1D). To confirm *Rit2* expression in DA neurons of the SNc in our experimental setting, we performed multiplex *in situ* hybridization (RNAscope® ISH technology) on mouse midbrain sections. Strong Rit2 mRNA signal was evident in SNc DA (TH+) neurons from control AAV-injected mice, and it was significantly reduced in mice injected with AAV-A53T-aSyn (Fig. 1E-F and Fig. S1C). Together, our results show that *RIT2* is expressed in both mouse and human DA neurons. *RIT2* expression is also reduced in DA neurons from idiopathic PD patients and in different cellular and animal models of PD, suggesting a possible role for Rit2 in both familial and idiopathic PD biology.

*Overexpression of Rit2 rescues ALP deficits in G2019S-LRRK2 cells*

It has been extensively reported that both aSyn and LRRK2 affect the autophagic process [46, 47, 48, 49]. Furthermore, we recently found that the reduction of pS129-aSyn-positive inclusions in G2019S-LRRK2 cells, following exposure to a LRRK2 kinase inhibitor, depends on functioning lysosomal activity[38]. As an unbiased approach, we used the RT² Profiler™ PCR Array for autophagy to measure the expression levels of 84 genes implicated in different stages of the ALP. Since G2019S-LRRK2 cells displayed lower *RIT2* mRNA levels, we decided to reconstitute *RIT2* expression in these cells, using high efficiency nucleofection of a construct containing the human *RIT2* gene (Fig. S1D-E) and investigate gene expression changes with respect to non-nucleofected G2019S-LRRK2 cell lines (Fig. S2). *RIT2* overexpression affected

several genes related to autophagy; specifically, *WIPI1* and *DRAM1* genes were upregulated by *RIT2* overexpression. WIPI1 promotes autophagy and autophagosome formation [50, 51], and DRAM1 is implicated in lysosomal acidification, clearance of autophagosomes and fusion of autophagosomes with lysosomes[52]. Overall, the results obtained from the array suggested that the ALP is impacted by the overexpression of *RIT2*, at least at the transcriptional level. Therefore, we looked at specific stages of the ALP to investigate the functionality of the pathway, starting with monitoring the overall autophagic flux.

G2019S-LRRK2 cells were transiently nucleofected with *RIT2* or GFP as a control. After 72 hours of overexpression, cellular extracts were prepared and LC3B levels were measured via Western blotting to quantify the dynamics of the autophagic process (Fig. 2A) [53]. The LC3B-II/LC3B-I ratio was not significantly changed between non-transfected G2019S-LRRK2 cells, GFP-transfected cells or cells transfected with Rit2 (Fig. 2B). In parallel, we assessed the LC3B-II/b-actin ratio in the same cellular extracts, which was also not affected by Rit2 overexpression (Fig. 2C). These results indicate that Rit2 overexpression does not affect the overall autophagic flux. Then, we utilized the Cyto-ID assay to visualize autophagosomes and autolysosomes and observed that Rit2 overexpression increased the number of Cyto-ID-stained vesicles (Fig. 2D-E). Given the importance of later fusion steps and our previous results showing impaired lysosome function in the same cell lines, we subsequently evaluated the endpoint effector of the ALP, the lysosome. We investigated lysosomal morphology and number employing the lysosomotropic dye Lysotracker Red, which accumulates in cellular acidic compartments (Fig. 3A). We observed that Rit2 overexpression increases the number of lysosomes (Fig. 3B) and decreases their size (Fig. 3C). The results from LC3B western blotting and Lysotracker experiments suggest that the increase in the number of Cyto-ID-positive vesicles might derive from an accumulation of autolysosomes/lysosomes and not from an increased production of autophagosomes. Given these morphological alterations, usually

coupled to abnormal lysosome function, we measured the proteolytic activity of lysosomes using the DQ-Red-BSA assay. DQ-Red-BSA is degraded by proteases in the acidic environment of the lysosome and an increase of fluorescent spots indicates an enhanced amount of cleaved DQ-Red-BSA, correlating with proteolytic capacity of the cell. The overexpression of Rit2 significantly enhanced the number of fluorescent spots per cell (Fig. 3D-E), indicating an increase in lysosomal proteolysis. Taken together these results reveal that Rit2 does not affect the overall autophagic flux, but rescues the morphological and functional deficits of the lysosomes we previously identified in G2019S-LRRK2 neuroblastoma cells[38]. We replicated some of the above-mentioned experiments in WT-LRRK2 neuroblastoma cells to determine if the effect was specific for the G2019S mutation. Successful nucleofection is again shown by mRNA (Fig. S1F) and protein levels (Fig. S3H). Autophagosome/autolysosome number, measured using the CytoID assay, was not changed when Rit2 was overexpressed in WT-LRRK2 cells (Fig. S3A-B). Lysosome number (Fig. S3C-E) and functionality, measured by Lysotracker Red (Fig. S3C-E) and DQ-Red-BSA (Fig. S3F-G) staining respectively, were not significantly changed, when Rit2 was overexpressed in these cells. Thus, Rit2 overexpression appears to rescue dysfunctional lysosomes caused by G2019S-LRRK2 while not affecting phenotypes in WT-LRRK2 expressing cells. In addition, we also investigated total aSyn levels, which were not changed by Rit2 overexpression in the WT-LRRK2 cell line (Fig. S3H-I).

*pS129-aSyn positive inclusions in G2019S-LRRK2 cells are reduced by Rit2 overexpression*

A significant proportion of PD patients carrying the G2019S mutation exhibit LB pathology[54, 55] and, this mutation has been shown to promote the accumulation of pS129-aSyn in experimental models[25]. SH-SY5Y neuroblastoma cells stably overexpressing G2019S-LRRK2 display inclusion-like structures staining positively for pS129-aSyn, while WT-LRRK2 cells only exhibited diffuse, barely detectable pS129-aSyn staining comparable to naïve cells (Fig.

4A). Enhanced expression of Rit2 showed beneficial effects on different stages of the ALP; therefore, we hypothesized that it might play a role in the degradation of pS129-aSyn. Thus, we decided to investigate the effects of Rit2 on pathological inclusions. G2019S-LRRK2 cells were transiently nucleofected with Rit2 and after 72 hours fixed and processed for pS129-aSyn staining. Overexpression of Rit2 significantly reduced the number of objects positively stained for pS129-aSyn per cell (Fig. 4A-B). Control GFP nucleofection did not alter pS129-aSyn inclusion number (Fig. S4A-B). Total aSyn levels, measured with Western blotting, were not changed by Rit2 overexpression (Fig. S4C-D), indicating a likely specific effect on inclusions of the pathologic form.

*Rit2 overexpression reduces kinase activity of recombinant LRRK2*

Our results indicate that Rit2 overexpression in G2019S-LRRK2 cells phenocopies pharmacological LRRK2 kinase inhibition in ALP and pS129-aSyn modulation, as we recently reported[38]. Thus, we hypothesized that LRRK2 and Rit2 could play a role in a common molecular mechanism. We explored the possibility that LRRK2 kinase inhibition could influence *RIT2* mRNA levels, with LRRK2 acting upstream of *RIT2*. We treated G2019S-LRRK2 cells with different concentrations of the LRRK2-selective kinase inhibitor PF-06447475[56] and we assessed *RIT2* mRNA levels using ddPCR. No difference in *RIT2* gene expression levels were observed upon pharmacological LRRK2 kinase inhibition (Fig. S4E). Since LRRK2 kinase inhibition did not affect *RIT2* expression, we explored the hypothesis that Rit2 might directly interact with LRRK2. We first used proximity ligation assay (PLA) for Rit2 and LRRK2 in SH-SY5Y cell lines and observed that overexpressed WT LRRK2 and Rit2 displayed a robust level of PLA interaction signal. This was strongly reduced in G2019S-LRRK2 cells (Fig. S5A-B). To rule out an effect of the different LRRK2 protein expression levels in these cell lines (as we previously reported [57]), we performed the same PLA experiment

in HEK293T cells with transient, stoichiometrically comparable expression of Rit2 and LRRK2 (either WT or G2019S). WT LRRK2 and Rit2 expression again led to a robust PLA signal and the G2019S LRRK2 mutation decreased the interaction between the two proteins (Fig. S5C-D). PLA is a measure of close proximity of two proteins in the cellular environment (<40nm), but it does not demonstrate physical interaction. Therefore, we co-immunoprecipitated LRRK2 from HEK293T cells transfected with either Rit2, LRRK2 (WT or G2019S) or both proteins. We observed LRRK2 and Rit2 co-precipitation, indicating a direct and physical interaction between the two proteins (Fig. S5E). We then confirmed the physical interaction in mouse brain samples (midbrain and striatum pooled together) to investigate the interaction of endogenous Rit2 and LRRK2. We observed LRRK2 co-precipitation, when Rit2 was pulled down (Fig. S5F). Furthermore, both Rit2 and LRRK2 levels were reduced in the supernatants of the Co-IP, when compared to the IgG control (Fig. S5F), indicating a depletion due to the pulled-down proteins. This interaction and the phenocopy of LRRK2 inhibition led us to hypothesize that Rit2 overexpression might inhibit LRRK2 kinase activity. LRRK2 phosphorylation was measured using Western blotting at two distinct residues (S935 and S1292), which are responsive to pharmacological LRRK2 inhibition[38, 58]. The autophosphorylation of Serine 1292 (pS1292) is a validated readout of LRRK2 kinase activity [58]. We previously found that G2019S-LRRK2 cells harbor a 3-4-fold increase of relative pS1292-LRRK2 when compared to WT-LRRK2 cells[38]. The measurement of LRRK2 phosphorylation by Western blot following overexpression of *RIT2* revealed a significant decrease in the ratio of pS1292-LRRK2/LRRK2 (Fig. S6A-B). Differently from LRRK2 kinase inhibitor treatment, pS935-LRRK2 levels were not decreased, but rather significantly increased (Fig. S6C-D). Moreover, total LRRK2 levels in G2019S-LRRK2 cells overexpressing Rit2 were also increased (Fig. S6E). This effect is distinct from LRRK2 kinase inhibitors, which have been shown to reduce total LRRK2 through protein destabilization likely due to

dephosphorylation at the S935 residue[59]. Consistent with a lack of S935 dephosphorylation with Rit2 overexpression, our results indicate that Rit2 does not impair LRRK2 protein stability. We further measured pS1292-LRRK2 levels also using PLA to enhance the specificity and sensitivity of the analysis, as previously validated[60]. Naïve SH-SY5Y and WT LRRK2 cells displayed negligible levels of pLRRK2 PLA signal, consistent with a very low basal activation of LRRK2[58], whereas G2019S LRRK2 cells displayed a dramatic increase in PLA signal (Fig. 4C). The overexpression of Rit2, in line with the Western blot data, produced a significant reduction of pS1292-LRRK2 PLA signal. In order to validate the assay, we used pharmacological inhibition of LRRK2 as positive control, which consistently completely abolished the PLA signal (Fig. 4C-D). In summary, we show that Rit2 directly interacts with LRRK2 in the cell and leads to decrease of S1292-LRRK2 phosphorylation, thus limiting LRRK2 kinase activity.

*Enhanced Rit2 expression in the mouse midbrain counteracts aSyn-dependent deficits and DA neuron loss*

To determine if the beneficial effects of Rit2 could also be translated *in vivo*, we modeled PD pathology in mice by unilaterally injecting an Adeno-Associated virus 2/9 (AAV) expressing the human A53T-aSyn (herein AAV-A53T-aSyn). We used DAT-Ires-Cre mice that specifically express the Cre recombinase in DAT-expressing neurons[61]. This allowed us to manipulate gene expression in a neuron-specific manner, as Rit2 is specifically downregulated in DA neurons from PD patients (Fig. 1A). The AAV-mediated overexpression of aSyn in the mouse midbrain has previously been shown to induce progressive SNc neuron loss, aSyn pathology and motor deficits[62]. Sixteen weeks following overexpression of A53T-aSyn (in combination with AAV-GFP), we observed motor abnormalities in the cylinder, open field and amphetamine tests. Mice expressing A53T-aSyn displayed an ipsilateral rotation phenotype

(Fig. 5A) and a preferential use of the ipsilateral forepaw (Fig. S7A), but no changes in the horizontal activity in the open field (Fig. 5B). In addition, A53T-aSyn overexpression induced a loss of TH-positive neurons in the midbrain (Fig. 5C-E) coupled to a loss of striatal DA terminals (Fig. 5F-G), mimicking the progressive nigrostriatal degeneration observed in PD. Overexpression of A53T-aSyn also tended to decrease the number of NeuN-positive cells in the ipsilateral SNc (Fig. 5E). To further ensure that overexpression of A53T-aSyn did not cause a downregulation of TH expression without cell loss, we counted the percentage of double-positive cells for GFP and TH in the ipsilateral SNc of AAV-GFP and AAV-GFP+A53T-aSyn injected mice. Both groups showed a percentage of double-positive cells of around 90%, suggesting that A53T-aSyn overexpression did not alter TH expression in dopaminergic neurons (Fig. S7C). Mice were co-injected with AAV-A53T-aSyn and the Cre dependent AAV-CAG-Flex-*Rit2*-EGFP (AAV-Rit2) or AAV-CAG-Flex-EGFP (AAV-GFP) control, to achieve overexpression selectively in DA neurons. This strategy ensured that the observed phenotypes would be attributed to the effect of Rit2 in this neuronal population. Rit2 overexpression was confirmed by western blotting of ventral midbrain protein lysates (Fig. S8C). The loss of TH-positive neurons in the SNc (Fig. 5D) and of DA terminals in the striatum (Fig. 5G) were greatly attenuated by the co-expression of *Rit2*, when compared to GFP control, and also significantly preserved NeuN+ cells in the ipsilateral SNc (Fig. 5E). Overexpression of Rit2 alone did not cause alterations to midbrain neuron number nor striatal terminal density, but interestingly, strongly promoted locomotor activity. We observed a marked increase in horizontal activity (Fig. 5B) in the open field, along with an increased number of contralateral rotations in the cylinder test (Fig. 5A).

*Enhanced Rit2 expression reduces pS129-aSyn load and total aSyn levels in the mouse midbrain*

Viral overexpression of A53T-aSyn in the mouse SNc also led to a significant increase of total aSyn protein levels measured by Western blotting (Fig. 6A). The concomitant overexpression of Rit2 produced a reduction of total aSyn, when compared to AAV-GFP co-injection (Fig. 6B). Importantly, viral A53T-aSyn overexpression significantly increased the burden of pS129-aSyn in DA neurons, when compared to AAV-GFP-injected animals (Fig. 6D). The co-injection of AAV-Flex-Rit2 significantly reduced pS129-aSyn levels in western blotting (Fig. 6C) and immunostaining (Fig. 6D-E) in midbrain DA neurons. This indicates that enhanced Rit2 expression counteracts pS129-aSyn accumulation not only in recombinant neuroblastoma cell lines, but importantly also in an *in vivo* PD mouse model, providing effective neuroprotection in a non-LRRK2 modeling paradigm. In addition, we investigated the autophagic flux in tissue using western blotting for LC3B and could not detect any alteration in the LC3B-II/LC3B-I ratio among the experimental groups (Fig. S8A-B). This is consistent with the results obtained in the G2019S-LRRK2 cells, where the overall autophagic flux was not altered by Rit2 overexpression.

*Rit2 overexpression prevents aSyn-induced hyperactivation of endogenous LRRK2 kinase*

We show that viral co-expression of Rit2 with A53T-aSyn in the mouse rescues neuronal loss and aSyn accumulation. In a recent study, viral overexpression of aSyn in rats led to increased kinase activity of endogenous LRRK2, observed as well in the midbrain of idiopathic PD patients, in the absence of any LRRK2 mutation [60]. Here we report that Rit2 reduces phosphorylation levels of S1292-LRRK2 in recombinant neuroblastoma cells (Fig. 4C-D) and is neuroprotective in animals with no LRRK2 mutations (Fig. 5), therefore we assessed the impact of Rit2 on S1292 autophosphorylation in the mouse DA neurons. The validated pS1292-LRRK2/total LRRK2 PLA method was employed in mouse brain sections (Fig. 7A), to increase specificity and decrease background with respect to standard IHC staining [60]. The

injection of AAV-A53T-aSyn induced a strong increase in the number of PLA dots, indicating a significant enhancement of endogenous LRRK2 phosphorylation at S1292 and thus an increase in kinase activity. Rit2 co-expression completely prevented the overactivation of endogenous LRRK2 that was elicited by A53T-aSyn (Fig. 7B). Importantly, total LRRK2 levels were not changed in any of the conditions analyzed (Fig S8C-D), supporting a specific kinase-regulating effect. In summary, viral Rit2 overexpression in the mouse SNc DA neurons conferred neuroprotection and reduced aSyn neuropathology through prevention of endogenous LRRK2 overactivation. However, the effects on lysosome function were observed upon Rit2 overexpression, and thus we set out to explore whether Rit2 has a physiological role in the ALP.

*Rit2 is required for correct lysosome function in cells and neurons*

Enhanced Rit2 expression in pathological conditions, like G2019S-LRRK2 mutation, reduces the accumulation of pS129-aSyn *in vitro* and *in vivo* and rescues lysosomal deficits. However, the precise function of endogenous Rit2 in the ALP is unclear. Therefore, we used previously characterized SH-SY5Y Rit2 knock-out (KO) cells [63] to investigate the physiological involvement of Rit2 in different stages of the ALP. First, we used the Cyto-ID assay to stain autophagosomes/autolysosomes and Rit2 KO cells displayed an increase in the number of these vesicles (Fig. 8A-B). We confirmed this result by Western blotting for LC3B and show that the Rit2-KO increases the number of autophagosomes, as represented by the LC3B-II/actin ratio. Furthermore, also the LC3B-II/LC3B-I ratio was increased in Rit2-KO cells (Fig. S9A-C). Then, we investigated the number and morphology of lysosomes and Rit2 KO cells displayed an increased diameter and a drastically reduced number of lysosomes (Fig. 8C-E). In addition, when using the DQ-Red BSA assay to investigate proteolytic activity of the lysosomes, the Rit2 KO led to a major decrease in both the number and intensity of DQ-Red-BSA spots,

indicating Rit2 is important for lysosomal catabolism (Fig. 8F-H). Of note, these phenotypes are similar to what we observed in G2019S-LRRK2 cells (bearing a downregulation of Rit2 expression, Fig. 1C) and indicate that the loss of Rit2 affects ALP functionality and is required for lysosome activity. To confirm that these phenotypes are caused by the loss of Rit2 in the cells, we carried out a rescue experiment, where we overexpressed Rit2 in the Rit2-KO cells. Nucleofection efficiency was similar to the other neuroblastoma cell lines, as protein (Fig. S9D) and mRNA levels (Fig. S9E) of Rit2 were correctly augmented by overexpression. Rit2 overexpression did not alter the number of autophagosome/autolysosomes (Fig. S9F-G) However, the overexpression of Rit2 in Rit2-KO cells increases the number of lysosomes (Fig. S9H-I) and the intensity of the DQ-Red-BSA staining (Fig. S9J-K), indicating Rit2-dependency of these phenotypes. Furthermore, we investigated total aSyn and LRRK2 levels in Rit2-KO cells with and without Rit2 overexpression. Total aSyn levels were significantly lower in Rit2-KO+Rit2 cells when compared to SH-SY5Y naïve cells (Fig. S9L-N), but both aSyn and LRRK2 levels did not differ in Rit2-KO cells with or without Rit2 expression (Fig. S9J-L). To assess the role of Rit2 in neuronal lysosomes, we used primary mouse dopaminergic neurons. Neurons were infected with either lentiviral particles expressing a scramble shRNA or a shRNA directed against Rit2 and expressing GFP in the same construct. The most efficient shRNA was tested in NIH-3T3 cells using western blotting (Fig. S10A) and the knock-down efficiency in primary neurons was determined via qPCR and was about 90% (Fig. S10B). Analysis of Rit2 protein levels by western blotting (Fig. S10C-D) corroborated the significant downregulation caused by Rit2-shRNA treatment. The infection with the two lentiviral constructs did not alter TH levels (Fig. S10E) or LC3B-II/LC3B-I ratio (Fig. S10F) in the midbrain cultures. We then employed the Lysotracker Red and DQ-Red BSA assays to explore lysosome morphology and function in this model as well. Both lysosome number and morphology were altered consistently with neuroblastoma cells. DA neurons displayed a

decreased number of lysosomes and an increase in their size with Rit2 KD (Fig. 9A-C). Moreover, lysosomal proteolytic activity was reduced with Rit2 KD, similar to the results in SH-SY5Y cells (Fig. 9D-F). In summary, we show that Rit2 modulates the ALP and is specifically required for correct morphology and functionality of the lysosomes, strengthening a role of Rit2 in the ALP and consistently, impacting aSyn accumulation.

**Discussion**

In this study, we aim at evaluating the neuroprotective role of a novel, underexplored target against aSyn neuropathology and elucidate its role in the ALP. We validated the potential of the small GTPase Rit2 in complementary *in vitro* and *in vivo* models of PD and revealed the cellular mechanism involved. In recent GWAS, *RIT2* has been associated with PD [28] and neuropsychiatric disorders[64, 65, 66]. Here, we show *RIT2* mRNA levels are reduced in DA neurons from idiopathic PD patients, in G2019S-LRRK2 overexpressing cells and an *in vivo* PD mouse model. Altogether, expression analysis shows that *RIT2* is expressed by DA neurons and reduced in PD conditions.

The downregulation of *RIT2* mRNA levels constitutes the rationale to transiently overexpress Rit2 in G2019S-LRRK2 cells. Rit2 overexpression was effective in increasing lysosome numbers and reducing their size. Moreover, Rit2 was able to rescue the impaired proteolytic function of lysosomes. In summary, enhanced Rit2 expression provided similar rescue to what was observed with the application of a pharmacological LRRK2 kinase inhibitor.

Consistently, the overexpression of Rit2 reduced the number of pS129-aSyn inclusions in G2019S-LRRK2 cells. It has already been reported that autophagy impairment might constitute a causative factor in aSyn accumulation[67, 68, 69] and autophagy/lysosome markers are altered in PD brain areas affected by LB pathology[12, 70]. In our study, we specifically focused on macroautophagy since, in our cell model, this major form of autophagy was significantly

affected. Nevertheless, we do not exclude an involvement of CMA that is also profoundly implicated in LRRK2 biology and aSyn pathology[49, 67, 71, 72]. Notably, the impairment of (macro)autophagy leads to a compensatory activation of CMA and vice versa[73]. Our results suggest that Rit2 and LRRK2 function in a common pathway and physically interact. We found that *in vitro* Rit2 overexpression modulates the phosphorylation levels, and thus kinase activity, of LRRK2. Importantly, S1292 phosphorylation was reduced by Rit2 overexpression, whereas pS935-LRRK2 was significantly increased, critically differentiating Rit2-related effects from those of pharmacological LRRK2 kinase inhibition (which targets both phospho-sites). The G2019S-LRRK2 mutation is known to enhance aSyn inclusion formation after application of aSyn preformed fibrils. Indeed, it has been reported that LRRK2 kinase inhibition is beneficial against aSyn aggregation and neurodegeneration, highlighting that these effects are dependent on LRRK2 kinase activity[25] and even more important because PD-associated mutations in LRRK2 increase its kinase activity[74]. Similar beneficial effects on aSyn inclusion formation and neuron loss were achieved by reducing total LRRK2 levels using antisense oligonucleotides against LRRK2[75], strengthening the important role of the LRRK2 kinase in aSyn aggregation and associated to defective autophagy. In addition, we show that total LRRK2 protein levels were not reduced when overexpressing Rit2, contrasting with the effect of LRRK2 kinase inhibitors [59]. Phosphorylation of S935-LRRK2 is required for a stable binding to 14-3-3 proteins and a reduction in pS935-LRRK2 was shown to reduce this interaction. The disrupted interaction leads to mislocalization of LRRK2 into cytoplasmic pools and therefore, the S935-dependent 14-3-3 binding is thought to protect LRRK2 protein from degradation[76, 77]. The exact mechanism behind LRRK2 destabilization is not yet understood, but it is believed to rely on LRRK2 kinase activity, since mice expressing a kinase-dead mutation in LRRK2 display reduced LRRK2 protein levels[78, 79]. Understanding the exact regulation of LRRK2 protein degradation is a key point to predict side effects of LRRK2 kinase inhibitors, as it has been

reported to produce lung and kidney pathology, similar to observations in LRRK2 KO mice[78]. LRRK2 inhibitors are envisaged to be administered not only to LRRK2-PD patients, but also to idiopathic PD patients, as indicated by the increase of pS1292-LRRK2 levels in urinary exosomes and brain tissue[60, 80]. We found that Rit2 overexpression is capable of reducing pS1292-LRRK2 levels, without affecting S935-LRRK2 phosphorylation and total protein stability. These findings indicate that a potential strategy based on targeting Rit2 or its associated pathway(s) could be efficient in inhibiting LRRK2 while avoiding peripheral side effects induced by LRRK2 kinase inhibitors and related to reduction of total protein levels. Notably, targeting Rit2 could be a direct way to impact autophagy and aSyn aggregation. In addition, we show that the beneficial effects are specific to the mutated form of LRRK2 and not its WT form, further enlarging the possible therapeutic window.

Accordingly, our results indicate that Rit2 overexpression not only rescued motor impairments, but also strongly attenuated the loss of DA neurons and striatal DA terminals in mice. Moreover, total aSyn levels and pS129-aSyn pathology were reduced by Rit2 *in vivo*. In our cell model total levels of aSyn were not changed, but pathological pS129-aSyn was strongly reduced. This might be due to the cellular model, with overall low endogenous levels of total aSyn protein. In summary, our results suggest that enhanced Rit2 expression has specific beneficial effects on aSyn inclusion clearance, rather than a general effect on aSyn protein levels.

Viral overexpression of Rit2 in DA neurons, independently from aSyn overexpression, induced motor hyperactivity and this might be due to altered extracellular DA levels or release dynamics. It has been previously reported that Rit2 interacts directly with DAT, is required for DA trafficking, and is necessary for the inactivation of DAT [33]. This suggests that these modulations could be responsible for the increased locomotion in mice. In fact, the genetic deletion of DAT in rats increases extracellular DA lifetime, resulting in locomotor hyperactivity

[81]. Interestingly, the conditional KO of Rit2 in mouse midbrain DA neurons decreases total DAT protein in the striatum, strengthening the possible modulation of DAT by Rit2 [35].

Lastly, the reduction of pS1292-LRRK2 levels *in vitro* and the recent observation that virally overexpressed aSyn in rats increases endogenous LRRK2 kinase activity [60], led us to investigate LRRK2 kinase activity in our mouse model. Using a viral vector encoding A53T-aSyn we confirmed the increased pS1292-LRRK2 levels in DA neurons, indicating an increased kinase activity. The co-expression of Rit2 completely prevented the increase of pS1292-LRRK2 levels. As previously reported, aSyn overexpression results in an increase of endogenous LRRK2 activity, impacting the ALP and worsening aSyn pathology[60]. Even though we used a mutant version of aSyn for this set of experiments, WT aSyn is believed to involve similar mechanisms of neurodegeneration, but with a slower effect[92]. These results suggest that the activation of wild-type LRRK2 plays a role in idiopathic PD pathogenesis and consequently holds a strong pathogenic implication in most PD cases.

However, upstream modifiers of LRRK2 and related mechanisms are mostly unknown. *Rab7L1*, a PD risk factor[82], has recently been suggested to recruit LRRK2 to the Golgi-network[83] and stressed lysosomes [84], and to stimulate its kinase activity[85]. Interestingly, Rab7L1 is a Rab GTPase, part of the RAS superfamily[86] to which Rit2 also belongs[29]. Moreover, we previously proposed a novel hypothesis, in which GTPase-MAPK signaling is involved in the regulation of autophagy[36]. Our study provides evidence for a molecular mechanism leading to LRRK2 kinase inhibition, with Rit2 acting as a direct modifier of LRRK2. This could partly explain the reduced penetrance of the G2019S-LRRK2 mutation, when considering possible differential expression. In addition, we show the involvement of Rit2 in the ALP and its diverse effects on the lysosome, depending on its expression levels. Enhanced Rit2 expression rescues the G2019S-LRRK2-induced lysosomal defects, whereas the reduction of Rit2 levels in neuroblastoma cells and primary DA neurons induces defects in

the ALP and specifically to lysosome biology. These defects are comparable to the ones detected in G2019S-LRRK2 cells, indicating that they might be caused by the reduced Rit2 expression. This notion is further supported by the rescue of ALP defects by re-expression of Rit2 in Rit2-KO cells. In fact, genetic alterations in Rit2 can alter its expression levels, via length differences in short tandem repeats within the promoter[87].

Reduced Rit2 levels, as observed in post-mortem PD brains, strengthen the role of Rit2 as a PD risk factor, possibly by modulating the ALP. Further studies are needed to elucidate the connection of ALP regulation and DAT endocytosis and trafficking.

In conclusion, we demonstrate that Rit2 acts both on autophagy-related processes and pS129-aSyn clearance. Our results suggest that inhibiting LRRK2 kinase activity through enhanced Rit2 expression is beneficial against ALP defects, aSyn pathology and could target not only G2019S-LRRK2 PD, but also idiopathic PD. Our results suggest Rit2, through modulation of LRRK2 activity, as a novel target for neuroprotection in PD and a modulator of the ALP.

## Methods

*Cell culture and transfection*

SH-SY5Y neuroblastoma cell lines stably overexpressing wild-type (WT) or G2019S-LRRK2 were previously described [88, 89] and maintained as in[38]. SH-SY5Y RIT2 KO cells were maintained in DMEM GlutaMAX medium supplemented with 10% FBS and 1% Penicillin/Streptomycin (P/S). SK-N-SH neuroblastoma cell lines stably overexpressing A35T-aSyn were recently described and maintained as in[89]. HEK293T cells were grown in culture medium composed of MEM supplemented with 10% FBS, 1% MEM non-essential amino acids, 1% L-Glutamine, 1% P/S.). All culture conditions were maintained strictly consistent across experimental groups and procedures.

Cells were transfected using the SF Cell Line 4D-Nucleofector™ X kit (Lonza) with the 4D Nucleofector X unit. Nucleofection was carried out according to the manufacturer's protocol. Briefly, 200.000 cells were resuspended in the nucleofection solution containing plasmid DNA (SC118279, Origene, eGFP in pcDNA3.1, 800 ng) and analysed after 72 h. For CO-IP experiments $2x10^6$ cells were resuspended in 100 µl of the nucleofection solution containing 2 µg of plasmid DNA. The plasmids used were: 2xMyc-LRRK2 in pCMV vector for the transient overexpression of both WT and G2019S LRRK2; hRIT2 CDS in pcDNA3.1 vector. The plasmids were nucleofected alone or in combination. Cells were processed for co-immunoprecipitation 48h post nucleofection.

*Primary dopaminergic neurons*

Primary dopaminergic neurons were prepared as described in[90]. Neurons were infected with shRNA (scramble or RIT2) at DIV 7 with MOI of 30 and live imaging assays were performed at DIV 14 as described for each assay.

*Droplet digital PCR and qPCR*

Total RNA was extracted using the RNeasy Plus Mini Kit (Qiagen). First strand cDNA was synthesized using the SuperScript VILO cDNA Synthesis Kit (Invitrogen). 1 ng of cDNA was used for each reaction to assess *RIT2* mRNA gene expression (Hs01046671_m1, FAM), multiplexed with a housekeeping gene (RPP30, HEX, BioRad cat# 10031243). PCR was carried out as suggested by the manufacturer using ddPCR Supermix for probes (BioRad, cat# 11969064001).

PCR program

| | | |
|---|---|---|
| 95°C | 10 min | |
| 94°C | 30 sec | } 40 cycles |
| 60°C | 1 min | |
| | | |
| 98°C | 10 min | |
| 4°C | ∞ | |

After PCR amplification, the plate was analyzed in the QX200 Droplet Reader. Data was analyzed using QuantaSoftTM software from BioRad. Results are reported as Fractional abundance of gene of interest respect to housekeeping gene.

The autophagy gene expression array (PAHS-084Z, Qiagen) for G2019S-LRRK2 cells without and with RIT2 overexpression was carried out according to the manufacturers protocol and as described in[38]. The experiment has been carried out with two technical replicates and quantitative PCR was performed in a CFX96 Touch™ Real-Time PCR Detection System (BioRad). qPCR samples for Rit2 levels in primary neurons were prepared as described above. qPCR was performed in the QuantStudio 5 Real-Time PCR System using the following oligos:

mTBP

FW: ACAGCCACTCTGGAGGAGAA

REV: GCCTGTTTCCGTAACCTCAA

mRit2

FW: GGAGCAGTTCCGTCAGGTATC

REV: ACTAAGCCTTGAAAAGCATCATCG

*Analysis of RIT2 mRNA levels from publicly available datasets*

Geo Dataset GSE2014 composed of SN tissues isolated by laser capture microdissection from sporadic PD patients and controls was analyzed with 206984_s_at probe for RIT2. Geo Dataset GSE46798 composed of human iPSC-derived DA neurons from A53T mutant and corrected control lines was analyzed with ILMN_1796673 probe for *RIT2*. Finally, Geo Dataset GSE17542 composed of laser captured SNpc and VTA from TH-GFP mice was analyzed with 1448125_at probe for *RIT2*.

*Western blotting and CO-IP*

Cells or tissue lysates for western blotting were prepared as previously described in [37]. Primary antibodies used: anti-LRRK2 1:20000 (Abcam, ab172378), anti-pS935-LRRK2 1:1000 (Abcam, ab172382), anti-pS1292-LRRK2 1:1000 (Abcam, ab206035), anti-LC3 1:1000 (Cell Signaling Technologies, 3868), anti-β-actin 1:6000 (Sigma Aldrich, A-5316), anti-aSyn (Abnova, MAB5383), anti-Myc (9E10 hybridoma supernatant, 1:100) total aSyn (CST 2628), pS129-aSyn (WAKO, 015-25191). Chemiluminescence images were acquired using Chemidoc Touch (BioRad) and relative band intensity levels were calculated using ImageLab software (BioRad). For CO-IP experiments cells were mechanically lysed in lysis buffer composed of 50 mM Tris-HCl (pH = 7.6), 150 mM NaCl, 1% IGEPAL CA-630, 0.1% SDS (Sodium

Dodecyl Sulfate), protease/phosphatase inhibitors cocktail (Roche, 4693124001 and 4906837001) and incubated 30 minutes on ice. Total lysates were cleared by centrifugation for 10 minutes at 13000xg at 4°C. Protein concentration was assessed by BCA assay (Pierce, Thermo Scientific, 23225) and samples were adjusted to a concentration of 1 mg/ml. Pre-clearing was performed incubating samples with protein G-agarose (Roche, 11719416001) with gentle agitation for 30 minutes, 4°C. After pre-clearing, 0.5 mg of protein extracts were incubated overnight at 4°C with 5 µg of rabbit anti-LRRK2 antibody (Abcam, ab133474), or with same species IgG (Sigma-Aldrich, 12-370) as negative control, followed by incubation with 100 ul of protein G-agarose for 2 hours at 4°C. After centrifugation protein G-agarose pellets were washed and resuspended in 2X sample buffer and processed for SDS-PAGE as in[38].

*Lysotracker Deep Red, DQ-Red-BSA and Cyto-ID staining*

To investigate lysosome morphology, we utilized the Lysotracker Deep Red dye (Molecular Probes, L12492) following the manufacturer´s instructions, as in[38]. To study the proteolytic activity of lysosomes, the fluorescent DQ-Red-BSA dye (Molecular Probes, D12051) was used following manufacturer´s instructions, as in[38]. To investigate autophagic vesicles we used the CYTO-ID® Autophagy Detection Kit in live cells, which uses a novel dye that selectively labels accumulated autophagic vacuoles. The assay was carried out following manufacturer`s instructions. Briefly, 2ul of CYTO-ID® Green Detection Reagent were diluted in the assay buffer and then incubated for 30 minutes in the incubator. Imaging was carried out in complete media. In Lysotracker and Cyto-ID experiments, the number of vesicles per cell was obtained by using Cell Profiler software to assess the number of fluorescent puncta and divide it by the number of nuclei (representing the number of cells) in the same image field.

*Immunofluorescence and Immunohistochemistry*

Cells were fixed in 4% PFA, permeabilized, blocked and incubated with primary and secondary antibodies, as described in [38]. The primary antibodies were mouse anti-pS129-aSyn 1:2000 (Abcam, ab184674). The secondary antibodies were: Donkey anti-Mouse Secondary Antibody, Alexa Fluor 555 (A31570). Visualization was performed using a Leica SP8-X confocal laser scanning microscope system equipped with an oil immersion 63X objective and images were analysed using CellProfiler to quantify the number and intensity of investigated objects (object size in pixel units: pS129-aSyn 20-250; pipelines available upon request). Immunohistochemistry (IHC) was performed as described in[90]. For DA neuron survival quantification, sections of midbrain (4 sections interval) were stained with NeuN (Millipore, MAB377, 1:500) and TH (Pel-Freez Biologicals, P60101, 1:1000) antibodies, followed by incubation with Cy3 (Jackson Immuno, 715-165-150, 1:200) and Alexa Fluor 647 (Life Technologies, A-21448, 1:400) respectively. Images were acquired using a slide scanner (TissueScope™, Huron Digital Pathology). Both NeuN and TH positive neurons were counted using a stereology software with optical fractioning (Stereo Investigator, mbf bioscience). For fluorescence quantification of the striatal dopamine terminals, sections were labeled with a TH antibody (P60101) and incubated with Alexa Fluor 647 (Life Technologies, A-21448, 1:400). For aSyn neuropathology, sections were labeled for pS129-aSyn (*custom antibody*, 73C6 1µg/ml, see following section) followed by Alexa Fluor 647 (Life Technologies, A-31571, 1:400). We used our custom 73C6 antibody for pS129-aSyn quantification because the signal obtained on brain sections was stronger and more specific than with ab184674 (used on cells). Images were acquired with a confocal microscope (LSM700, Carl Zeiss) and fluorescence quantification was obtained by using Corrected Total Cell Fluorescence with ImageJ software.

*73C6 antibody production and purification*

Briefly, mice were immunized with a peptide containing amino acids 111 to 135 (C-terminal) from human aSyn. B-cells were harvested and fused with myeloma cells. Hybridomas were maintained in DMEM high glucose supplemented with 10% Ultra-low IgG Fetal Bovin Serum (FBS) and Penicillin/Streptomycin (Gibco) and filtered through a 0.2µm filter. For purification, Protein-G agarose (Thermo-Fisher, cat# P120399) was used according to manufacturer's instructions. Final IgG concentration was determined with spectrometry (Nanodrop One, Thermo-Fisher). Antibody specificity was determined using Western Blotting on HEK293 cells transfected with either WT-aSyn or S129A-aSyn, with or without concomitant transfection with the PLK2 kinase (Supplementary Fig S9).

*Animals*

Heterozygous DAT-Ires-Cre mice aged between two and three months from Jackson Laboratory were used (males and females). Housing, breeding and procedures were approved by the CPAUL (Comité de protection des animaux de l'Université Laval) and the CCPA (Comité canadien de protection des animaux).

*Stereotaxic injection of AAV vectors*

Mice were deeply anesthetized with isoflurane (3-4% for induction and 2% for maintenance with 0,5% oxygen). AAV-emCBA-GFP-Flex (7.5E12), AAV-CMVie-hSynP-synA53T (7.5E12) + AAV-emCBA-GFP-Flex, AAV-CAG-Flex-*Rit2*-EGFP, AAV-CAG-Flex-*Rit2*-EGFP (7E12 GC/ml) + AAV-CMVie-hSynP-synA53T were unilaterally injected in the right substantia nigra. A total volume of 1ul was injected at 2nl/sec at the following coordinates: -3,5mm (A/P); +1mm (M/L); +4mm (D/V) from bregma. Mice were euthanized 4 months after surgery.

*Behavioral tests*

*Open field*

Mice were placed in the room one hour prior to testing for habituation, and then were placed in the open field for 60 minutes. Open fields (**) were used in the 2-animal monitor mode and the activity of the mice was recorded automatically with the VersaMax software. The total distance traveled (cm), horizontal activity (number of beam breaks) and vertical activity (number of beam breaks) were analyzed. The test was performed after 4 months following injection.

*Cylinder, rotation and amphetamine test*

Mice were placed, one hour prior to testing, in the room for habituation and were then placed in a cylinder with a diameter of 10 cm. Tests were performed 4 months after injection and were recorded by video. For the cylinder and rotation tests, mice were placed in the cylinder for 5 minutes. Forepaw use and complete rotations were analyzed manually by an investigator. For the amphetamine test, mice were injected with amphetamine at 5mg/kg of body weight. After 15 minutes, they were placed in the cylinder for 30 minutes. Their complete rotations were counted manually by an investigator.

*Fluorescence in situ hybridization*

RNAscope probes for mouse TH and *RIT2* (TH – 317621, RIT2 – 58904) were designed by Advanced Cell Diagnostics (Newark, CA, USA). The *in situ* hybridization was carried out following the manufacturers protocol for fixed and frozen tissue and as described in [91].

*Proximity ligation assay (PLA)*

Cells for PLA were processed as for ICC experiments. *In vivo*, 60 µm thick sections were used for PLA staining. Sections were washed twice in 1x PBS and then blocked for 60 minutes in

blocking solution (1x PBS +1% NDS + 0,2% Triton X100) at RT. After blocking the manufacturer's protocol was followed. Primary antibodies (pS1292 LRRK2, Abcam ab203181; total LRRK2, UC Davis #75-36253 or ab133474, Rit2, Origene TA501704) were diluted 1:500 in Duolink II Antibody Diluent (1x) and incubated overnight at 4°C shaking. After 2 washes of 5 minutes in 1x PBS + 0,1% Triton-X100, sections were incubated with PLA probes (Duolink II anti-Mouse MINUS and Duolink II anti-Rabbit PLUS) 1:5 in Antibody Diluent and incubated for 90 min at 37°C shaking. Washes in 1x PBS + 0,1% Triton-X100 were repeated and then sections were incubated in ligation solution (1x Duolink II Ligation stock + Ligase 1:40) for 45 min at 37°C shaking. After ligation sections were washed 2x 5 min in 1x PBS and then incubated with an amplification solution (1x Duolink II Amplification stock + Polymerase 1:80) for 100 min at 37°C shaking. After amplification sections were washed twice in 1x PBS for 10 min and then mounted using Fluoroshield mounting medium. Images were acquired with a confocal microscope (LSM700, Zeiss, or Leica SP8-X) and analysis of PLA spots was carried out using the “Particle Analysis” function in ImageJ or Cellprofiler (pipelines available upon request).

*Statistical analysis*

Statistical analyses were performed using GraphPad Prism 8. One-way ANOVA was used in experiments comparing 3 or more groups, followed by Bonferroni´s or Sidak post-hoc test for pairwise comparisons. With 2 experimental groups, the unpaired two-tailed Student´s t-test or two-tailed Mann-Whitney test was utilized. Threshold for significance was set at $p<0.05$. Data distribution was assessed using the D`Agostino-Pearson test for normal distribution. All experiments were performed in a minimum of 3 independent biological replicates.

**Acknowledgments**

The authors are thankful to: lab member Giulia Lamonaca for their invaluable assistance and support; Dr. Francesca Pischedda and Prof. Giovanni Piccoli (University of Trento, Italy) for their help with the pS935-LRRK2 western blot; Anne Picard for the RT-PCR of autophagy genes; Dr. Alexandros Lavdas for the analysis of Lysotracker images. We thank Veronique Rioux for the technical assistance and Modesto Peralta for comments on the manuscript. We thank the CERVO Centre Molecular Tool Platform (https://neurophotonics.ca/fr/pom) for the production of the viral vectors used. The authors thank the Department of Innovation, Research and University of the Autonomous Province of Bozen/Bolzano for covering the Open Access publication costs.

**Author contributions**

JO and AMC contributed to conceptualization, methodology, formal analysis, investigation, data curation, writing – original draft, writing – review and editing and visualization; GF SP and SM contributed to methodology, formal analysis, investigation, data curation for some experiments; EL and VB contributed resources; CC contributed to the planning of some experiments and to revising the manuscript. AAH, PPP contributed to Eurac funding acquisition; CG contributed to methodology, formal analysis, investigation, data curation for some experiments. ML and MV contributed equally to conceptualization, methodology, formal analysis, data curation, writing – original draft, writing – review and editing, supervision, project administration, funding acquisition.

**Conflict of interest**

The authors declare no competing interests.

**Funding**

This work was supported by Parkinson Canada (grant number 2018-00157 to ML and MV), the Weston Brain Institute (grant number RR191071 to ML and MV), the Canadian Institute of Health Research to ML (420504), the Autonomous Province of Bozen/Bolzano for core funding to the Institute for Biomedicine of Eurac Research to MV. AMC received a scholarship from the Fonds de Recherche du Québec–Santé. ML receives salary support from Fonds de Recherche du Québec–Santé, Chercheur-Boursier Senior in partnership with Parkinson Québec (34974). JO is holding a Basic research fellowship from Parkinson Canada.

**DATA AVAILABILITY**

The datasets generated and/or analyzed during the current study, and the Cell Profiler pipelines generated by for image analyses, are available upon reasonable request to both the corresponding authors.

**Figure legends**

**Figure 1:** Rit2 *is expressed in human and mouse brain, and is reduced in both sporadic PD patients and in cells overexpressing LRRK2.* A) Geo dataset comparing *RIT2* expression levels in DA neurons of the SNc isolated by laser capture microdissection. mRNA levels were reduced by 2.2-fold in DA neurons from sporadic PD patients, when compared to healthy controls (GSE20141, controls=8, PD=10). B) Geo dataset (GSE46798) comparing Rit2 expression in iPSC-derived DA neurons with A53T-aSyn mutation to control mutation-corrected neurons (n=3). C) Droplet Digital PCR was carried out to assess *RIT2* mRNA levels in recombinant neuroblastoma cell lines. Ratio of *RIT2* mRNA, normalized to RPP30, is reduced in WT and G2019S LRRK2 cells (n=3). D) Geo dataset (GSE17542) comparing *Rit2* expression in SNc and VTA from TH-GFP mice (n=3). E) Quantification of Rit2 mRNA levels in dopaminergic neurons in the midbrain. Viral aSyn expression decreases Rit2 mRNA levels (n=6). F) Fluorescent in situ hybridization (RNAscope®) was employed to show *Rit2* mRNA expression in DA neurons of the mouse SNc and TH and aSyn staining were visualised using immunostaining. Data are median (min-max) or means±SEM.*$p<0.05$, **$p<0.01$ two-tailed Student´s t-test. # $p<0.05$ unpaired t-test with Welch's correction after D`Agostino-Pearson test for normal distribution. **$p<0.01$, ***$p<0.001$, one-way ANOVA followed by Bonferroni´s post-hoc test.

**Figure 2:** *Overexpression of* Rit2 *does not affect overall autophagic flux.* A) The autophagic flux was assessed in G2019S-LRRK2, G2019S LRRK2+ Rit2 and G2019S_LRRK2 +GFP cells upon treatment with CQ (100 μM, 3h) and WB for LC3B. B) The ratio between LC3B-II and LC3B-I was not different, suggesting no differences in autophagic flux (n=3). C) Quantification of LC3B levels (normalized to β-actin) indicated no differences upon Rit2

overexpression or CQ-treatment (n=3). D) CytoID assay was employed to visualize autophagosome and autolysosome distribution. E) Quantification of CytoID-positive puncta revealed a significant increase in G2019S-LRRK2 cells, when Rit2 was overexpressed (n=4). Data are median (min-max) or means±SEM. In imaging experiments analysis was conducted on 700-1000 cells per group in each experiment.

***p<0.01, unpaired two tailed Student´s t-test.

**Figure 3:** *Rit2 overexpression is rescuing lysosomal morphology and proteolytic activity in G2019S-LRRK2 cells.* A) Cell processing with the Lysotracker Red dye was performed to visualize lysosomes G2019S-LRRK2 and G2019S LRRK2+ Rit2 cells. B) The number of lysosomes per cell was quantified and revealed an increase, when Rit2 was transfected in G2019S LRRK2 cells (n=3). C) The average size of lysosomes was assessed, and a significant decrease of the diameter was measured when Rit2 was transfected to G2019S-LRRK2 cells (n=3). D) The DQ-Red-BSA assay was employed to assess the proteolytic activity of lysosomes. E) Quantification of DQ-Red-BSA fluorescent spots revealed a significant increase in G2019S LRRK2 cells, with Rit2 overexpression (n=3).

In imaging experiments analysis was conducted on 700-1000 cells per group in each experiment.

*p<0.05, ***p<0.001, unpaired two tailed Student´s t-test.

**Figure 4:** *RIT2 overexpression reduces pS129-aSyn positive inclusions and reduces pS1292-LRRK2.* A) Representative images showing pS129-aSyn immunostaining in SH-SY5Y, WT-LRRK2 and G2019S-LRRK2 cells with or without Rit2 overexpression. B) Quantification pS129-aSyn in cell overexpressing either G2019S-LRRK2 alone or G2019S-LRRK2 with Rit2 (n=4). C) PLA was used to quantify phosphorylation of Serine 1292 of LRRK2 in

neuroblastoma cell lines. D) The G2019S-LRRK2 mutation increases Serine 1292 phosphorylation, which is reduced by Rit2 overexpression or treatment with PF-475 LRRK2 kinase inhibitor (n=4). Data are presented as median (min-max). In imaging experiments analysis was conducted on 700-1000 cells per group in each experiment.

*p<0.05, **p<0.01, ****p<0.0001 two-tailed Student's t-test.

**Figure 5**: *Enhanced* Rit2 *expression in the mouse midbrain counteracts aSyn-dependent deficits and DA neuron loss.* A) Overexpression of A53T-aSyn increases the number of ipsilateral rotations and co-injection with AAV-Rit2 or injection of AAV-Rit2 alone increases the number of contralateral rotations. B) Overexpression of Rit2 alone or with aSyn significantly increases horizontal activity in the open field ($n^{GFP}$=7, $n^{aSyn}$=9, $n^{aSyn+RIT2}$=8, $n^{RIT2}$=6 for behavioural tests). C) IHC for TH was used to count dopaminergic neurons in the midbrain. D) Overexpression of A53T-aSyn alone induces a significant loss of DA neurons, which is attenuated by co-injection of AAV-Flex-Rit2. E) aSyn overexpression tends to reduce the number of NeuN+ cells in the ipsilateral SNc and concomitant overexpression of Rit2 significantly preserves NeuN+ cells (5 animals/group). F) IHC for TH was used to measure the density of DA projections in the striatum. G) Overexpression of A53T-aSyn decreases the number of TH+ axons in the striatum, which is attenuated by the co-injection of AAV-Flex-Rit2 (n=5/group for IHC experiments).

Data represented as mean ± SEM *p<0,05 **p<0,01 ***p<0,001 ****p<0,0001, one-way ANOVA followed by Bonferroni's post-hoc test. Scale bar = 500um.

**Figure 6**: *Enhanced* Rit2 *expression reduces total aSyn and pS129-aSyn levels.* A) Total aSyn levels in mice injected with AAV-A53T-aSyn alone or in combination with AAV-Flex-Rit2 were assessed blotting for total and phosphorylated aSyn and β-actin. B) Quantification of total

aSyn levels, normalized on β-actin (n=4). Co-injection of AAV-Flex-*Rit2* significantly reduces aSyn levels in the ipsilateral side. C) Quantification of pS129-aSyn levels, normalized on β-actin (5 animals/group). Co-injection of AAV-Flex-Rit2 significantly reduces aSyn levels in the ipsilateral side. D) Quantification of pS129-aSyn levels, normalized on total aSyn. Co-injection of AAV-Flex-Rit2 does not alter pS129-aSyn/aSyn ratio. E) IHC staining of pS129-aSyn and TH in the midbrain of AAV GFP, AAV-A53T-aSyn and AAV-A53T-aSyn + AAV-Flex-*Rit2* injected mice. F) Quantification of pS129-aSyn intensity. AAV-A53T-aSyn injection significantly increases the intensity of pS129-aSyn signal, which is reduced by the co-injection of AAV-Flex-*Rit2* (5 animals/group). Scale bar = 20um.

Data represented as mean ± SEM. *p<0.05, **p<0.01, ***p<0.001 ****p<0.0001, one-way ANOVA followed by the Bonferroni´s post-hoc test.

**Figure 7:** *In vivo aSyn overexpression increases endogenous LRRK2 activity, which is prevented by Rit2 co-expression.* A) PLA analysis of AAV-GFP, AAV-A53T-aSyn and AAV-A53T-aSyn+AAV-Flex-Rit2 injected mice in TH-positive neurons in the SNc. B) Quantification of PLA counts in TH-positive neurons shows a significant increase of endogenous LRRK2 kinase activity with AAV-A53T-aSyn injection. The increase is completely prevented by co-injection of AAV-Flex-Rit2 with AAV-A53T-aSyn (AAV-GFP=6 animals, AAV-A53T-aSyn=6 animals, AAV-A53T-aSyn+AAV-Flex-Rit2=5 animals).

Data represented as mean ± SEM. *p<0.05, one-way ANOVA followed by Bonferroni´s post-hoc test.

**Figure 8:** *Lysosomal morphology and proteolytic activity are altered in Rit2 KO neuroblastoma cells.* A) CytoID assay was employed to visualize autophagosome and autolysosome distribution. B) Quantification of CytoID-positive puncta revealed a significant

increase in Rit2 KO cells (n=3). C) Cell processing with the Lysotracker Red dye was performed to visualize number and size of lysosomes. D) The number of lysosomes per cell was quantified and revealed a decrease, with Rit2 KO (n=6). E) The average size of lysosomes was assessed, and a significant increase of the diameter was measured in Rit2 KO cells (n=6). F) The DQ-Red-BSA assay was employed to assess the proteolytic activity of lysosomes. G-H) Quantification of DQ-Red-BSA fluorescent spots revealed a significant decrease of number and intensity in Rit2 KO cells (n=3). In imaging experiments and analysis was conducted on 700-1000 cells per group in each experiment.

Data represented as median (min-max). *p<0.05, ***p<0.001, ****p<0.0001 unpaired two tailed Student´s t-test.

**Figure 9:** *Rit2 KD leads to abnormal lysosomal morphology and proteolytic activity in primary dopaminergic neurons.* A) Lysosomes were visualized with the Lysotracker Red dye in neurons. B) The number of lysosomes per cell was quantified and revealed a decrease when Rit2 levels were reduced (n=3). C) The average size of lysosomes was assessed, and a significant increase of the diameter was measured upon Rit2 KD (n=3). D) The DQ-Red-BSA assay was employed to assess the proteolytic activity of lysosomes. E-F) Quantification of DQ-Red-BSA fluorescent spots revealed a significant decrease of number and intensity in Rit2 KD neurons (n=3).

Data represented as median (min-max). *p<0.05, ***p<0.001, unpaired two tailed Student´s t-test.

# References


1. Tysnes O-B, Storstein A. Epidemiology of Parkinson's disease. *Journal of Neural Transmission* **124**, 901-905 (2017).

2. Poewe W*, et al.* Parkinson disease. *Nat Rev Dis Primers* **3**, 17013 (2017).

3. Lesage S, Brice A. Parkinson's disease: from monogenic forms to genetic susceptibility factors. *Hum Mol Genet* **18**, R48-59 (2009).

4. Dauer W, Przedborski S. Parkinson's disease: mechanisms and models. *Neuron* **39**, 889-909 (2003).

5. Deng H, Wang P, Jankovic J. The genetics of Parkinson disease. *Ageing Res Rev* **42**, 72-85 (2018).

6. Dickson DW. Neuropathology of Parkinson disease. *Parkinsonism & Related Disorders* **46**, S30-S33 (2018).

7. Goedert M, Spillantini MG, Del Tredici K, Braak H. 100 years of Lewy pathology. *Nat Rev Neurol* **9**, 13-24 (2013).

8. Kenney DL, Benarroch EE. The autophagy-lysosomal pathway: General concepts and clinical implications. *Neurology* **85**, 634-645 (2015).

9. Finkbeiner S. The Autophagy Lysosomal Pathway and Neurodegeneration. *Cold Spring Harb Perspect Biol* **12**, (2020).

10. Nixon RA. The role of autophagy in neurodegenerative disease. *Nat Med* **19**, 983-997 (2013).

11. Anglade P*, et al.* Apoptosis and autophagy in nigral neurons of patients with Parkinson's disease. *Histol Histopathol* **12**, 25-31 (1997).

12. Dehay B*, et al.* Pathogenic lysosomal depletion in Parkinson's disease. *J Neurosci* **30**, 12535-12544 (2010).

13. Paisan-Ruiz C, Lewis PA, Singleton AB. LRRK2: cause, risk, and mechanism. *J Parkinsons Dis* **3**, 85-103 (2013).

14. Fuji RN*, et al.* Effect of selective LRRK2 kinase inhibition on nonhuman primate lung. *Sci Transl Med* **7**, 273ra215 (2015).

15. Miklossy J*, et al.* LRRK2 expression in normal and pathologic human brain and in human cell lines. *J Neuropathol Exp Neurol* **65**, 953-963 (2006).

16. Trinh J, Farrer M. Advances in the genetics of Parkinson disease. *Nat Rev Neurol* **9**, 445-454 (2013).

17. Beccano-Kelly DA*, et al.* Synaptic function is modulated by LRRK2 and glutamate release is increased in cortical neurons of G2019S LRRK2 knock-in mice. *Front Cell Neurosci* **8**, 301 (2014).

18. Beccano-Kelly DA*, et al.* LRRK2 overexpression alters glutamatergic presynaptic plasticity, striatal dopamine tone, postsynaptic signal transduction, motor activity and memory. *Hum Mol Genet* **24**, 1336-1349 (2015).

19. Parisiadou L*, et al.* LRRK2 regulates synaptogenesis and dopamine receptor activation through modulation of PKA activity. *Nat Neurosci* **17**, 367-376 (2014).

20. Piccoli G*, et al.* LRRK2 controls synaptic vesicle storage and mobilization within the recycling pool. *J Neurosci* **31**, 2225-2237 (2011).

21. Saez-Atienzar S*, et al.* The LRRK2 inhibitor GSK2578215A induces protective autophagy in SH-SY5Y cells: involvement of Drp-1-mediated mitochondrial fission and mitochondrial-derived ROS signaling. *Cell Death Dis* **5**, e1368 (2014).

22. Manzoni C, Lewis PA. LRRK2 and Autophagy. *Adv Neurobiol* **14**, 89-105 (2017).

23. Manzoni C*, et al.* Pathogenic Parkinson's disease mutations across the functional domains of LRRK2 alter the autophagic/lysosomal response to starvation. *Biochem Biophys Res Commun* **441**, 862-866 (2013).

24. Schapansky J*, et al.* Familial knockin mutation of LRRK2 causes lysosomal dysfunction and accumulation of endogenous insoluble alpha-synuclein in neurons. *Neurobiol Dis* **111**, 26-35 (2018).

25. Volpicelli-Daley LA*, et al.* G2019S-LRRK2 Expression Augments alpha-Synuclein Sequestration into Inclusions in Neurons. *J Neurosci* **36**, 7415-7427 (2016).

26. Nalls MA*, et al.* Large-scale meta-analysis of genome-wide association data identifies six new risk loci for Parkinson's disease. *Nat Genet* **46**, 989-993 (2014).

27. Nalls MA*, et al.* Expanding Parkinson’s disease genetics: novel risk loci, genomic context, causal insights and heritable risk. *bioRxiv*, 388165 (2019).

28. Pankratz N*, et al.* Meta-analysis of Parkinson's disease: identification of a novel locus, RIT2. *Annals of neurology* **71**, 370-384 (2012).

29. Lee CH, Della NG, Chew CE, Zack DJ. Rin, a neuron-specific and calmodulin-binding small G-protein, and Rit define a novel subfamily of ras proteins. *J Neurosci* **16**, 6784-6794 (1996).

30. Hoshino M, Nakamura S. Small GTPase Rin induces neurite outgrowth through Rac/Cdc42 and calmodulin in PC12 cells. *J Cell Biol* **163**, 1067-1076 (2003).

31. Shi GX, Han J, Andres DA. Rin GTPase couples nerve growth factor signaling to p38 and b-Raf/ERK pathways to promote neuronal differentiation. *The Journal of biological chemistry* **280**, 37599-37609 (2005).

32. Spencer ML, Shao H, Tucker HM, Andres DA. Nerve growth factor-dependent activation of the small GTPase Rin. *The Journal of biological chemistry* **277**, 17605-17615 (2002).

33. Navaroli DM*, et al.* The plasma membrane-associated GTPase Rin interacts with the dopamine transporter and is required for protein kinase C-regulated dopamine transporter trafficking. *J Neurosci* **31**, 13758-13770 (2011).

34. Fagan RR*, et al.* Dopamine transporter trafficking and Rit2 GTPase: Mechanism of action and in vivo impact. *The Journal of biological chemistry* **295**, 5229-5244 (2020).

35. Sweeney CG*, et al.* Conditional, inducible gene silencing in dopamine neurons reveals a sex-specific role for Rit2 GTPase in acute cocaine response and striatal function. *Neuropsychopharmacology*, (2019).

36. Obergasteiger J, Frapporti G, Pramstaller PP, Hicks AA, Volta M. A new hypothesis for Parkinson's disease pathogenesis: GTPase-p38 MAPK signaling and autophagy as convergence points of etiology and genomics. *Mol Neurodegener* **13**, 40 (2018).

37. Rui Q, Ni H, Li D, Gao R, Chen G. The Role of LRRK2 in Neurodegeneration of Parkinson Disease. *Curr Neuropharmacol* **16**, 1348-1357 (2018).

38. Obergasteiger J*, et al.* Kinase inhibition of G2019S-LRRK2 enhances autolysosome formation and function to reduce endogenous alpha-synuclein intracellular inclusions. *Cell Death Discov* **6**, 45 (2020).

39. Latourelle JC, Dumitriu A, Hadzi TC, Beach TG, Myers RH. Evaluation of Parkinson disease risk variants as expression-QTLs. *PLoS One* **7**, e46199 (2012).

40. Bossers K*, et al.* Analysis of gene expression in Parkinson's disease: possible involvement of neurotrophic support and axon guidance in dopaminergic cell death. *Brain pathology* **19**, 91-107 (2009).

41. Zheng B*, et al.* PGC-1alpha, a potential therapeutic target for early intervention in Parkinson's disease. *Sci Transl Med* **2**, 52ra73 (2010).

42. Lesnick TG*, et al.* A genomic pathway approach to a complex disease: axon guidance and Parkinson disease. *PLoS Genet* **3**, e98 (2007).

43. Ryan SD*, et al.* Isogenic human iPSC Parkinson's model shows nitrosative stress-induced dysfunction in MEF2-PGC1alpha transcription. *Cell* **155**, 1351-1364 (2013).

44. Zhou Q, Li J, Wang H, Yin Y, Zhou J. Identification of nigral dopaminergic neuron-enriched genes in adult rats. *Neurobiology of aging* **32**, 313-326 (2011).

45. Phani S, Gonye G, Iacovitti L. VTA neurons show a potentially protective transcriptional response to MPTP. *Brain Res* **1343**, 1-13 (2010).

46. Bravo-San Pedro JM*, et al.* The LRRK2 G2019S mutant exacerbates basal autophagy through activation of the MEK/ERK pathway. *Cell Mol Life Sci* **70**, 121-136 (2013).

47. Schapansky J, Nardozzi JD, Felizia F, LaVoie MJ. Membrane recruitment of endogenous LRRK2 precedes its potent regulation of autophagy. *Hum Mol Genet* **23**, 4201-4214 (2014).

48. Bellomo G, Paciotti S, Gatticchi L, Parnetti L. The vicious cycle between alpha-synuclein aggregation and autophagic-lysosomal dysfunction. *Mov Disord* **35**, 34-44 (2020).

49. Ho PW*, et al.* Age-dependent accumulation of oligomeric SNCA/alpha-synuclein from impaired degradation in mutant LRRK2 knockin mouse model of Parkinson disease:

role for therapeutic activation of chaperone-mediated autophagy (CMA). *Autophagy*, 1-24 (2019).

50. Tsuyuki S*, et al.* Detection of WIPI1 mRNA as an indicator of autophagosome formation. *Autophagy* **10**, 497-513 (2014).

51. Xiao FH*, et al.* Transcriptome evidence reveals enhanced autophagy-lysosomal function in centenarians. *Genome Res* **28**, 1601-1610 (2018).

52. Zhang XD, Qi L, Wu JC, Qin ZH. DRAM1 regulates autophagy flux through lysosomes. *PLoS One* **8**, e63245 (2013).

53. Klionsky DJ*, et al.* Guidelines for the use and interpretation of assays for monitoring autophagy (4th edition)(1). *Autophagy* **17**, 1-382 (2021).

54. Kalia LV*, et al.* Clinical correlations with Lewy body pathology in LRRK2-related Parkinson disease. *JAMA Neurol* **72**, 100-105 (2015).

55. Volta M*, et al.* Chronic and acute LRRK2 silencing has no long-term behavioral effects, whereas wild-type and mutant LRRK2 overexpression induce motor and cognitive deficits and altered regulation of dopamine release. *Parkinsonism Relat Disord* **21**, 1156-1163 (2015).

56. Daher JP*, et al.* Leucine-rich Repeat Kinase 2 (LRRK2) Pharmacological Inhibition Abates alpha-Synuclein Gene-induced Neurodegeneration. *The Journal of biological chemistry* **290**, 19433-19444 (2015).

57. Obergasteiger J, Uberbacher C, Pramstaller PP, Hicks AA, Corti C, Volta M. CADPS2 gene expression is oppositely regulated by LRRK2 and alpha-synuclein. *Biochem Biophys Res Commun* **490**, 876-881 (2017).

58. Kluss JH*, et al.* Detection of endogenous S1292 LRRK2 autophosphorylation in mouse tissue as a readout for kinase activity. *NPJ Parkinsons Dis* **4**, 13 (2018).

59. Lobbestael E, Civiero L, De Wit T, Taymans JM, Greggio E, Baekelandt V. Pharmacological LRRK2 kinase inhibition induces LRRK2 protein destabilization and proteasomal degradation. *Sci Rep* **6**, 33897 (2016).

60. Di Maio R*, et al.* LRRK2 activation in idiopathic Parkinson's disease. *Sci Transl Med* **10**, (2018).

61. Backman CM*, et al.* Characterization of a mouse strain expressing Cre recombinase from the 3' untranslated region of the dopamine transporter locus. *Genesis* **44**, 383-390 (2006).

62. Oliveras-Salva M*, et al.* rAAV2/7 vector-mediated overexpression of alpha-synuclein in mouse substantia nigra induces protein aggregation and progressive dose-dependent neurodegeneration. *Mol Neurodegener* **8**, 44 (2013).

63. Uenaka T*, et al.* In silico drug screening by using genome-wide association study data repurposed dabrafenib, an anti-melanoma drug, for Parkinson's disease. *Hum Mol Genet* **27**, 3974-3985 (2018).

64. Liu X*, et al.* Genome-wide Association Study of Autism Spectrum Disorder in the East Asian Populations. *Autism Res* **9**, 340-349 (2016).

65. Hamedani SY*, et al.* Ras-like without CAAX 2 (RIT2): a susceptibility gene for autism spectrum disorder. *Metab Brain Dis* **32**, 751-755 (2017).

66. Glessner JT*, et al.* Strong synaptic transmission impact by copy number variations in schizophrenia. *Proc Natl Acad Sci U S A* **107**, 10584-10589 (2010).

67. Cuervo AM, Stefanis L, Fredenburg R, Lansbury PT, Sulzer D. Impaired degradation of mutant alpha-synuclein by chaperone-mediated autophagy. *Science* **305**, 1292-1295 (2004).

68. Komatsu M*, et al.* Loss of autophagy in the central nervous system causes neurodegeneration in mice. *Nature* **441**, 880-884 (2006).

69. Lynch-Day MA, Mao K, Wang K, Zhao M, Klionsky DJ. The role of autophagy in Parkinson's disease. *Cold Spring Harbor perspectives in medicine* **2**, a009357 (2012).

70. Chu Y, Dodiya H, Aebischer P, Olanow CW, Kordower JH. Alterations in lysosomal and proteasomal markers in Parkinson's disease: relationship to alpha-synuclein inclusions. *Neurobiol Dis* **35**, 385-398 (2009).

71. Orenstein SJ*, et al.* Interplay of LRRK2 with chaperone-mediated autophagy. *Nat Neurosci* **16**, 394-406 (2013).

72. Webb JL, Ravikumar B, Atkins J, Skepper JN, Rubinsztein DC. Alpha-Synuclein is degraded by both autophagy and the proteasome. *The Journal of biological chemistry* **278**, 25009-25013 (2003).

73. Kaushik S, Massey AC, Mizushima N, Cuervo AM. Constitutive activation of chaperone-mediated autophagy in cells with impaired macroautophagy. *Mol Biol Cell* **19**, 2179-2192 (2008).

74. West AB*, et al.* Parkinson's disease-associated mutations in leucine-rich repeat kinase 2 augment kinase activity. *Proc Natl Acad Sci U S A* **102**, 16842-16847 (2005).

75. Zhao HT*, et al.* LRRK2 Antisense Oligonucleotides Ameliorate alpha-Synuclein Inclusion Formation in a Parkinson's Disease Mouse Model. *Mol Ther Nucleic Acids* **8**, 508-519 (2017).

76. Dzamko N*, et al.* Inhibition of LRRK2 kinase activity leads to dephosphorylation of Ser(910)/Ser(935), disruption of 14-3-3 binding and altered cytoplasmic localization. *Biochem J* **430**, 405-413 (2010).

77. Nichols RJ*, et al.* 14-3-3 binding to LRRK2 is disrupted by multiple Parkinson's disease-associated mutations and regulates cytoplasmic localization. *Biochem J* **430**, 393-404 (2010).

78. Herzig MC*, et al.* LRRK2 protein levels are determined by kinase function and are crucial for kidney and lung homeostasis in mice. *Hum Mol Genet* **20**, 4209-4223 (2011).

79. Mercatelli D*, et al.* Leucine-rich repeat kinase 2 (LRRK2) inhibitors differentially modulate glutamate release and Serine935 LRRK2 phosphorylation in striatal and cerebrocortical synaptosomes. *Pharmacol Res Perspect* **7**, e00484 (2019).

80. Fraser KB*, et al.* Ser(P)-1292 LRRK2 in urinary exosomes is elevated in idiopathic Parkinson's disease. *Mov Disord* **31**, 1543-1550 (2016).

81. Leo D*, et al.* Pronounced Hyperactivity, Cognitive Dysfunctions, and BDNF Dysregulation in Dopamine Transporter Knock-out Rats. *J Neurosci* **38**, 1959-1972 (2018).

82. Satake W*, et al.* Genome-wide association study identifies common variants at four loci as genetic risk factors for Parkinson's disease. *Nat Genet* **41**, 1303-1307 (2009).

83. Madero-Perez J*, et al.* RAB7L1-Mediated Relocalization of LRRK2 to the Golgi Complex Causes Centrosomal Deficits via RAB8A. *Front Mol Neurosci* **11**, 417 (2018).

84. Eguchi T*, et al.* LRRK2 and its substrate Rab GTPases are sequentially targeted onto stressed lysosomes and maintain their homeostasis. *Proc Natl Acad Sci U S A* **115**, E9115-E9124 (2018).

85. Purlyte E*, et al.* Rab29 activation of the Parkinson's disease-associated LRRK2 kinase. *EMBO J* **37**, 1-18 (2018).

86. Wang S*, et al.* A role of Rab29 in the integrity of the trans-Golgi network and retrograde trafficking of mannose-6-phosphate receptor. *PLoS One* **9**, e96242 (2014).

87. Emamalizadeh B*, et al.* The human RIT2 core promoter short tandem repeat predominant allele is species-specific in length: a selective advantage for human evolution? *Molecular Genetics and Genomics* **292**, 611-617 (2017).

88. Vancraenenbroeck R*, et al.* In silico, in vitro and cellular analysis with a kinome-wide inhibitor panel correlates cellular LRRK2 dephosphorylation to inhibitor activity on LRRK2. *Front Mol Neurosci* **7**, 51 (2014).

89. Volta M*, et al.* Elevated levels of alpha-synuclein blunt cellular signal transduction downstream of Gq protein-coupled receptors. *Cellular Signalling* **30**, 82-91 (2017).

90. Doucet-Beaupré H*, et al.* Lmx1a and Lmx1b regulate mitochondrial functions and survival of adult midbrain dopaminergic neurons. *Proceedings of the National Academy of Sciences of the United States of America* **113**, E4387-E4396 (2016).

91. Salesse C*, et al.* Opposite Control of Excitatory and Inhibitory Synapse Formation by Slitrk2 and Slitrk5 on Dopamine Neurons Modulates Hyperactivity Behavior. *Cell Rep* **30**, 2374-2386 e2375 (2020).

92. Lu, J., Sun, F., Ma, H., Qing, H. & Deng, Y. Comparison between α-synuclein wild-type and A53T mutation in a progressive Parkinson's disease model. *Biochem Biophys Res Commun* **464**, 988-993, doi:10.1016/j.bbrc.2015.07.007 (2015).

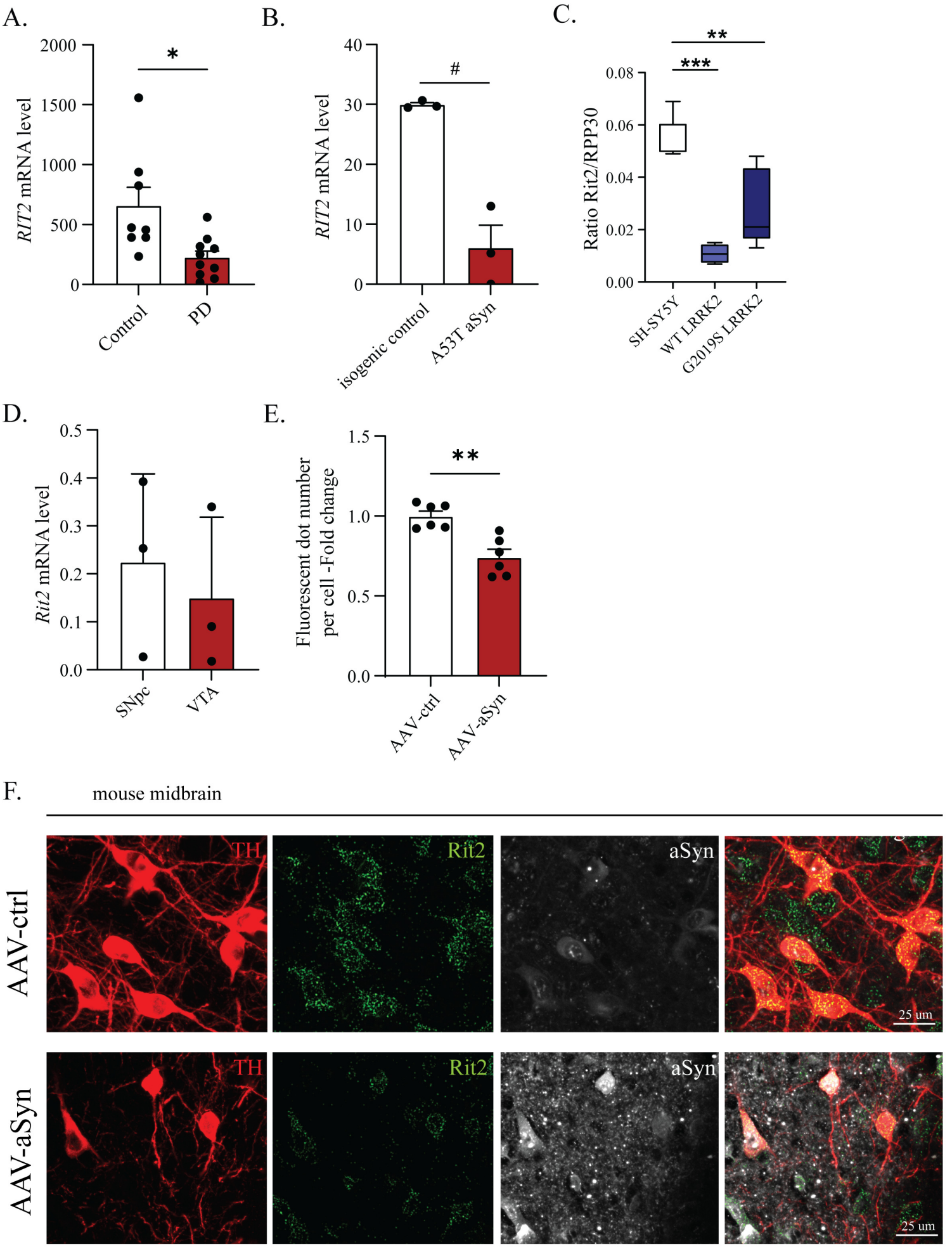
A.
RIT2 mRNA level
2000
1500
1000
500
0
*
Control
PD
B.
RIT2 mRNA level
40
30
20
10
0
#
isogenic control
A53T aSyn
C.
Ratio Rit2/RPP30
0.08
0.06
0.04
0.02
0.00
**
***
SH-SY5Y
WT LRRK2
G2019S LRRK2
D.
Rit2 mRNA level
0.5
0.4
0.3
0.2
0.1
0.0
SNpc
VTA
E.
Fluorescent dot number per cell -Fold change
1.5
1.0
0.5
0.0
**
AAV-ctrl
AAV-aSyn
F.
mouse midbrain
AAV-ctrl
AAV-aSyn
TH
Rit2
aSyn
25 um

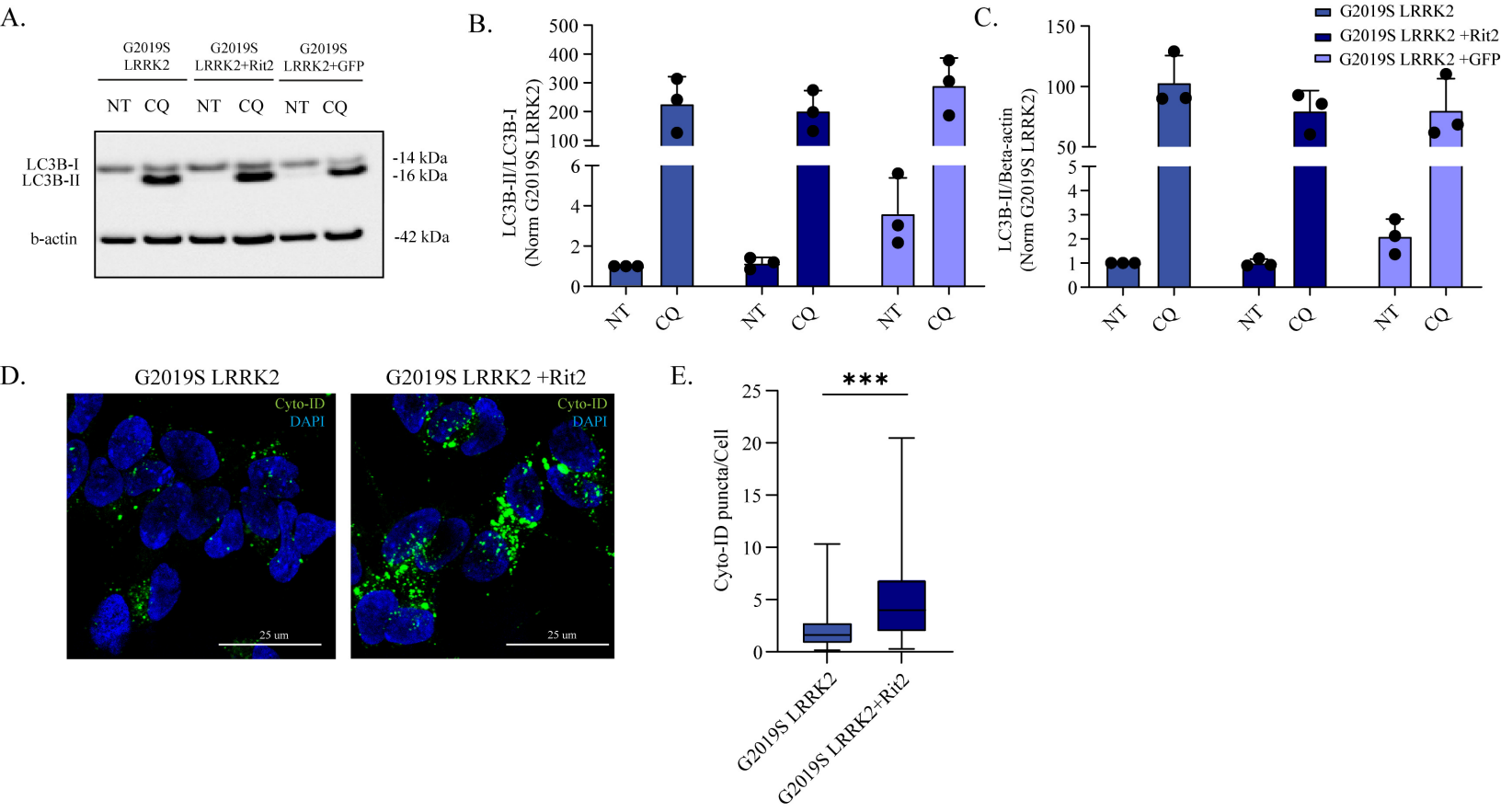
A.
G2019S LRRK2
G2019S LRRK2+Rit2
G2019S LRRK2+GFP
NT CQ NT CQ NT CQ
LC3B-I
LC3B-II
b-actin
-14 kDa
-16 kDa
-42 kDa
B.
LC3B-II/LC3B-I (Norm G2019S LRRK2)
NT CQ NT CQ NT CQ
C.
G2019S LRRK2
G2019S LRRK2 +Rit2
G2019S LRRK2 +GFP
LC3B-II/Beta-actin (Norm G2019S LRRK2)
NT CQ NT CQ NT CQ
D.
G2019S LRRK2
G2019S LRRK2 +Rit2
Cyto-ID
DAPI
25 um
E.
***
Cyto-ID puncta/Cell
G2019S LRRK2
G2019S LRRK2+Rit2

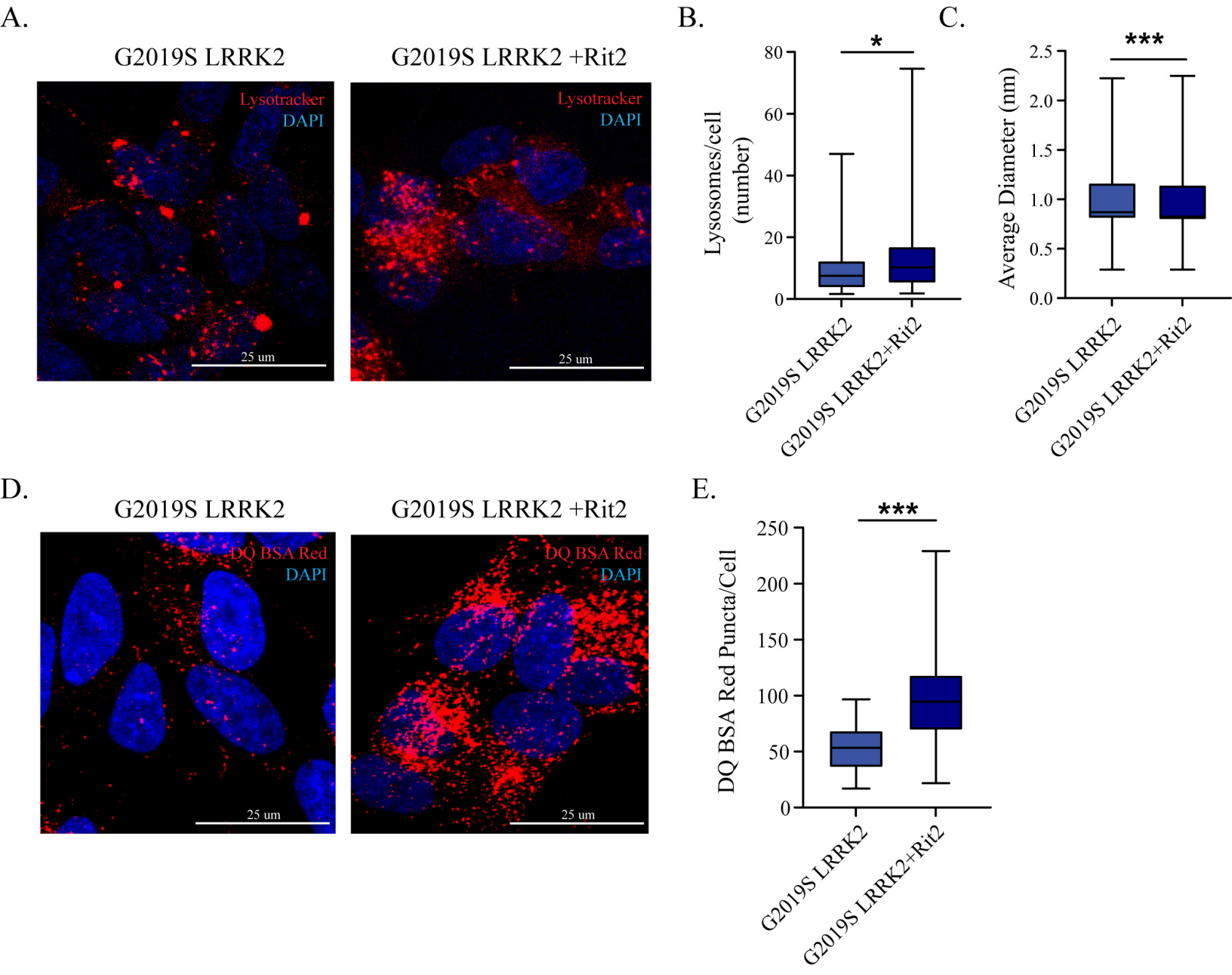
A.
G2019S LRRK2
G2019S LRRK2 +Rit2
Lysotracker
DAPI
25 um
B.
Lysosomes/cell (number)
*
G2019S LRRK2
G2019S LRRK2+Rit2
C.
Average Diameter (nm)
***
G2019S LRRK2
G2019S LRRK2+Rit2
D.
G2019S LRRK2
G2019S LRRK2 +Rit2
DQ BSA Red
DAPI
25 um
E.
DQ BSA Red Puncta/Cell
***
G2019S LRRK2
G2019S LRRK2+Rit2

A.

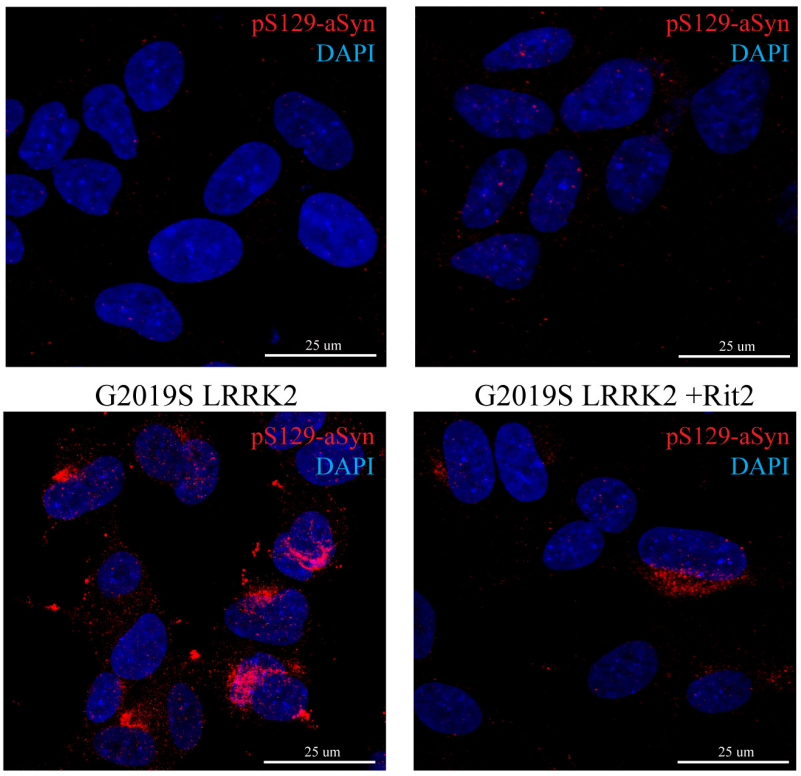
SH-SY5Y
WT LRRK2
G2019S LRRK2
G2019S LRRK2 +Rit2
pS129-aSyn
DAPI
25 um

B.

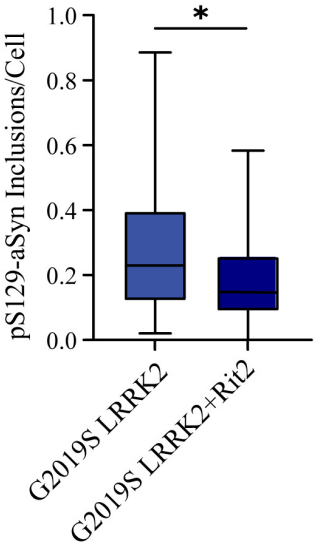
pS129-aSyn Inclusions/Cell
1.0
0.8
0.6
0.4
0.2
0.0
*
G2019S LRRK2
G2019S LRRK2+Rit2

C.

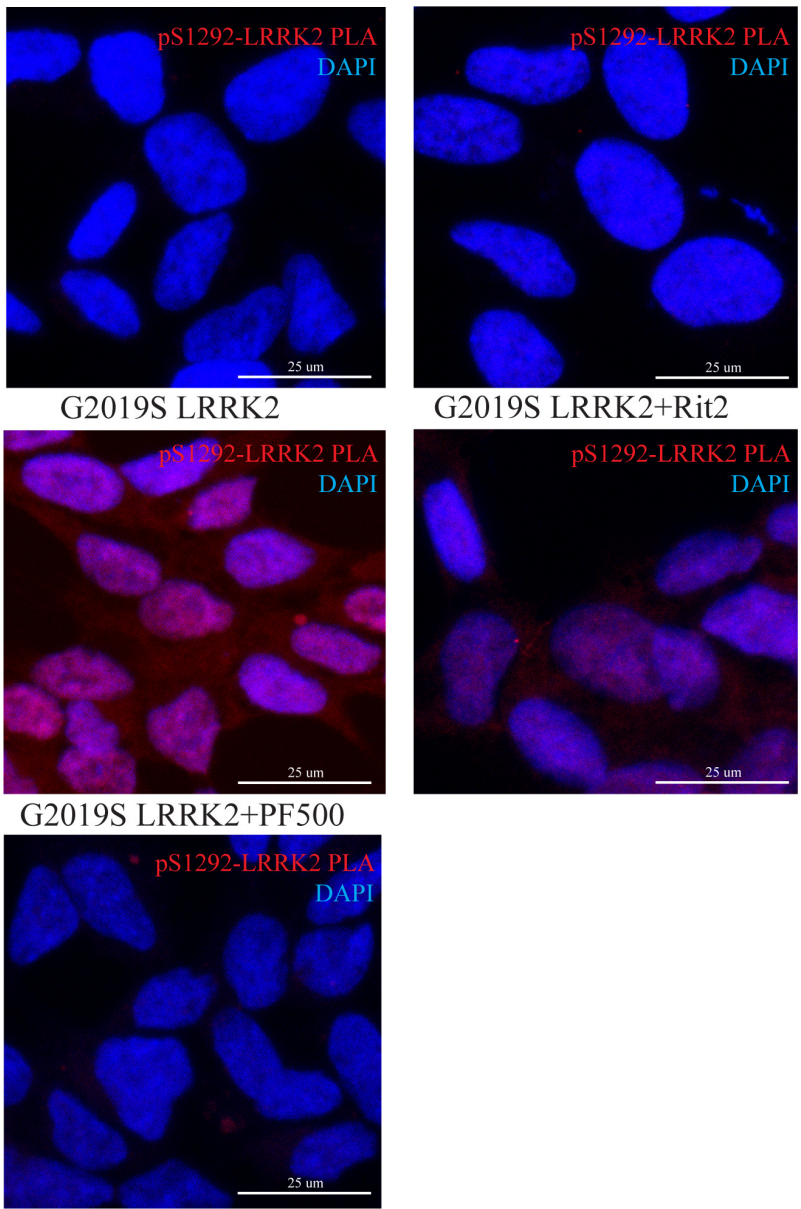
SH-SY5Y
WT LRRK2
G2019S LRRK2
G2019S LRRK2+Rit2
G2019S LRRK2+PF500
pS1292-LRRK2 PLA
DAPI
25 um

D.

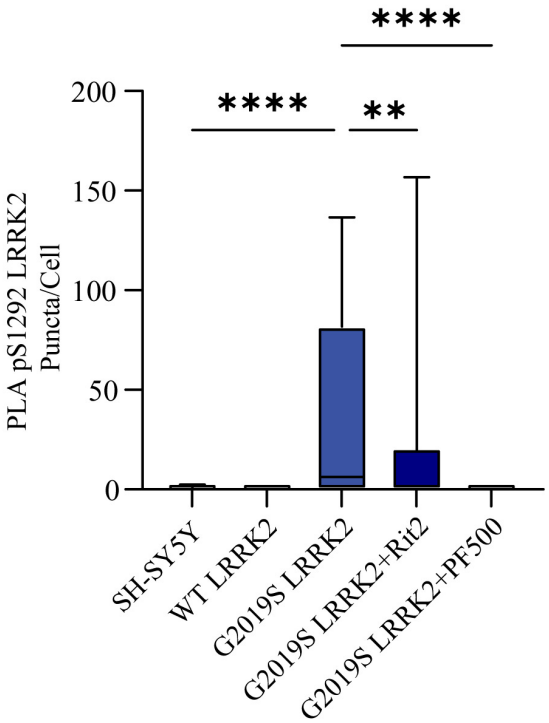
PLA pS1292 LRRK2 Puncta/Cell
200
150
100
50
0
****
****
**
SH-SY5Y
WT LRRK2
G2019S LRRK2
G2019S LRRK2+Rit2
G2019S LRRK2+PF500

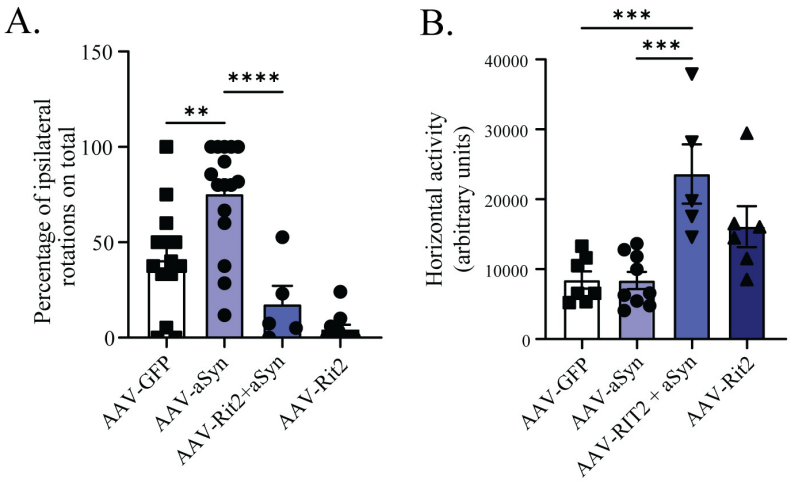
A.
Percentage of ipsilateral rotations on total
150
100
50
0
**
****
AAV-GFP
AAV-aSyn
AAV-Rit2+aSyn
AAV-Rit2
B.
Horizontal activity (arbitrary units)
40000
30000
20000
10000
0
***
***
AAV-GFP
AAV-aSyn
AAV-RIT2 + aSyn
AAV-Rit2

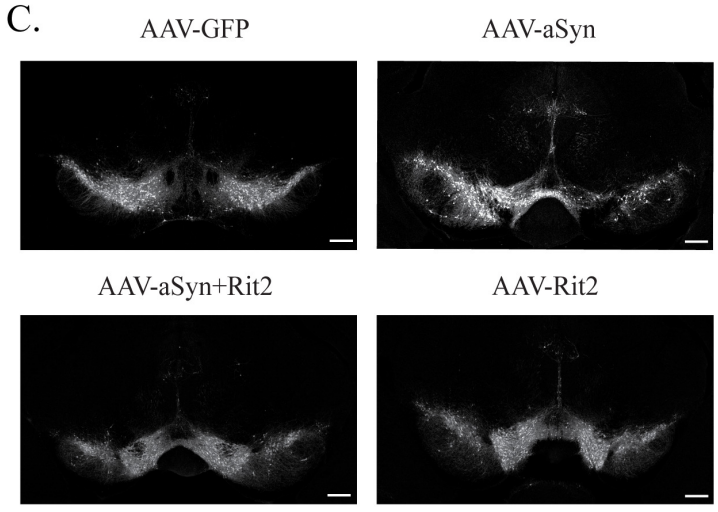
C.
AAV-GFP
AAV-aSyn
AAV-aSyn+Rit2
AAV-Rit2

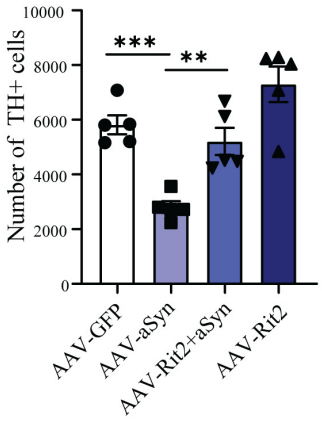
D.
Number of TH+ cells
10000
8000
6000
4000
2000
0
***
**
AAV-GFP
AAV-aSyn
AAV-Rit2+aSyn
AAV-Rit2

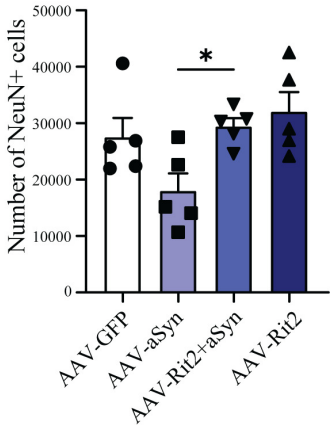
E.
Number of NeuN+ cells
50000
40000
30000
20000
10000
0
*
AAV-GFP
AAV-aSyn
AAV-Rit2+aSyn
AAV-Rit2

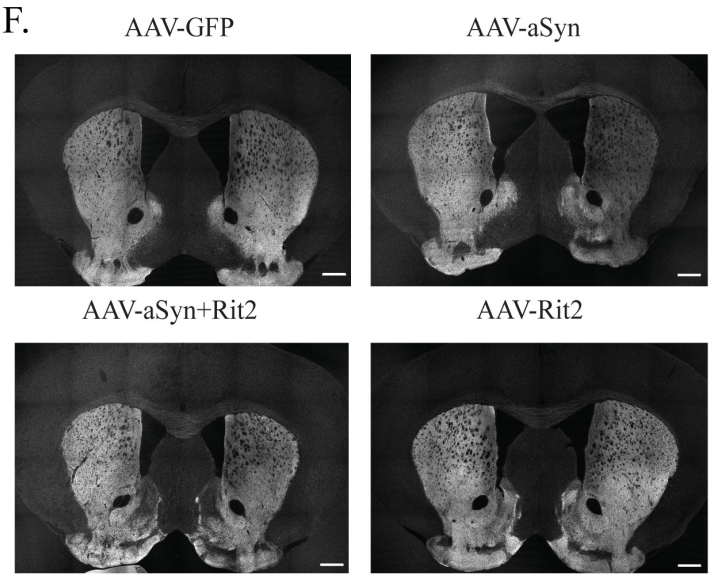
F.
AAV-GFP
AAV-aSyn
AAV-aSyn+Rit2
AAV-Rit2

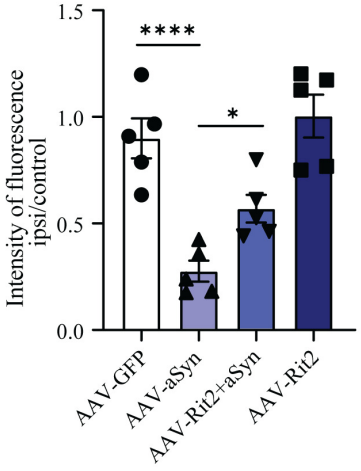
G.
Intensity of fluorescence ipsi/control
1.5
1.0
0.5
0.0
****
*
AAV-GFP
AAV-aSyn
AAV-Rit2+aSyn
AAV-Rit2

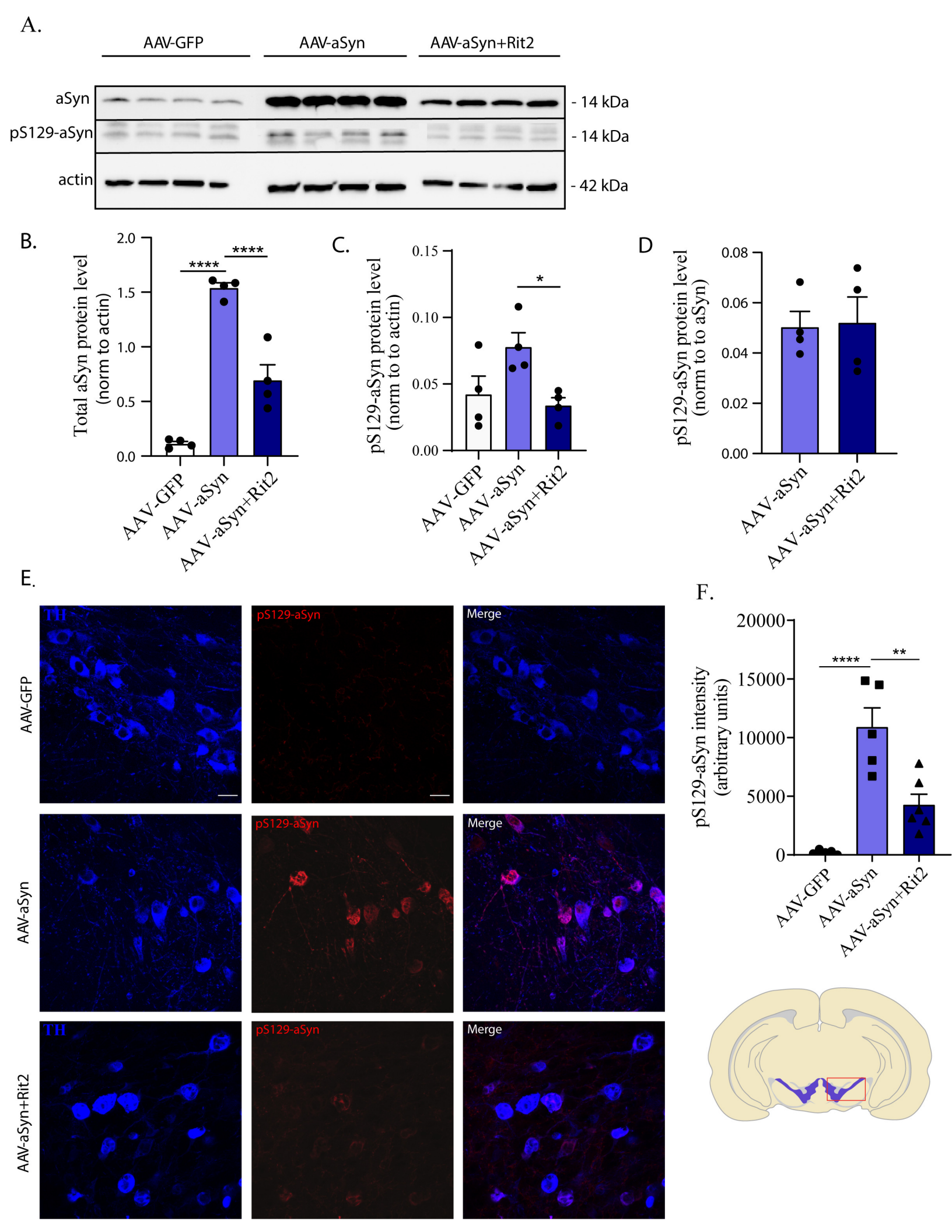
A.
AAV-GFP
AAV-aSyn
AAV-aSyn+Rit2
aSyn
pS129-aSyn
actin
- 14 kDa
- 14 kDa
- 42 kDa
B.
Total aSyn protein level (norm to actin)
2.0
1.5
1.0
0.5
0.0
****
****
AAV-GFP
AAV-aSyn
AAV-aSyn+Rit2
C.
pS129-aSyn protein level (norm to to actin)
0.15
0.10
0.05
0.00
*
AAV-GFP
AAV-aSyn
AAV-aSyn+Rit2
D
pS129-aSyn protein level (norm to to aSyn)
0.08
0.06
0.04
0.02
0.00
AAV-aSyn
AAV-aSyn+Rit2
E.
AAV-GFP
AAV-aSyn
AAV-aSyn+Rit2
TH
pS129-aSyn
Merge
F.
pS129-aSyn intensity (arbitrary units)
20000
15000
10000
5000
0
****
**
AAV-GFP
AAV-aSyn
AAV-aSyn+Rit2

A.

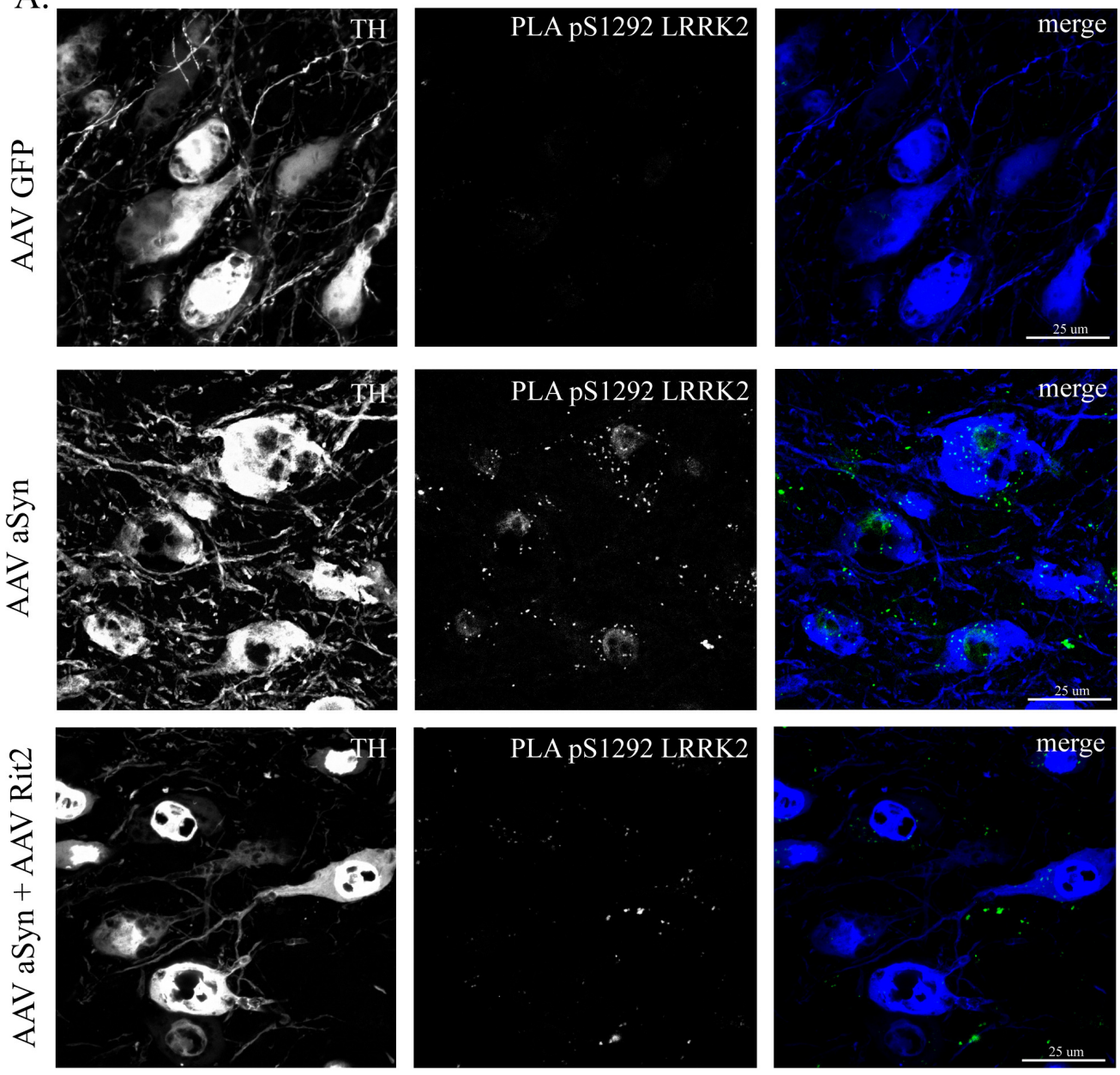
AAV GFP
AAV aSyn
AAV aSyn + AAV Rit2
TH
PLA pS1292 LRRK2
merge
25 um

B.

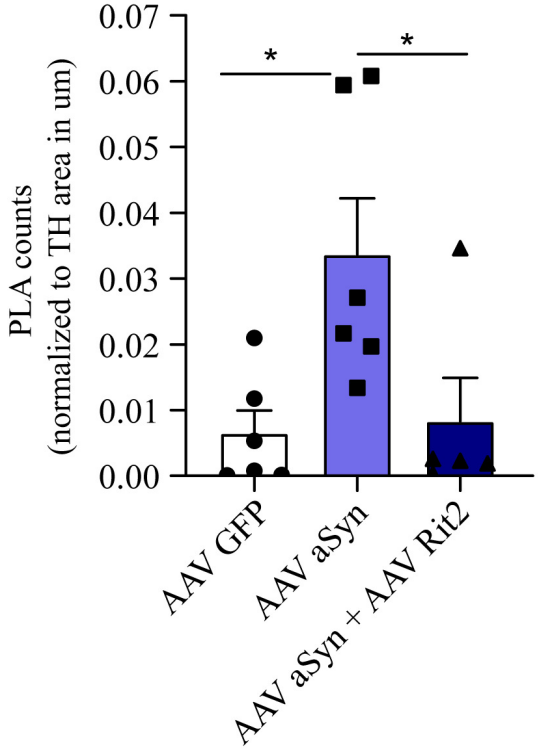
PLA counts
(normalized to TH area in um)
0.07
0.06
0.05
0.04
0.03
0.02
0.01
0.00
*
*
AAV GFP
AAV aSyn
AAV aSyn + AAV Rit2

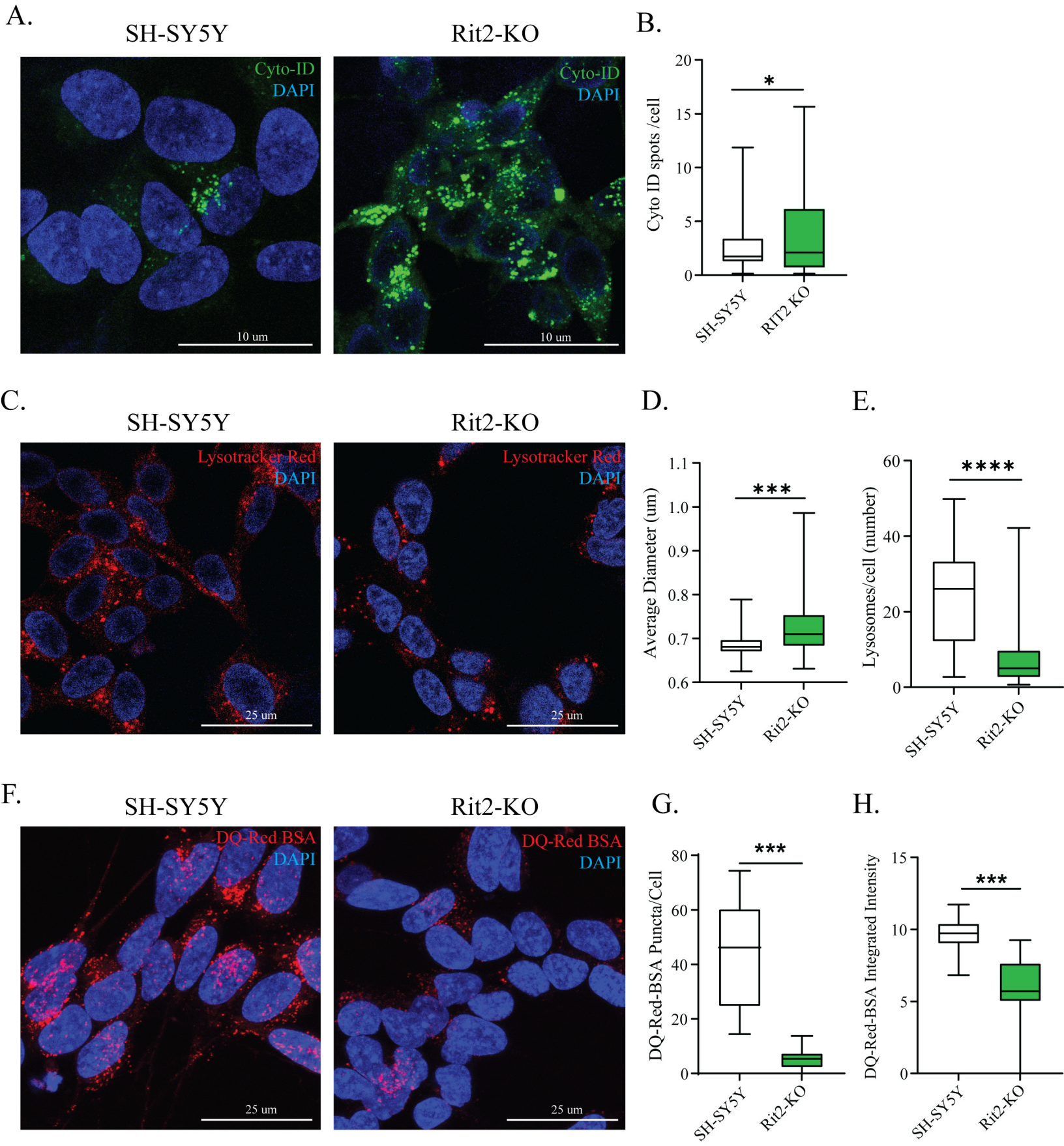
A.
SH-SY5Y
Rit2-KO
Cyto-ID
DAPI
10 um
B.
Cyto ID spots /cell
SH-SY5Y
RIT2 KO
C.
Lysotracker Red
25 um
D.
Average Diameter (um)
E.
Lysosomes/cell (number)
F.
DQ-Red BSA
G.
DQ-Red-BSA Puncta/Cell
H.
DQ-Red-BSA Integrated Intensity
Rit2-KO

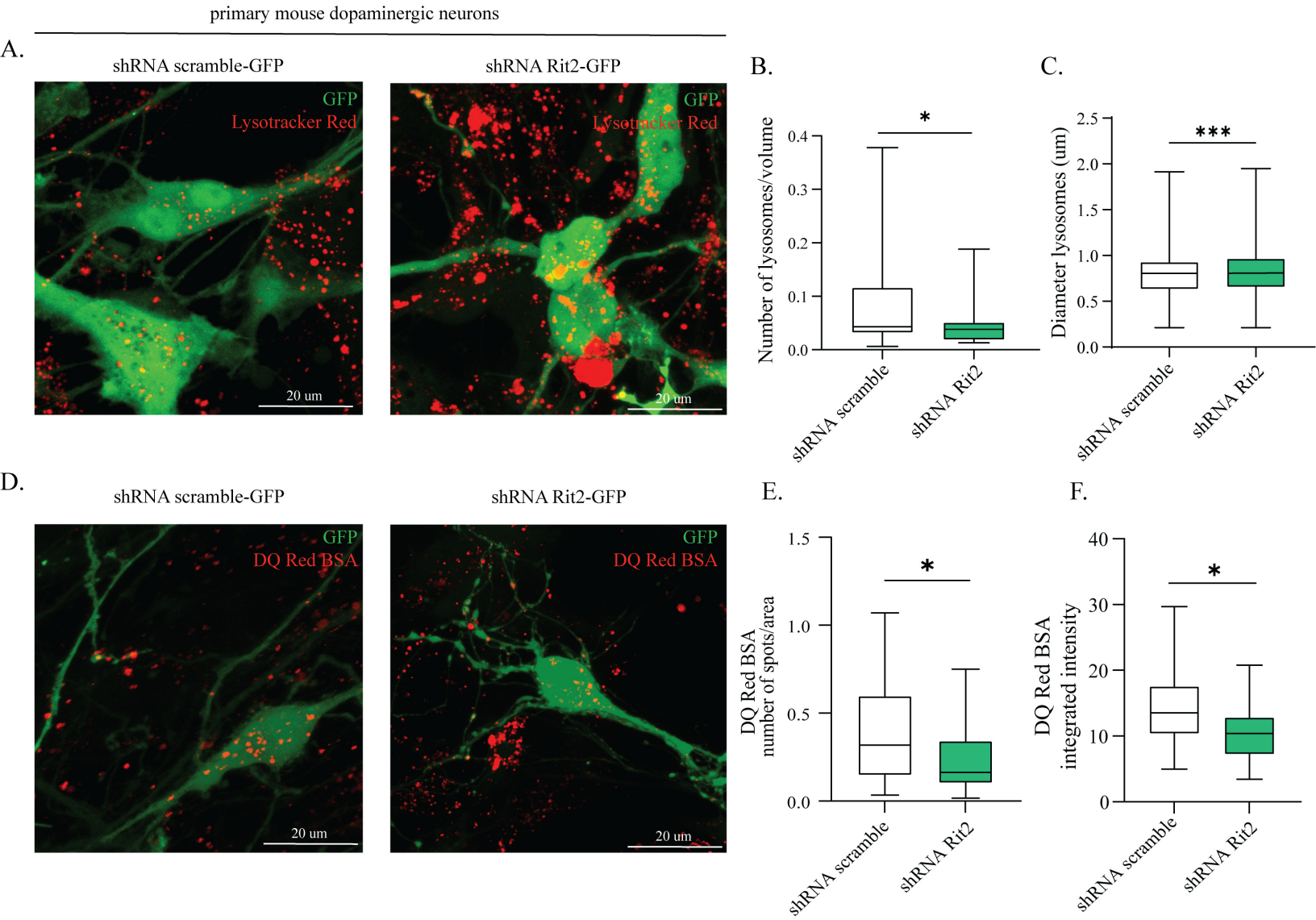
primary mouse dopaminergic neurons
A.
shRNA scramble-GFP
shRNA Rit2-GFP
GFP
Lysotracker Red
20 um
B.
C.
Number of lysosomes/volume
Diameter lysosomes (um)
shRNA scramble
shRNA Rit2
D.
shRNA scramble-GFP
shRNA Rit2-GFP
GFP
DQ Red BSA
20 um
E.
F.
DQ Red BSA number of spots/area
DQ Red BSA integrated intensity

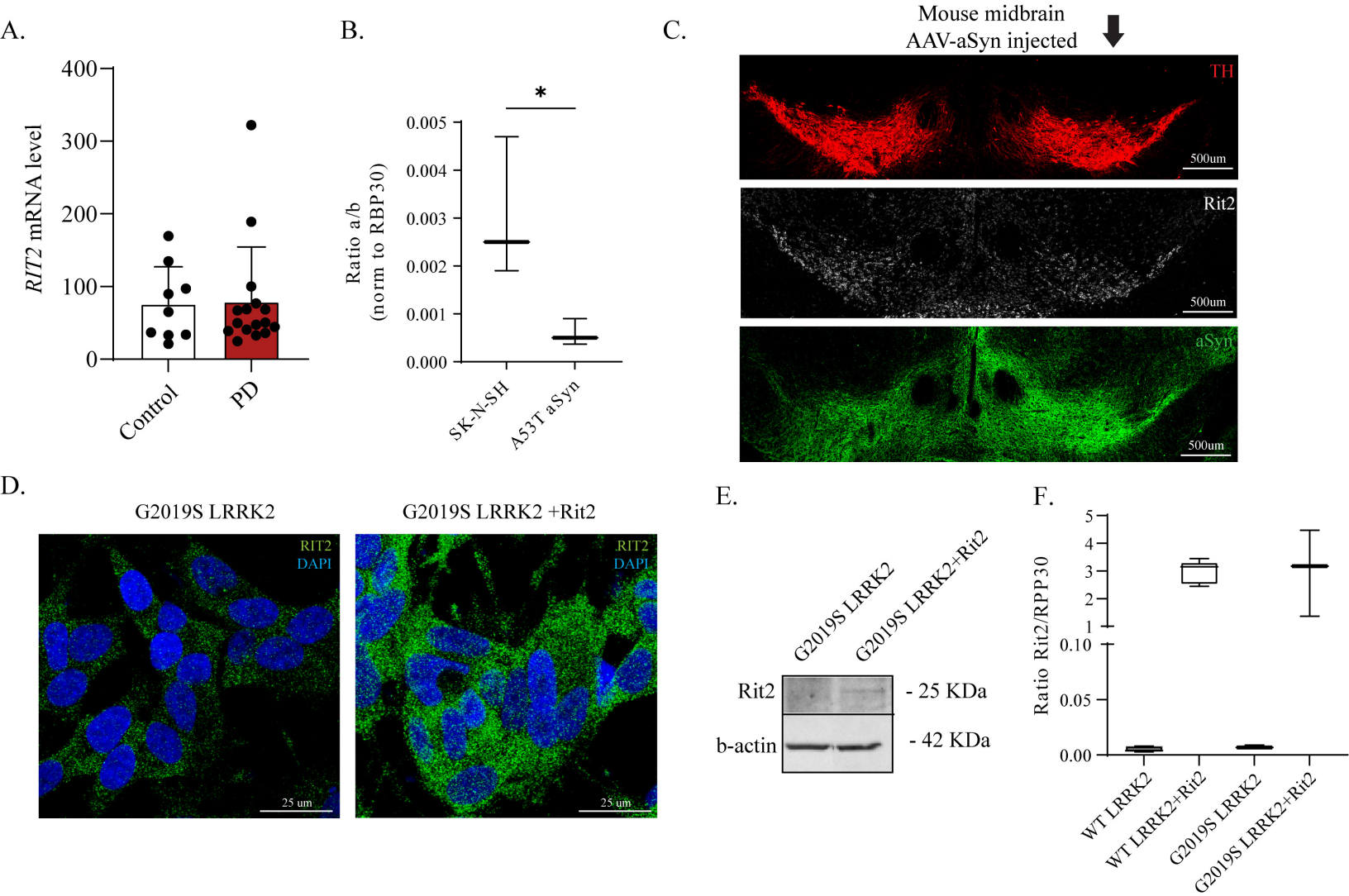
A.
400
300
200
100
0
RIT2 mRNA level
Control
PD
B.
0.005
0.004
0.003
0.002
0.001
0.000
Ratio a/b
(norm to RBP30)
*
SK-N-SH
A53T aSyn
C.
Mouse midbrain
AAV-aSyn injected
TH
500um
Rit2
500um
aSyn
500um
D.
G2019S LRRK2
G2019S LRRK2 +Rit2
RIT2
DAPI
25 um
RIT2
DAPI
25 um
E.
G2019S LRRK2
G2019S LRRK2+Rit2
Rit2
- 25 KDa
b-actin
- 42 KDa
F.
5
4
3
2
1
0.10
0.05
0.00
Ratio Rit2/RPP30
WT LRRK2
WT LRRK2+Rit2
G2019S LRRK2
G2019S LRRK2+Rit2

A.

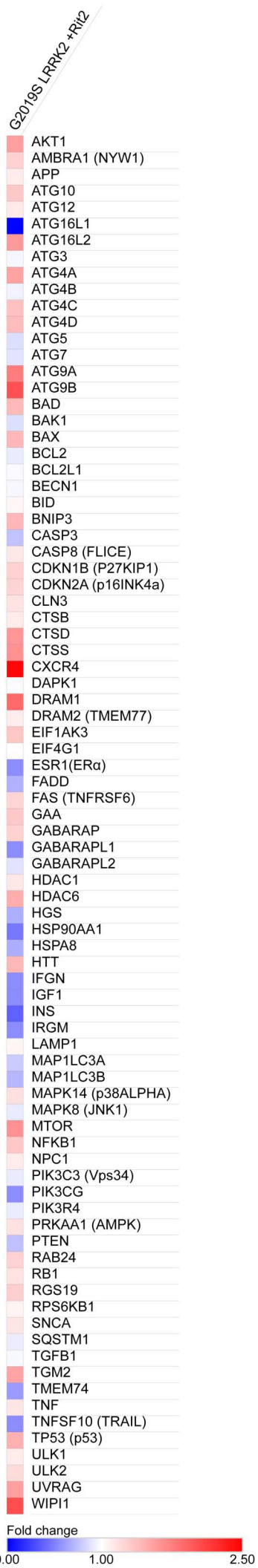
G2019S LRRK2 +Rit2
AKT1
AMBRA1 (NYW1)
APP
ATG10
ATG12
ATG16L1
ATG16L2
ATG3
ATG4A
ATG4B
ATG4C
ATG4D
ATG5
ATG7
ATG9A
ATG9B
BAD
BAK1
BAX
BCL2
BCL2L1
BECN1
BID
BNIP3
CASP3
CASP8 (FLICE)
CDKN1B (P27KIP1)
CDKN2A (p16INK4a)
CLN3
CTSB
CTSD
CTSS
CXCR4
DAPK1
DRAM1
DRAM2 (TMEM77)
EIF1AK3
EIF4G1
ESR1(ERα)
FADD
FAS (TNFRSF6)
GAA
GABARAP
GABARAPL1
GABARAPL2
HDAC1
HDAC6
HGS
HSP90AA1
HSPA8
HTT
IFGN
IGF1
INS
IRGM
LAMP1
MAP1LC3A
MAP1LC3B
MAPK14 (p38ALPHA)
MAPK8 (JNK1)
MTOR
NFKB1
NPC1
PIK3C3 (Vps34)
PIK3CG
PIK3R4
PRKAA1 (AMPK)
PTEN
RAB24
RB1
RGS19
RPS6KB1
SNCA
SQSTM1
TGFB1
TGM2
TMEM74
TNF
TNFSF10 (TRAIL)
TP53 (p53)
ULK1
ULK2
UVRAG
WIPI1
Fold change
0.00
1.00
2.50

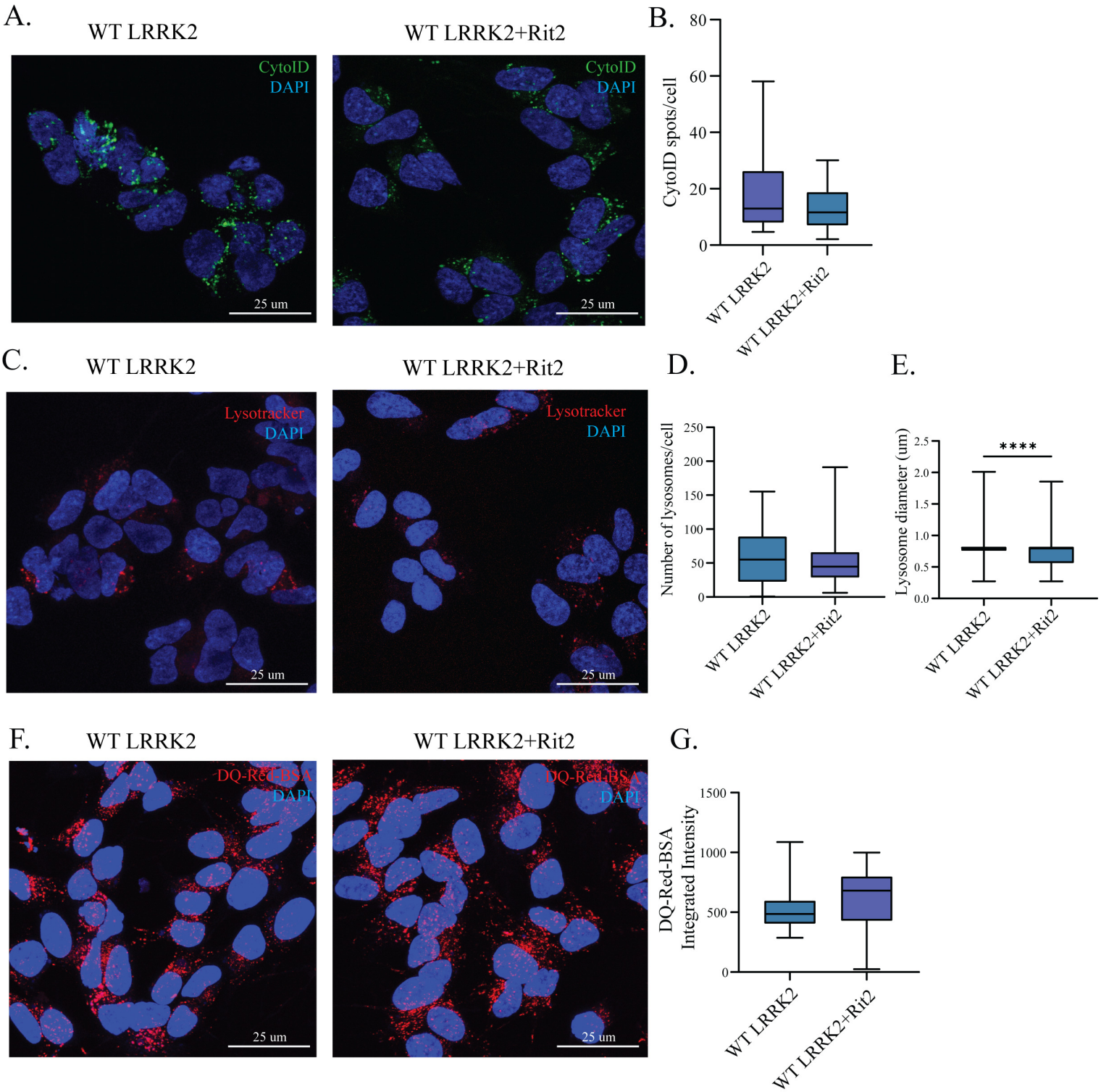
A.
WT LRRK2
WT LRRK2+Rit2
CytoID
DAPI
25 um
B.
CytoID spots/cell
80
60
40
20
0
WT LRRK2
WT LRRK2+Rit2
C.
Lysotracker
D.
Number of lysosomes/cell
250
200
150
100
50
E.
Lysosome diameter (um)
2.5
2.0
1.5
1.0
0.5
0.0
****
F.
DQ-Red-BSA
G.
DQ-Red-BSA Integrated Intensity
1500
1000
500
H.
LRRK2
-283KDa
aSyn
- 14 KDa
Rit2
- 25 KDa
b-actin
- 42 KDa
I.
Total aSyn/b-actin Ratio
J.
Total LRRK2/b-actin Ratio

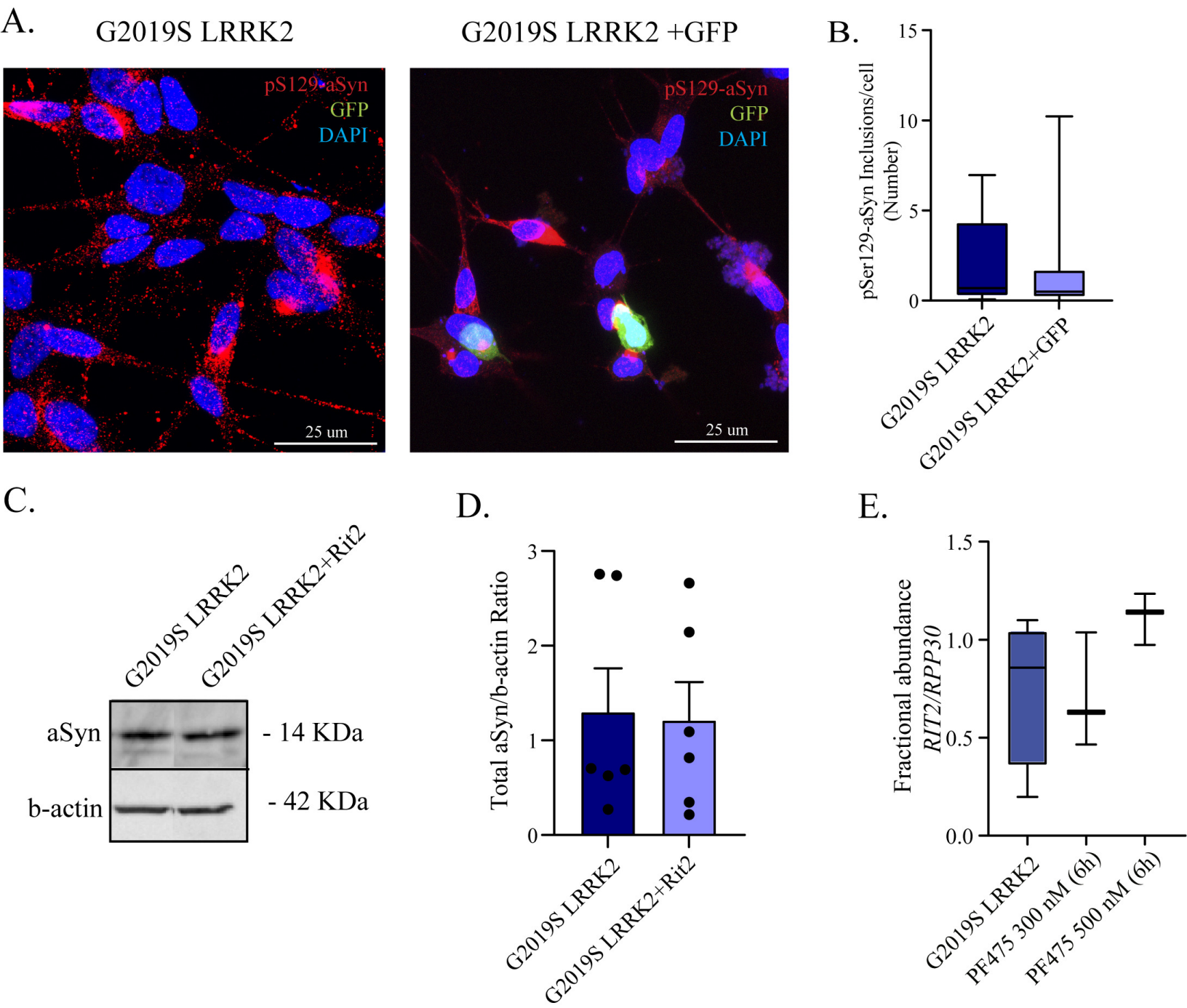
A.
G2019S LRRK2
G2019S LRRK2 +GFP
pS129-aSyn
GFP
DAPI
25 um
B.
pSer129-aSyn Inclusions/cell (Number)
15
10
5
0
G2019S LRRK2
G2019S LRRK2+GFP
C.
G2019S LRRK2
G2019S LRRK2+Rit2
aSyn
- 14 KDa
b-actin
- 42 KDa
D.
Total aSyn/b-actin Ratio
3
2
1
0
G2019S LRRK2
G2019S LRRK2+Rit2
E.
Fractional abundance
RIT2/RPP30
1.5
1.0
0.5
0.0
G2019S LRRK2
PF475 300 nM (6h)
PF475 500 nM (6h)

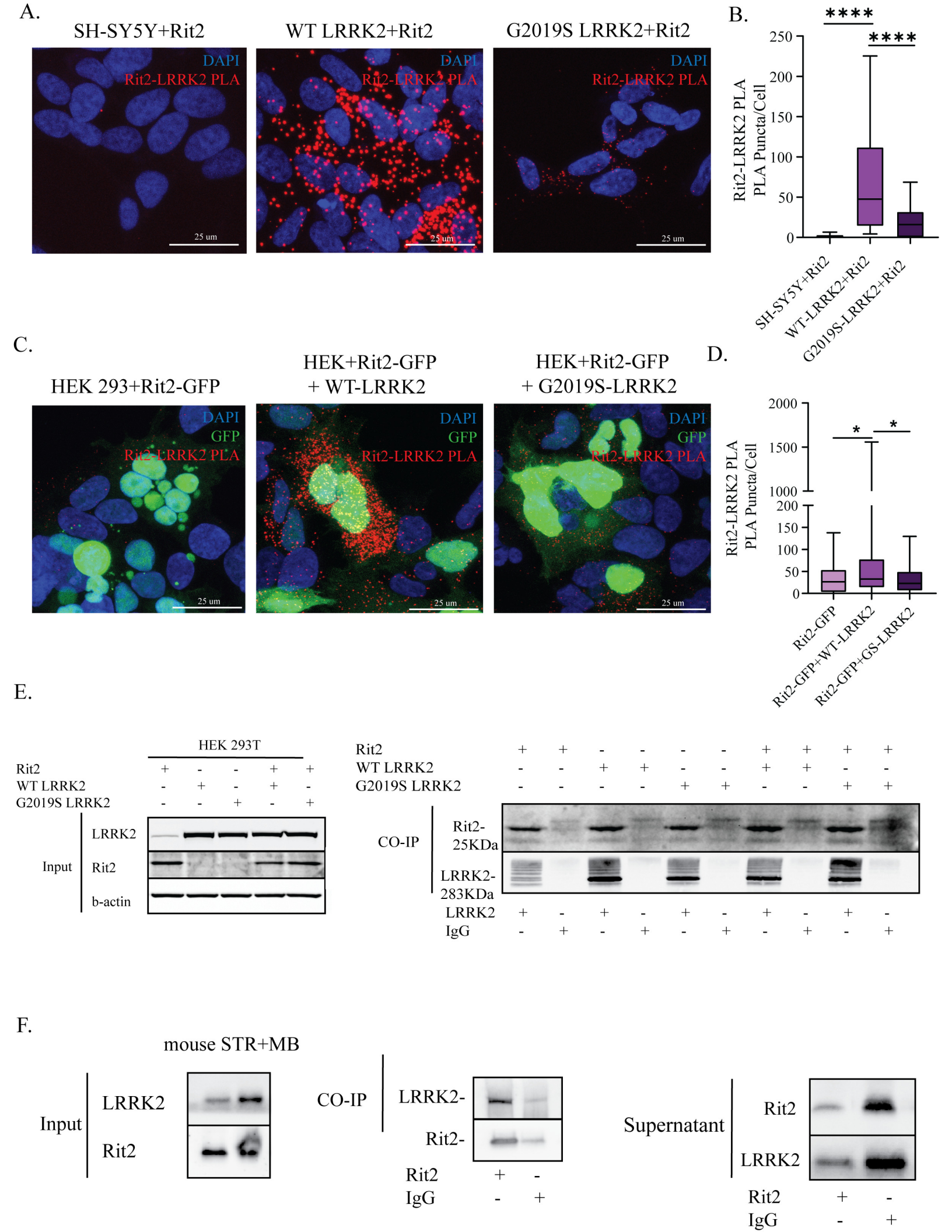
A.
SH-SY5Y+Rit2
WT LRRK2+Rit2
G2019S LRRK2+Rit2
DAPI
Rit2-LRRK2 PLA
25 um
B.
****
****
Rit2-LRRK2 PLA
PLA Puncta/Cell
250
200
150
100
50
0
SH-SY5Y+Rit2
WT-LRRK2+Rit2
G2019S-LRRK2+Rit2
C.
HEK 293+Rit2-GFP
HEK+Rit2-GFP
+ WT-LRRK2
HEK+Rit2-GFP
+ G2019S-LRRK2
DAPI
GFP
Rit2-LRRK2 PLA
25 um
D.
*
*
Rit2-LRRK2 PLA
PLA Puncta/Cell
2000
1500
1000
200
150
100
50
0
Rit2-GFP
Rit2-GFP+WT-LRRK2
Rit2-GFP+GS-LRRK2
E.
HEK 293T
Rit2
WT LRRK2
G2019S LRRK2
Input
LRRK2
Rit2
b-actin
CO-IP
Rit2-
25KDa
LRRK2-
283KDa
LRRK2
IgG
F.
mouse STR+MB
Input
LRRK2
Rit2
CO-IP
LRRK2-
Rit2-
Rit2
IgG
Supernatant
Rit2
LRRK2
Rit2
IgG

A.

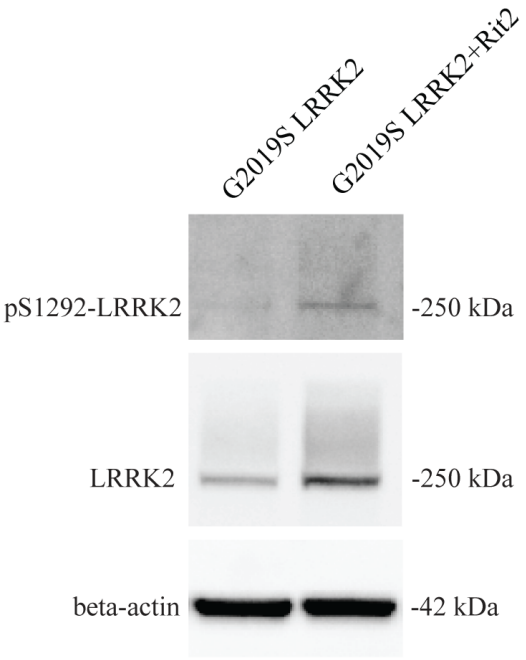
G2019S LRRK2
G2019S LRRK2+Rit2
pS1292-LRRK2
-250 kDa
LRRK2
-250 kDa
beta-actin
-42 kDa

B.

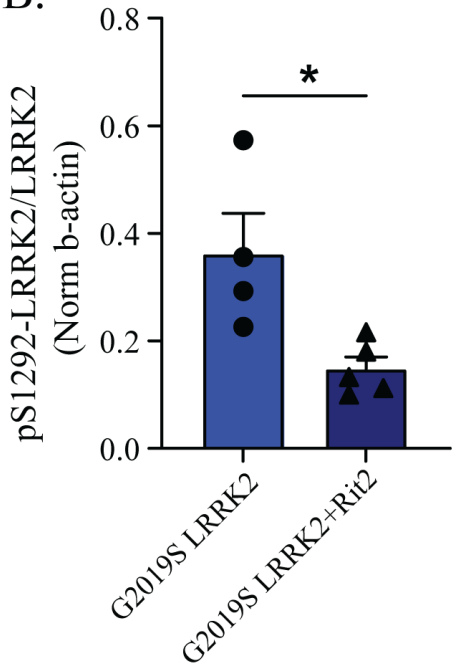
pS1292-LRRK2/LRRK2
(Norm b-actin)
0.8
0.6
0.4
0.2
0.0
*
G2019S LRRK2
G2019S LRRK2+Rit2

C.

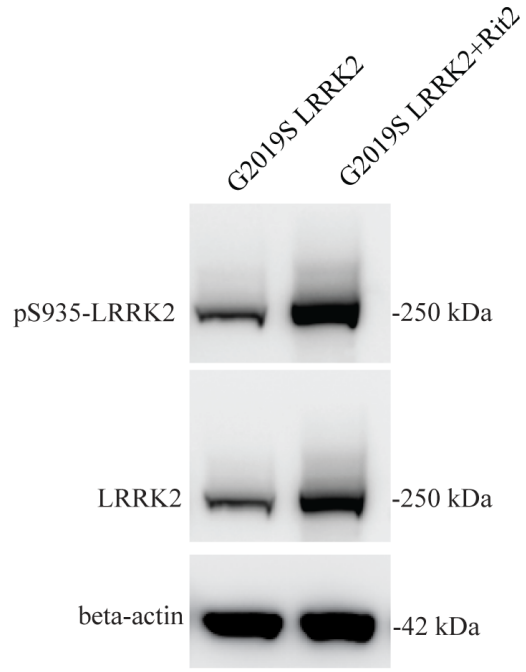
G2019S LRRK2
G2019S LRRK2+Rit2
pS935-LRRK2
-250 kDa
LRRK2
-250 kDa
beta-actin
-42 kDa

D.

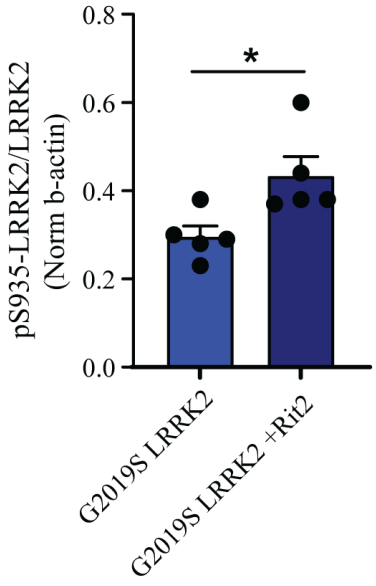
pS935-LRRK2/LRRK2
(Norm b-actin)
0.8
0.6
0.4
0.2
0.0
*
G2019S LRRK2
G2019S LRRK2 +Rit2

E.

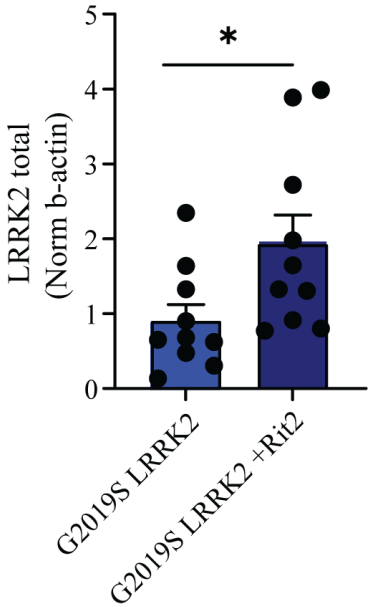
LRRK2 total
(Norm b-actin)
5
4
3
2
1
0
*
G2019S LRRK2
G2019S LRRK2 +Rit2

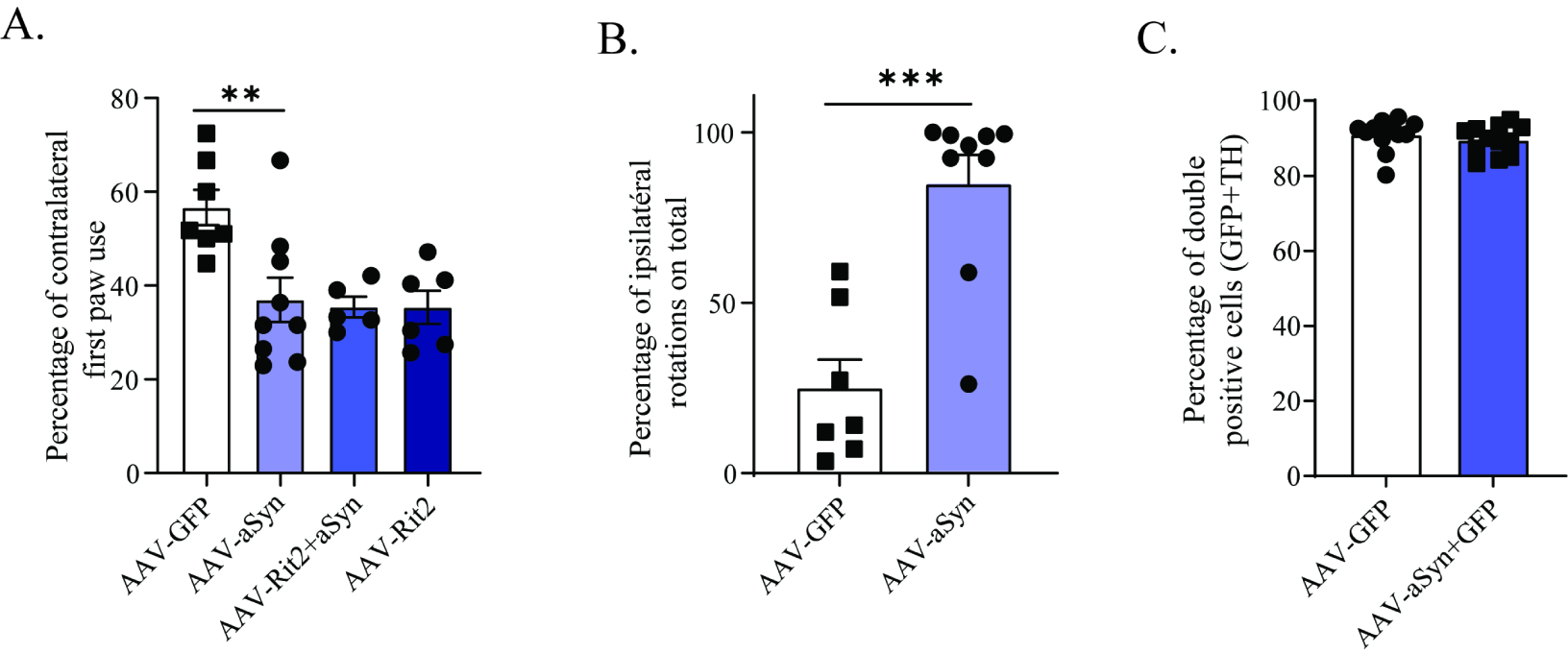
A.
B.
C.
Percentage of contralateral first paw use
80
60
40
20
0
**
AAV-GFP
AAV-aSyn
AAV-Rit2+aSyn
AAV-Rit2
Percentage of ipsilatéral rotations on total
100
50
0
***
AAV-GFP
AAV-aSyn
Percentage of double positive cells (GFP+TH)
100
80
60
40
20
0
AAV-GFP
AAV-aSyn+GFP

A.

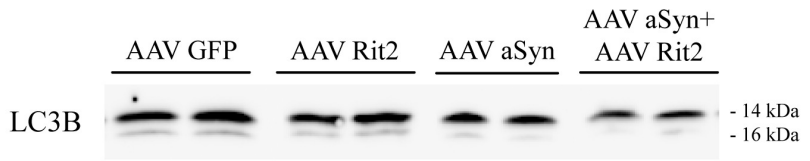
AAV GFP
AAV Rit2
AAV aSyn
AAV aSyn+
AAV Rit2
LC3B
- 14 kDa
- 16 kDa

B.

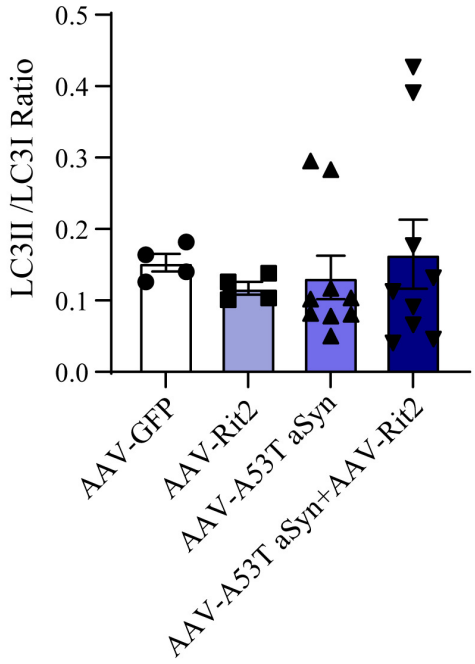
LC3II /LC3I Ratio
0.5
0.4
0.3
0.2
0.1
0.0
AAV-GFP
AAV-Rit2
AAV-A53T aSyn
AAV-A53T aSyn+AAV-Rit2

C.

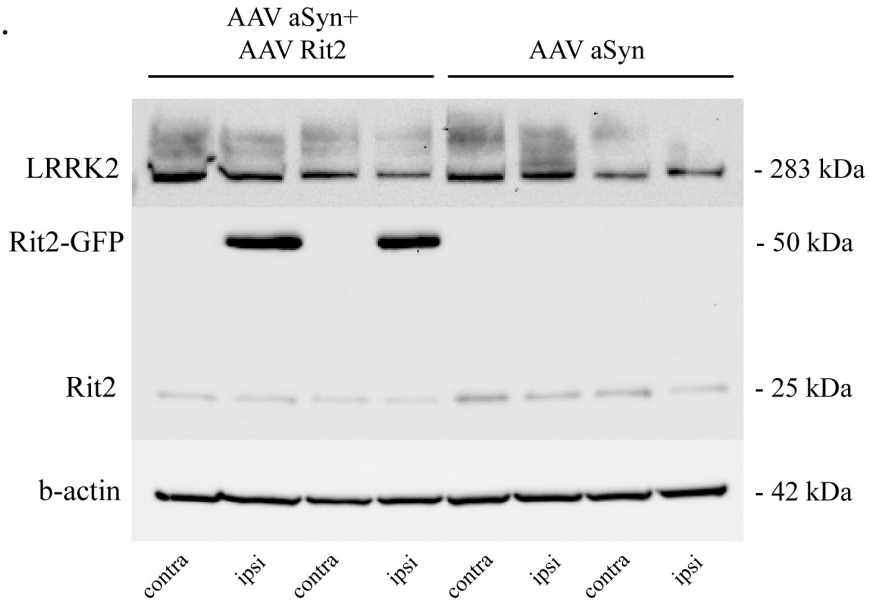
AAV aSyn+
AAV Rit2
AAV aSyn
LRRK2
Rit2-GFP
Rit2
b-actin
- 283 kDa
- 50 kDa
- 25 kDa
- 42 kDa
contra
ipsi
contra
ipsi
contra
ipsi
contra
ipsi

D.

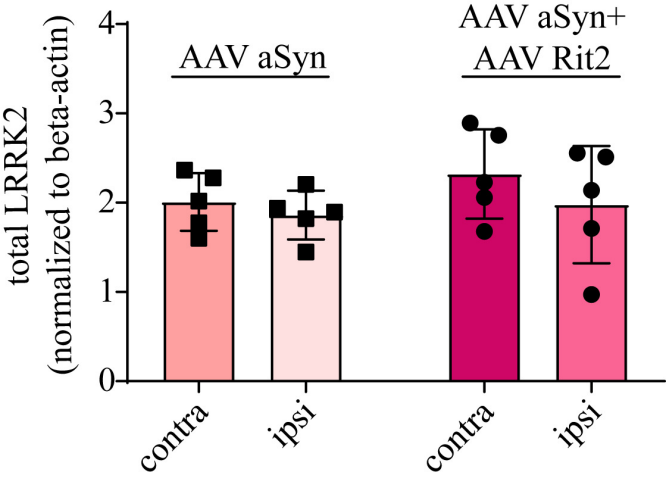
total LRRK2
(normalized to beta-actin)
4
3
2
1
0
AAV aSyn
AAV aSyn+
AAV Rit2
contra
ipsi
contra
ipsi

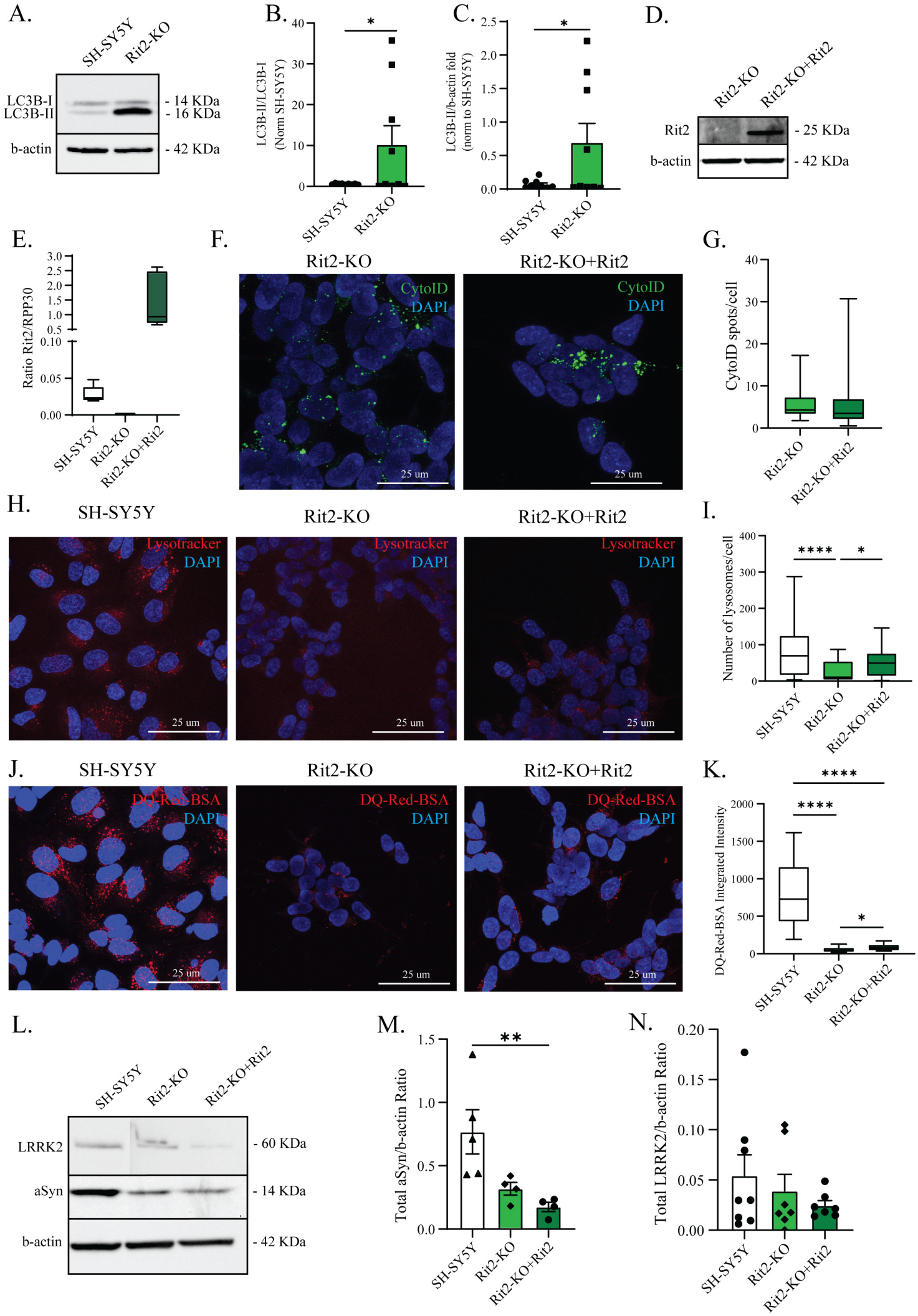
A.
SH-SY5Y
Rit2-KO
LC3B-I
LC3B-II
- 14 KDa
- 16 KDa
b-actin
- 42 KDa
B.
LC3B-II/LC3B-I (Norm SH-SY5Y)
*
SH-SY5Y
Rit2-KO
C.
LC3B-II/b-actin fold (norm to SH-SY5Y)
*
SH-SY5Y
Rit2-KO
D.
Rit2-KO
Rit2-KO+Rit2
Rit2
- 25 KDa
b-actin
- 42 KDa
E.
Ratio Rit2/RPP30
SH-SY5Y
Rit2-KO
Rit2-KO+Rit2
F.
Rit2-KO
Rit2-KO+Rit2
CytoID
DAPI
25 um
G.
CytoID spots/cell
Rit2-KO
Rit2-KO+Rit2
H.
SH-SY5Y
Rit2-KO
Rit2-KO+Rit2
Lysotracker
DAPI
25 um
I.
Number of lysosomes/cell
****
*
SH-SY5Y
Rit2-KO
Rit2-KO+Rit2
J.
SH-SY5Y
Rit2-KO
Rit2-KO+Rit2
DQ-Red-BSA
DAPI
25 um
K.
DQ-Red-BSA Integrated Intensity
****
****
*
SH-SY5Y
Rit2-KO
Rit2-KO+Rit2
L.
SH-SY5Y
Rit2-KO
Rit2-KO+Rit2
LRRK2
- 60 KDa
aSyn
- 14 KDa
b-actin
- 42 KDa
M.
Total aSyn/b-actin Ratio
**
SH-SY5Y
Rit2-KO
Rit2-KO+Rit2
N.
Total LRRK2/b-actin Ratio
SH-SY5Y
Rit2-KO
Rit2-KO+Rit2

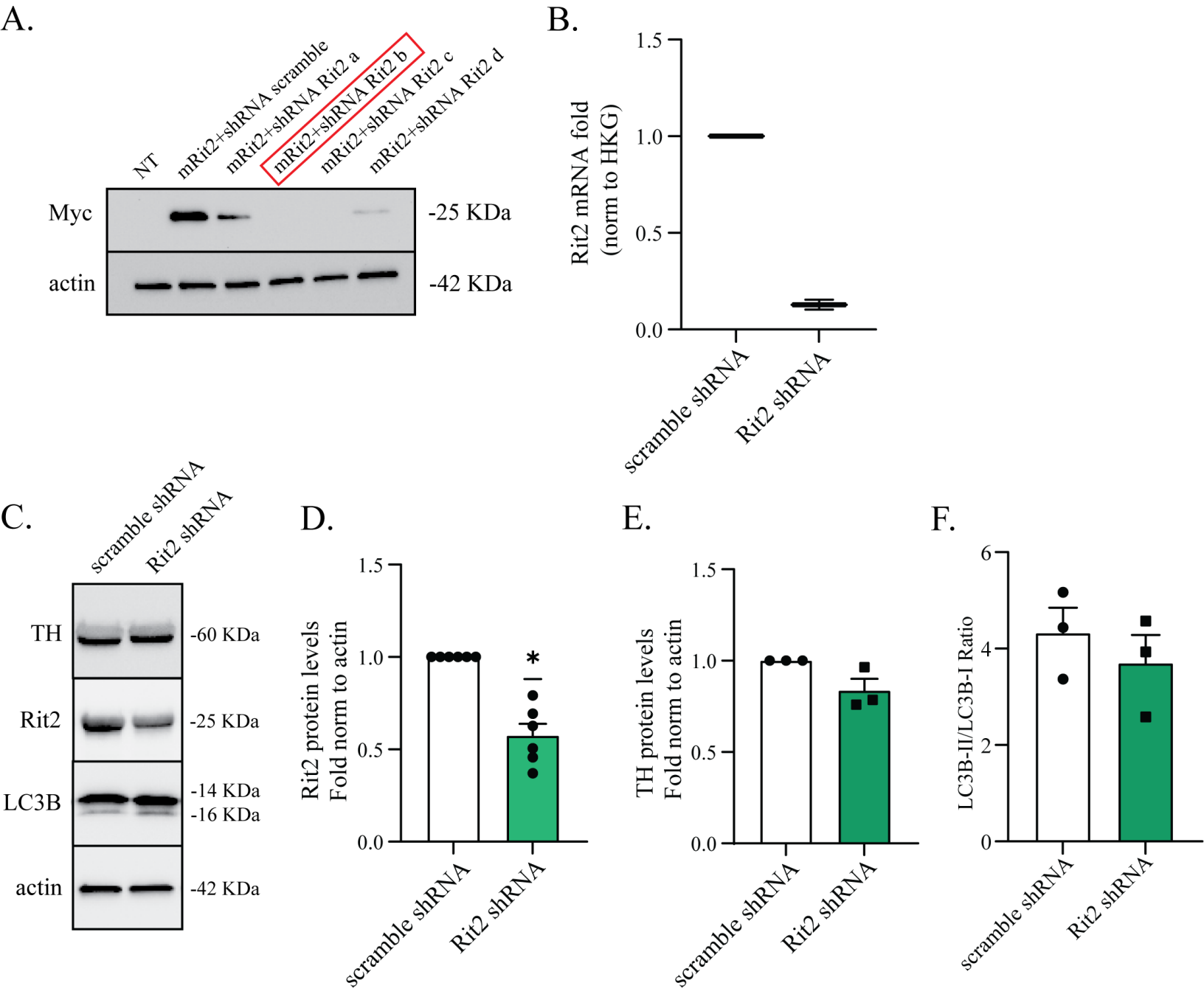
A.
NT
mRit2+shRNA scramble
mRit2+shRNA Rit2 a
mRit2+shRNA Rit2 b
mRit2+shRNA Rit2 c
mRit2+shRNA Rit2 d
Myc
actin
-25 KDa
-42 KDa
B.
Rit2 mRNA fold
(norm to HKG)
1.5
1.0
0.5
0.0
scramble shRNA
Rit2 shRNA
C.
scramble shRNA
Rit2 shRNA
TH
Rit2
LC3B
actin
-60 KDa
-25 KDa
-14 KDa
-16 KDa
-42 KDa
D.
Rit2 protein levels
Fold norm to actin
1.5
1.0
0.5
0.0
*
scramble shRNA
Rit2 shRNA
E.
TH protein levels
Fold norm to actin
1.5
1.0
0.5
0.0
scramble shRNA
Rit2 shRNA
F.
LC3B-II/LC3B-I Ratio
6
4
2
0
scramble shRNA
Rit2 shRNA

A.

AB73C6

| | | | | |
|---|---|---|---|---|
| aSyn | - | + | + | - |
| PLK2 | - | - | + | + |
| S129A asyn | - | - | - | + |